FINAL REPORT

NAG8-708-FINAL

HIGH TEMPERATURE FURNACE MODELING AND PERFORMANCE VERIFICATIONS

Submitted to

Richard M. Poorman
George C. Marshall Space Flight Center
National Aeronautics and Space Administration
Huntsville, Alabama 35812

Prepared by

James E. Smith, Jr., Ph.D.
Associate Professor and Chairman

Department of Chemical and Materials Engineering
College of Engineering
The University of Alabama in Huntsville
Huntsville, Alabama 35899

June 1992

FINAL REPORT

NAG8-708-FINAL

HIGH TEMPERATURE FURNACE MODELING AND PERFORMANCE VERIFICATIONS

Submitted to

Richard M. Poorman
George C. Marshall Space Flight Center
National Aeronautics and Space Administration
Huntsville, Alabama 35812

Prepared by

James E. Smith, Jr., Ph.D.
Associate Professor and Chairman

Department of Chemical and Materials Engineering
College of Engineering
The University of Alabama in Huntsville
Huntsville, Alabama 35899

June 1992

TABLE OF CONTENTS

FINAL REPORT

HIGH TEMPERATURE FURNACE MODELING AND PERFORMANCE VERIFICATIONS

1.0 INTRODUCTION

Under NASA Grant NAG8-708 we performed analytical, numerical, and experimental studies on two classes of high temperature materials processing sources for their potential use as directional solidification furnaces. The research concentrated on a commercially available high temperature furnace using a zirconia ceramic tube as the heating element and an Arc Furnace under design at NASA's MSFC, based on a ST International tube welder. The zirconia furnace was delivered, assembled, and analyzed for its potential to function as a directional solidification furnace. The work on the Arc Furnace was initially stalled due to the unavailability of the NASA prototype. A proposal was written and funded to purchase an additional arc welder to alleviate this problem. The ST International weld head and power supply were received in September 1988 and used to experimentally verify a portion of the numerical results generated by a thermal model using SINDA.

2.0 OBJECTIVES

There were five major objectives researched during the grant. The first objective was to assemble the zirconia furnace and construct components needed to successfully perform a series

of experiments. The second objective was to evaluate the zirconia furnace performance as-delivered from the manufacturer to evaluate its potential as a directional solidification furnace element. The third objective to establish a data base on materials used in furnace construction, with particular emphasis on emissivities, transmissivities and absorptivities as functions of wavelength and temperature. These data were used to develop a one-dimensional and two-dimensional spectral radiation heat transfer model for comparison with standard effective radiation heat transfer modeling techniques. These models were used to predict wall and crucible temperatures and may serve as an effective method to apply open loop control techniques to advanced high temperature resistance and arc furnaces. The fourth objective addressed the development of a SINDA model for the MSFC Arc Furnace and was used to begin preliminary numerical designs of sample holders and to estimate cooling media temperatures for the steady-state operation of the furnace. Finally, the fifth objective addressed the initial performance evaluation of the Arc furnace and associated equipment for directional solidification.

These objectives were met by the research. In addition, preliminary research was conducted to determine if a zirconia heating element could be developed that would function longer than the two commercially prepared elements purchased with the ARTCOR Model 460-15 Bench Top Tubular Laboratory Research Furnace. A zirconia heating element was prepared and its performance reported.

Objective 1.

One of the focuses of this research project was the evaluation and performance verification of existing furnace technologies. Two furnace types are being considered. They are the ARTCOR Model 460-15 Bench Top Tubular Laboratory Research Furnace and an Arc Furnace being constructed at NASA's MSFC which uses an ST International Orbital Tube Welding System as a heat source. This final report's first three sections concentrate on the ARTCOR Research Furnace.

Objective 2.

The second section contains an initial performance analysis of the zirconia furnace. The performance of the zirconia furnace was tested at different levels of applied power to the main zirconia heating element, namely 15%, 20%, 25% and 30%. The axial temperature profiles in the furnace were measured along the centerline for applied powers of 20% and 30%. Step change increase from 20% to 30% applied power and a linear ramp rate of 1% per minute from 0% to 15% applied power were studied. Limitation of 50% applied power were corrected with repair of the units controller. Power to higher levels was then applied.

Objective 3.

Experimental data on various ceramics and other materials needed for eventual design, construction and modeling of advanced high temperature electrical furnaces were collected from various

literature references. Spectral radiation data were collected on alumina, zirconia, and titania. The data were assembled to evaluate the material's emissivity, transmissivity, and absorptivity trends at various wavelengths and operating temperatures. Data for zirconia were used to estimate the effective emissivity for use with the high temperature optical pyrometer. Finally, the thermal and frequency characteristics of these data were used to formulate a one-dimensional and two-dimensional spectral model for comparison with effective radiation modeling approaches. FORTRAN computer programs were developed to solve these highly nonlinear problem. These efforts were coordinated with those of the UAH Center for Microgravity Studies to prevent duplication and to accelerate development of advance high temperature material processing technologies.

Objective 4.

Numerical Analysis of the MSFC Arc Furnace. An Arc Furnace for use on the KC-135 experimental aircraft was first proposed by Poorman (1986). The furnace uses an S.T. International orbital tube welding head and power supply to produce localized and extremely high temperatures. Several preliminary tests were conducted by Poorman on samples of Al, Cu and W using the configuration shown in Figure 1. We numerically characterized the processes and design parameters involved in the development of the Arc Furnace for use as a directional solidification furnace at temperatures exceeding those currently available, i.e. 1600^{o}C. This portion of the research was directed towards developing

scenarios for sample support, external furnace shielding, translation mechanisms, temperature limitations, and extensions of numerical characterizations to nonmetallic materials.

A numerical model developed for the Arc Furnace and described in following sections and was applied to a sample holder with physical properties of stainless steel, aluminum and copper. The goal of this numerical study was to estimate the performance of these holders under various isothermal external boundaries. The external boundary was held constant at temperatures consistent with air, water, and oil cooling (10, 38, 50, 100, 150 and 200^{o}C). Axial and radial profiles were determined for 75 mm long samples of tungsten held at each end by 25 mm long aluminum, copper, and stainless steel holders.

Objective 5.

Performance Verification of the Arc Furnace. The S.T. International weld head and power supply were received in September 1988, and after several repairs, was placed in service in February 1989. Tests were conducted on 3" stainless steel and aluminum tubing while using a specially designed water cooling system. The water cooling system keeps the weld head cool during high temperature operation associated with welding large diameter specimens at high currents. Details of this system are discussed in Section 3.5.

3.0 RESULTS AND DISCUSSION

This research supported a graduate student that prepared a thesis on the numerical modeling and experimental testing of the ARTCOR Model 460-15 Bench Top Tubular Laboratory Research Furnace. This thesis documents the work on this portion of the research and is attached as Appendix 1. The following sections directs the reader to the sections covering the specific research on each topic.

3.1 Objective 1. ARTCOR Furnace Assembly.

The ARTCOR zirconia furnace was received from NASA and required substantial assembly. A stand was constructed to support the furnace, optical pyrometer, and ventilator. This stand was designed to protect the furnace from vibrations and was fitted with clamps to hold accessories needed during the experiments. Detailed procedures are given in Chapter 3 of Appendix 1 under the topic commercial furnace. In addition, a research version was developed which was used to research the furnace and element performance. Information on the research version of the furnace is also provided in Chapter 3 of Appendix 1.

3.2 Objective 2. Zirconia Furnace Performance Verifications.

One requirement of this research was that the commercial zirconia furnace initially be evaluated in an as-received condition. No efforts were made to improve, modify, or alter in

any way its geometry, heat transfer characteristics, or control routines. It should be noted that free convection is used to cool the furnace casing. Also, since the furnace ends are open to the atmosphere, one recognizes that free convection and radiation losses will play major roles in the furnace's performance. Attempts to utilize this furnace for materials processing in a micro-gravity environment will require active cooling to correct this limitation.

A major problem with the commercial zirconia furnace was in the area of control. The furnace had no feed-back mechanism for thermal control or even a direct readout for furnace temperature. These problems were outlined in our semiannual and annual progress reports on this research. Basically the controller was found to be ineffective for controlling the furnace element, such that scientific temperature data could not be collected. No technique was available with this equipment to set or control the furnace to a desired operating temperature. In actual operations with this furnace, direct measurement of the temperature within the furnace and manual adjustment of the percentage power applied by the controller to the furnace are required get the furnace operating properly. Accurate temperature control is required to develop this type furnace for eventual directional solidification experiments.

The furnace support structure for the element did not produce dimensional stability that would facilitate consistent clearances around objects placed within the element. The dimensional limitation and measurement of the temperature

profiles were addressed in this research as part of the research furnace and reported in previous progress reports and reviewed in Chapter 3 of Appendix 1. In Appendix 1, some of the possible ways to correct the variations in element placement within the furnace are discussed. Some of these corrective techniques were incorporated in the research version discussed in the same chapter.

Element failure due to crack development were experienced with the commercial supplied elements. These problems were reported in previous progress reports and are reviewed in Appendix 1, Chapter 3. A research element was developed and cured in such a way that extended the life time of the element. Procedures used to prepare this element and measure the power consumed by the furnace and thermal distributions are discussed in Chapter 3, Appendix 1.

Detailed results on the above tasks can be found in our previous semiannual progress reports, the first annual report, and in Chapter 4, sections 4.2 of Appendix 1. The major results of this research show that the current configuration of the ARTCOR Model 460-15 Bench Top Tubular Laboratory Research Furnace lacks sufficient controls to provide scientific temperature data and dimensional stability to retail the element in a fixed location. Lack of element support on one end is an engineering problem that can be addressed with simple modifications as shown by using the research version prepared during this research.

The control problem is a larger problem that requires further research. The upgrade of the controller or the inclusion of a computer/controller combination that would permit feed-back control based on temperature measurements would greatly improve the research potential of this commercial furnace.

3.3 Objective 3. Zirconia Furnace Model Development.

In order to improve the performance of the furnace, an accurate model for the furnace has to be developed. Detailed models were developed for comparison with routine radiation heat transfer models which uses bulk radiation properties. A literature search was conducted on the spectral properties of furnace materials of construction namely alumina, zirconia,and titania. In addition, thermal properties of iron were also found and used in the numerical analysis. Radiation properties, which are functions of wavelength, were used to predict the radiation heat transfer of the crucible wall. At issue was the direct coupling of the sample to the furnace wall at specific frequencies for which the crucible wall is transparent. The 1-D and 2-D models take into account the absorption and conduction of the crucible wall to the iron sample.

Development of all aspects of this portion of the work along with a review of other measurement techniques are provided in Chapter 1, Chapter 2 (formulation of the one- and two-dimensional spectral radiation model) and Chapter 4 section 4.1, where the numerical results may be found.

The major finding of the numerical studies is that spectral radiation transfer plays a major role in zirconia type furnaces, and that with proper selection of the radial dimension of components used within the furnace, thermal gradients and their resulting losses can be minimized. Two papers, one on the one-dimensional model and its results and another on the two-dimensional model are in preparation. The one-dimensional model was submitted for review and returned for correction. It is currently in rewrite.

3.4 Objective 4. Arc Furnace Model Development.

A numerical model of the Arc Furnace was been developed to evaluate a conceptual design based on the work of Poorman. The studies were made using an idealized model with configuration shown in Figure 1, but with a sample rod only 20 mm long. Steady state idealized models of the Arc Furnace were numerically simulated using SINDA. This numerical model assumed symmetry; therefore, only half the configuration was modeled. Additionally, temperatures in the circumferential direction were assumed constant. The numerical model consisted of a 6.35 mm O.D. x 70 mm long sample of pure tungsten rod with 25 mm of rod inserted into each holder of 13 mm O.D. x 25 mm long stainless steel. This configuration provides only a 20 mm long tungsten sample rod. Since, symmetry was assumed, only 120 mm of the sample rod and one heat sink required numerical modeling. We limited our numerical analysis to a sample length of 70 mm, since this is our current experimental limit for preparing such a

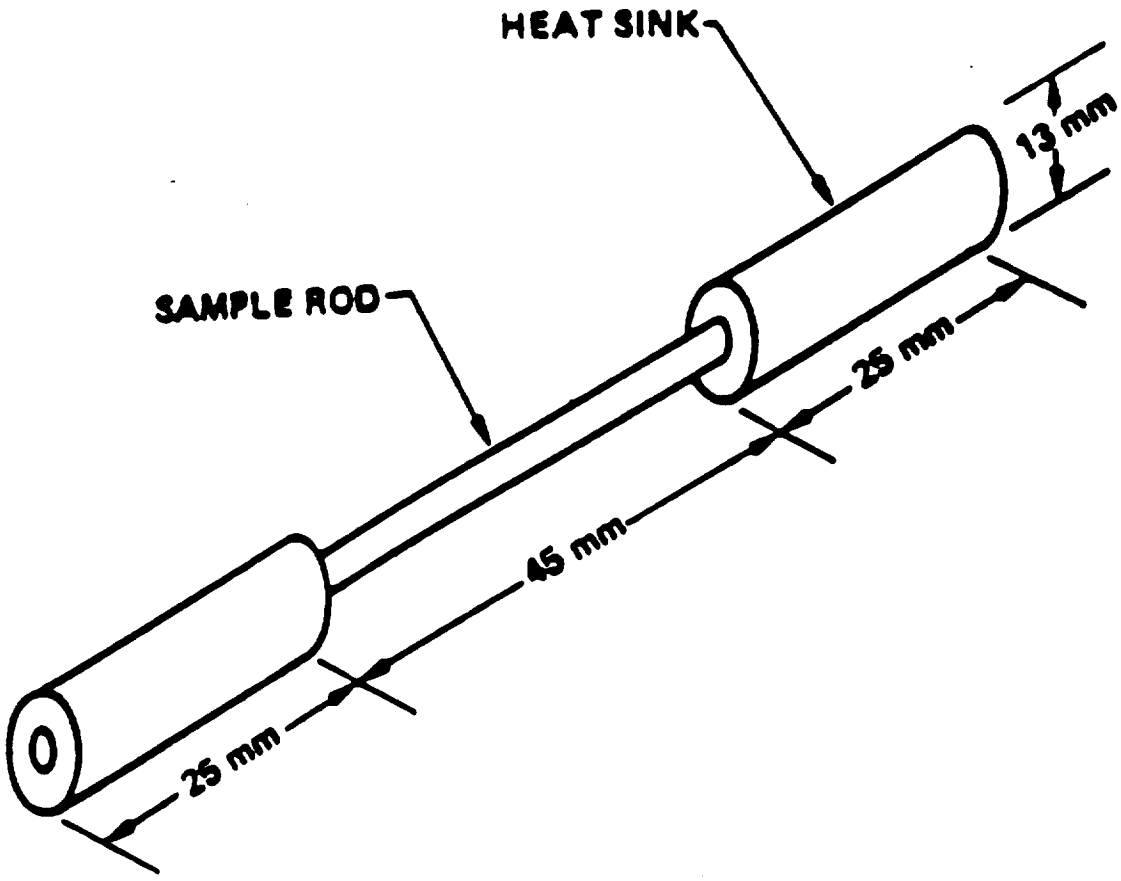

Figure 1. Arc Furnace sample and holder configuration as used by Poorman (1986).

sample by powdered metal sintering techniques. The numerical and experimental capabilities can easily be extended to a longer sample length.

The model developed included an isothermal boundary imposed at the end of the sample rod. The isothermal temperature was maintained at the melting point of pure tungsten (3387^{o}C). The isothermal surface of the stainless steel holder was set at the temperatures consistent with air, water and oil cooling (10-200^{o}C). Additionally, it was assumed that there was zero contact resistance between the tungsten sample rod and the stainless steel heat sink. An idealized radiation boundary was imposed on the exposed surface of the sample. This surface was radiation coupled to a constant 45^{o}C environment and was assumed to be a sufficient distance away from this environment to make the view factor equal 1. The emissivity of tungsten at 3315.5^{o}C, was assumed constant at 0.39 (Holman, 1981). To simplify the model, radiation exchange between the sample and sample holder was initially neglected.

The model was developed on a 1 mm grid spacing which required 222 nodes, with additional nodes for radiation to the environment. The steady state solutions took approximately 3 minutes of computer core time. The actual performance of the experimental furnace, processing a tungsten sample, should fall below this idealized case, due to the steady state assumption.

The power consumption as a function of the temperature of the quench block is shown in Figure 2. Power consumption ranges from 1.76 to 1.70 KW at a quench block temperature of 10 and

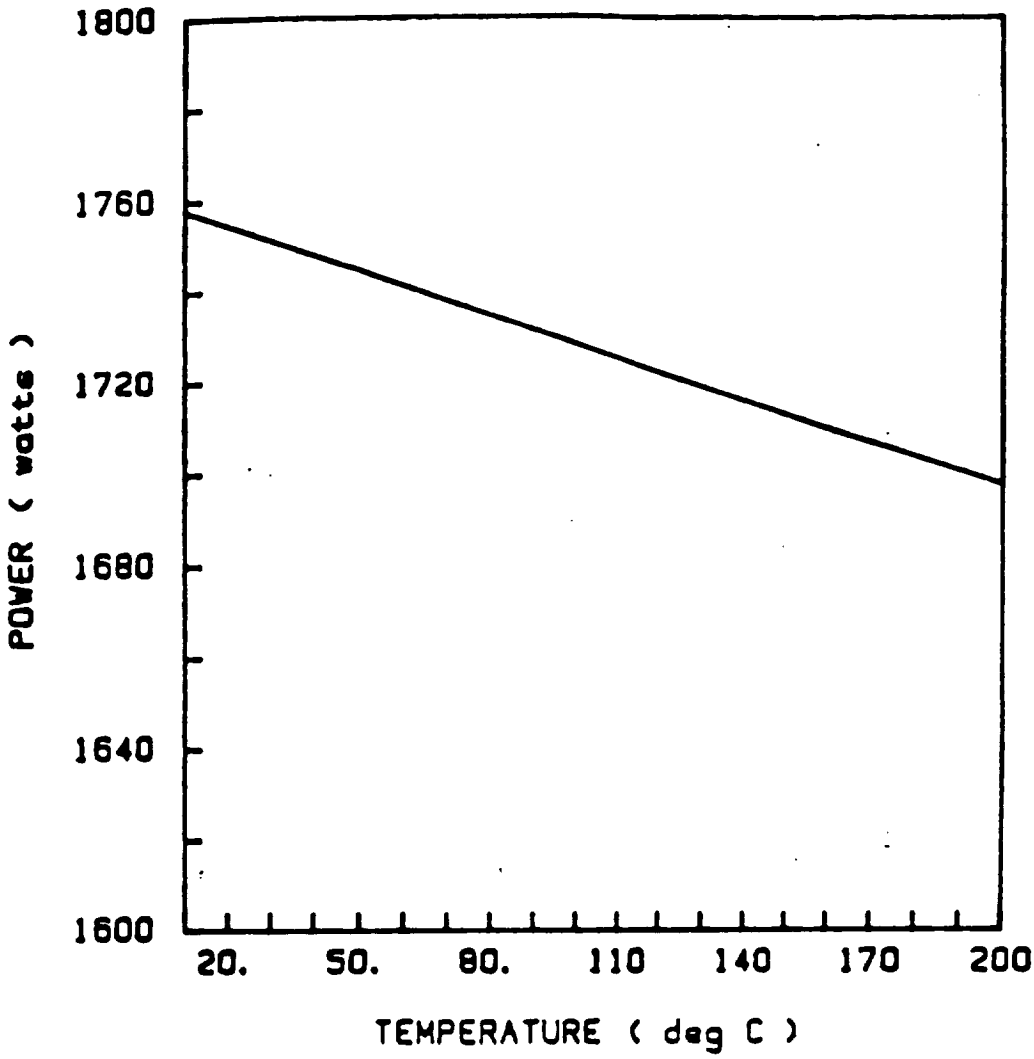

Figure 2. Steady-state power required for different quench block temperatures.

200°C, respectively. An increase in power of 0.32 watts is required for each degree centigrade when the quench block temperature is operated below 200°C. Values discussed here and in the figure are within the experimental range determined by Poorman (1986) for his 3.2 mm diameter tungsten sample. Centerline axial temperature profiles for tungsten samples calculated at various quench block temperatures are shown in Figure 3. An axial centerline gradient of 2650°C was calculated for the first 3mm of the sample. Figure 3 shows that this gradient is virtually constant for the first 2-3mm on either side of the arc location for the quench block temperatures imposed. The holder's isothermal boundary begins to influence the axial gradient in the sample at a distance of about 5 mm from the arc's location at 0 mm.

Several isotherms for the model were included in the contour plots shown in Figure 4. These temperature contours range from the quench block temperature to 3387°C and are plotted at their respective positions in the modeled portion of the sample. The calculations indicate that a relatively small, and extremely localized melt zone exists. In the first millimeter along the axial direction from the melt interface the temperature drops 187oC from the melting point of tungsten at 3387°C to 3200°C. Figures 4 a, b, c, and d show contour plots obtained for the Arc Furnace with isothermal boundaries of 50, 100, 150, and 200°C, respectively. In all four figures, the 500°C isotherm penetrates

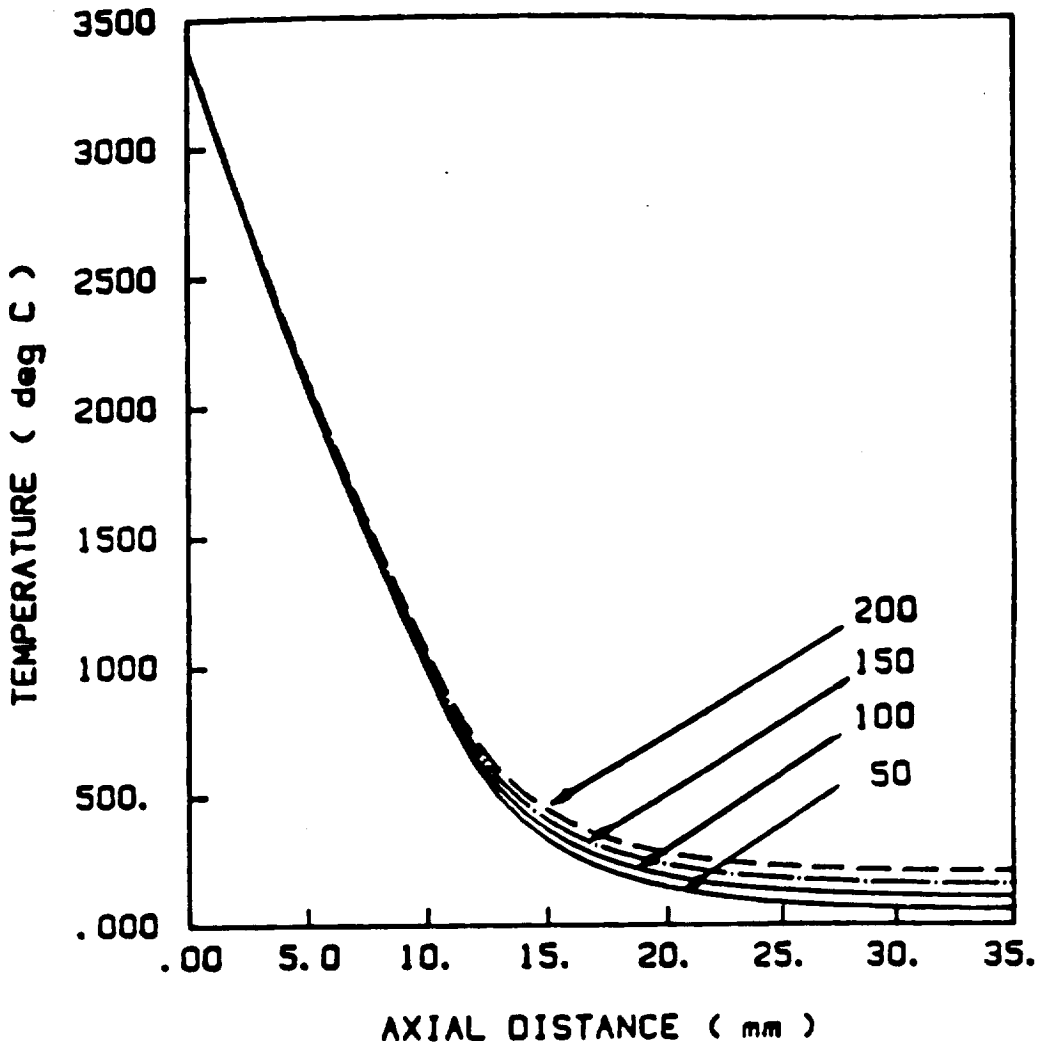

Figure 3. Centerline temperature profiles for different quench block temperatures for the tungsten/stainless steel holder model.

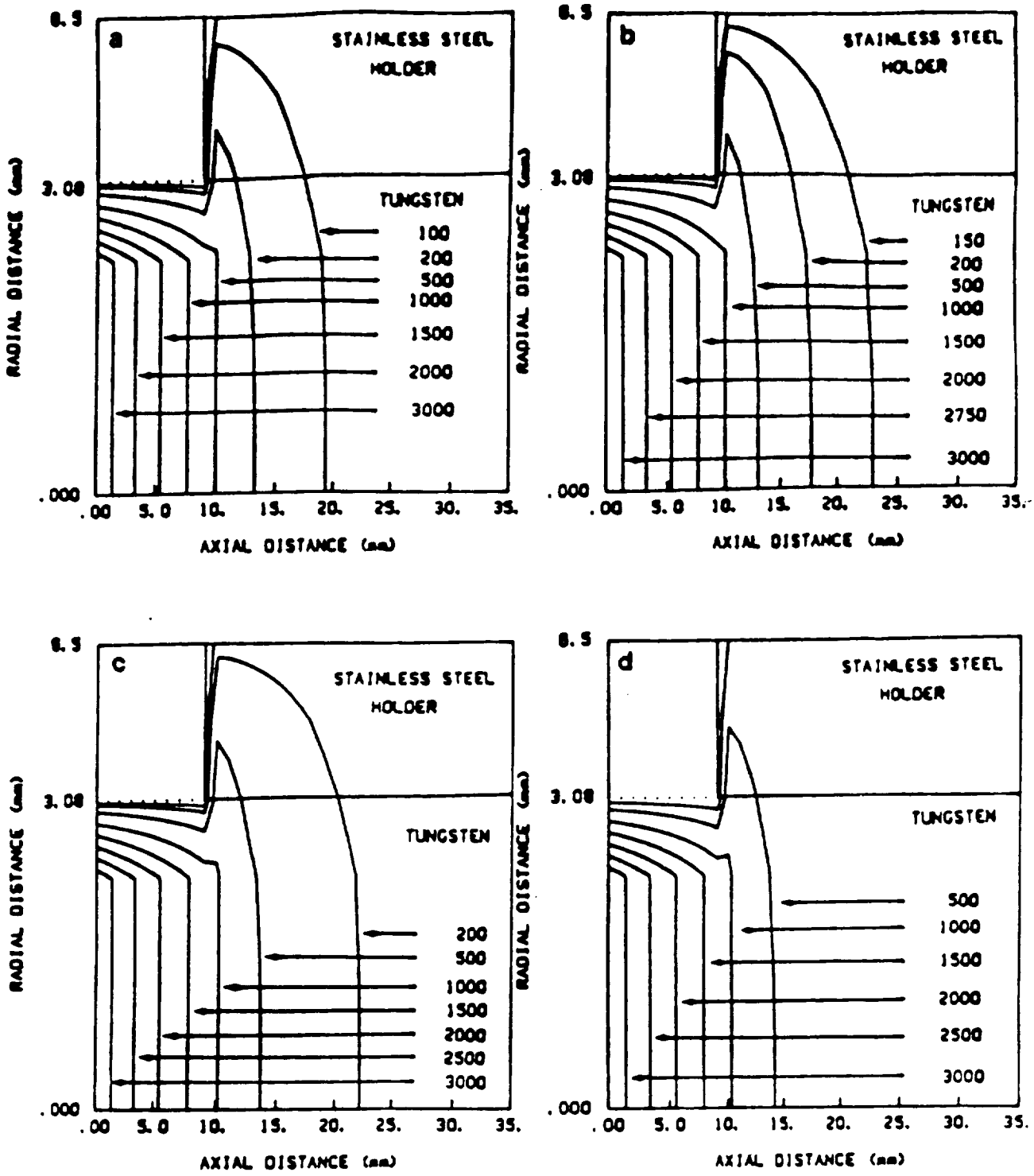

Figure 4. Contour plots obtained for the Arc Furnace with a tungsten sample and stainless steel holder. Boundary conditions on the external surface of the holder were controlled at a) 50°C, b) 100°C, c) 150°C, and d) 200°C.

well into the holder region. This temperature is approaching the melting point for aluminum holders. Even at temperatures as low as 10 and 38°C see Figures 5, this penetration is still apparent.

In all six figures one consistent trend can be seen. The isotherms in the samples from the center of the sample (0 mm in Figures 4 and 5) to about 10 mm are relatively constant no matter what cooling fluid temperature is used. This trend was also apparent in Figure 3. As previously discussed, the sample processing region are not greatly influenced by the quench block temperatures studied. Therefore, several different scenarios for cooling the Arc Furnace are possible, including forced air, water, or change of phase cooling approaches. As an example, one might choose to design a quench block and holder combination which would use the conversion of water to steam to remove heat and provide a constant reference temperature at the cooling block.

Radial profiles for these numerical calculations are shown in Figure 6 a, b, c, and d for the 50, 100, 150, and 200°C, respectively, and Figure 7 for the 10 and 38°C simulations. Again, these figures remain virtually unchanged in the region discussed above. In these figures, the zero line represents the centerline temperature, with the solid line representing the tungsten surface. The dashed line is the difference between the centerline profile and the profile at a radial distance of 2 mm, while the additional line is for the difference in the radial profile at 1 mm relative to the centerline. The largest

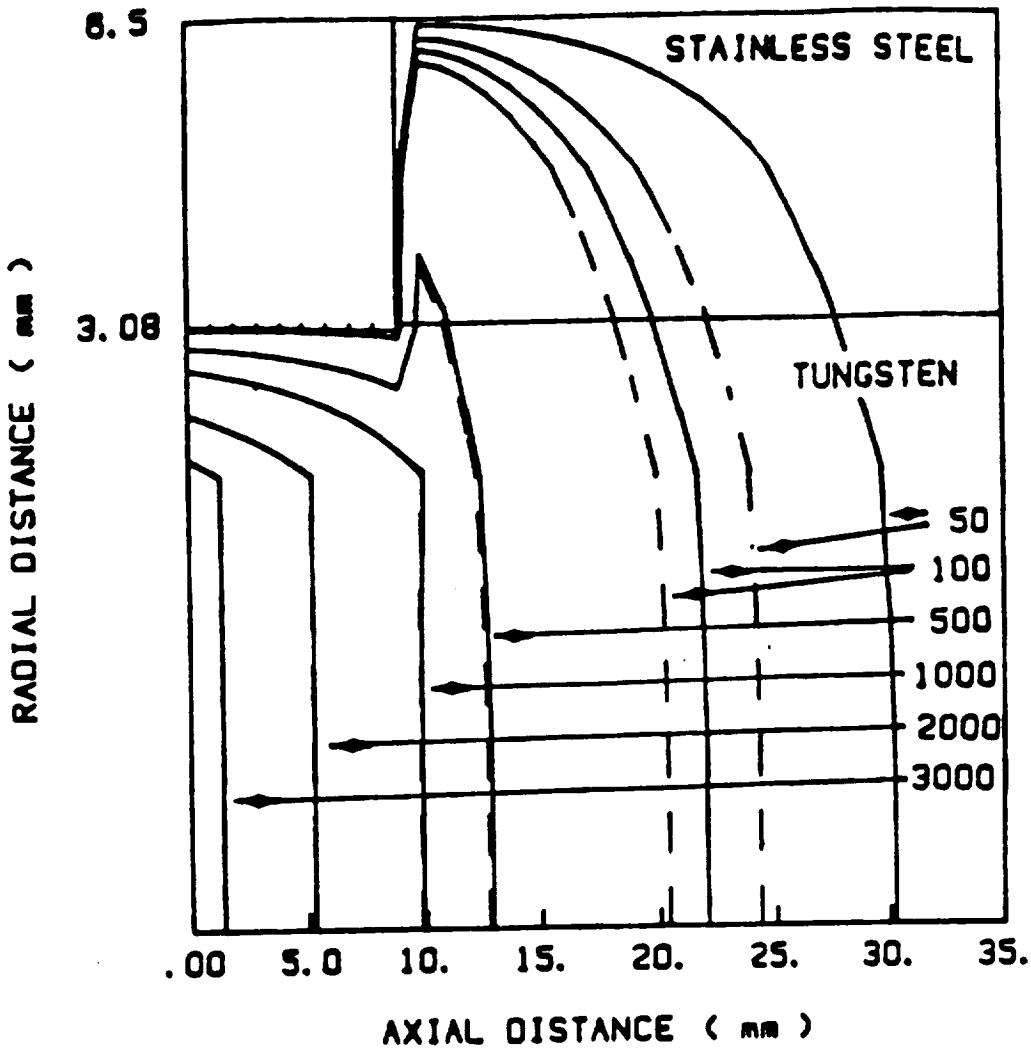

Figure 5. Contour plots obtained for the Arc Furnace with a tungsten sample and stainless steel holder. Boundary conditions on the external surface of the holder were controlled at 10°C (dashed line) and 38°C (solid line).

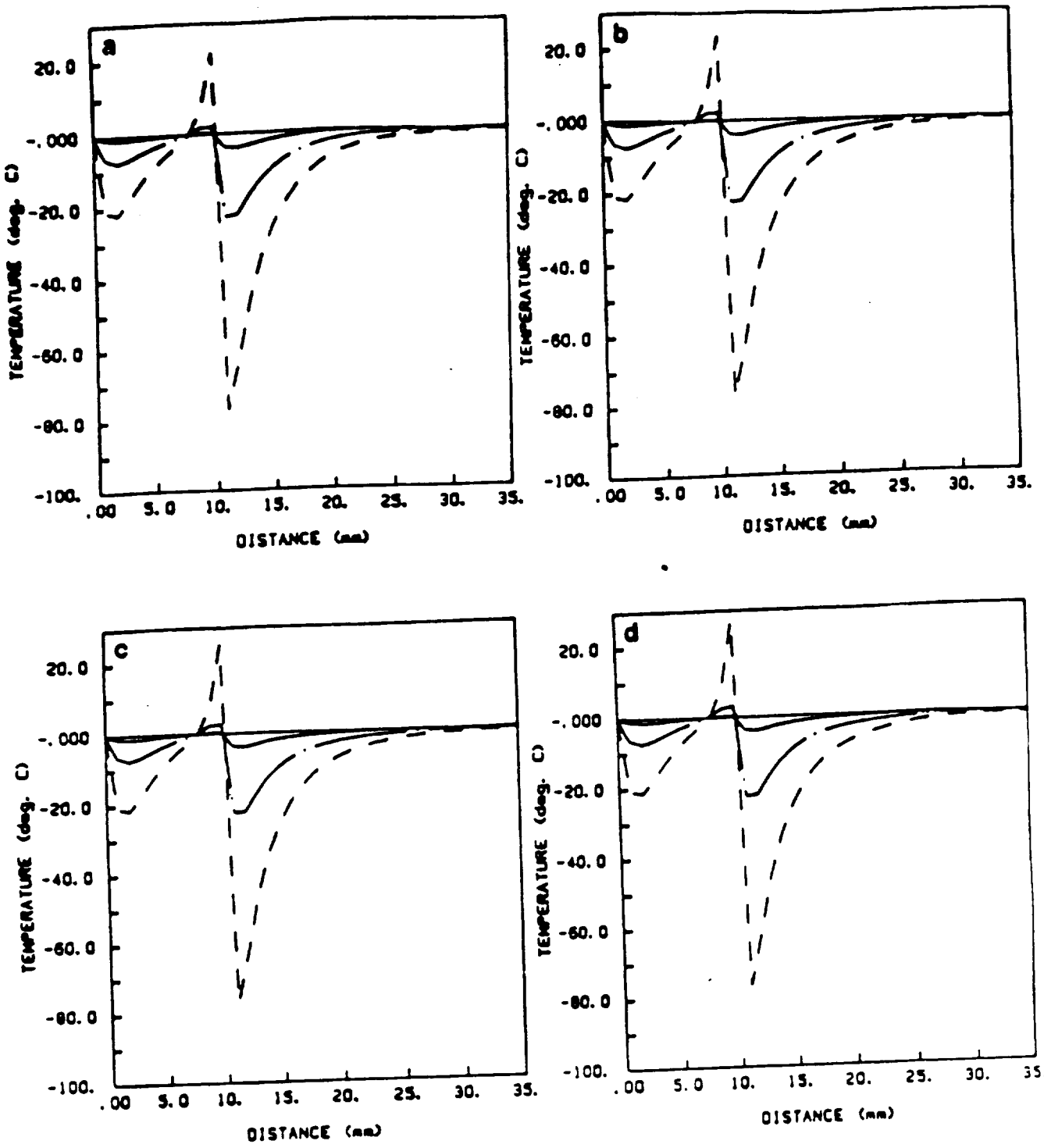

Figure 6. Radial temperature distributions relative to the centerline temperature for the Arc Furnace with a tungsten sample and stainless steel holder. Boundary conditions on the external surface of the holder were controlled at a) 50°C, b) 100°C, c) 150°C, and d) 200°C.

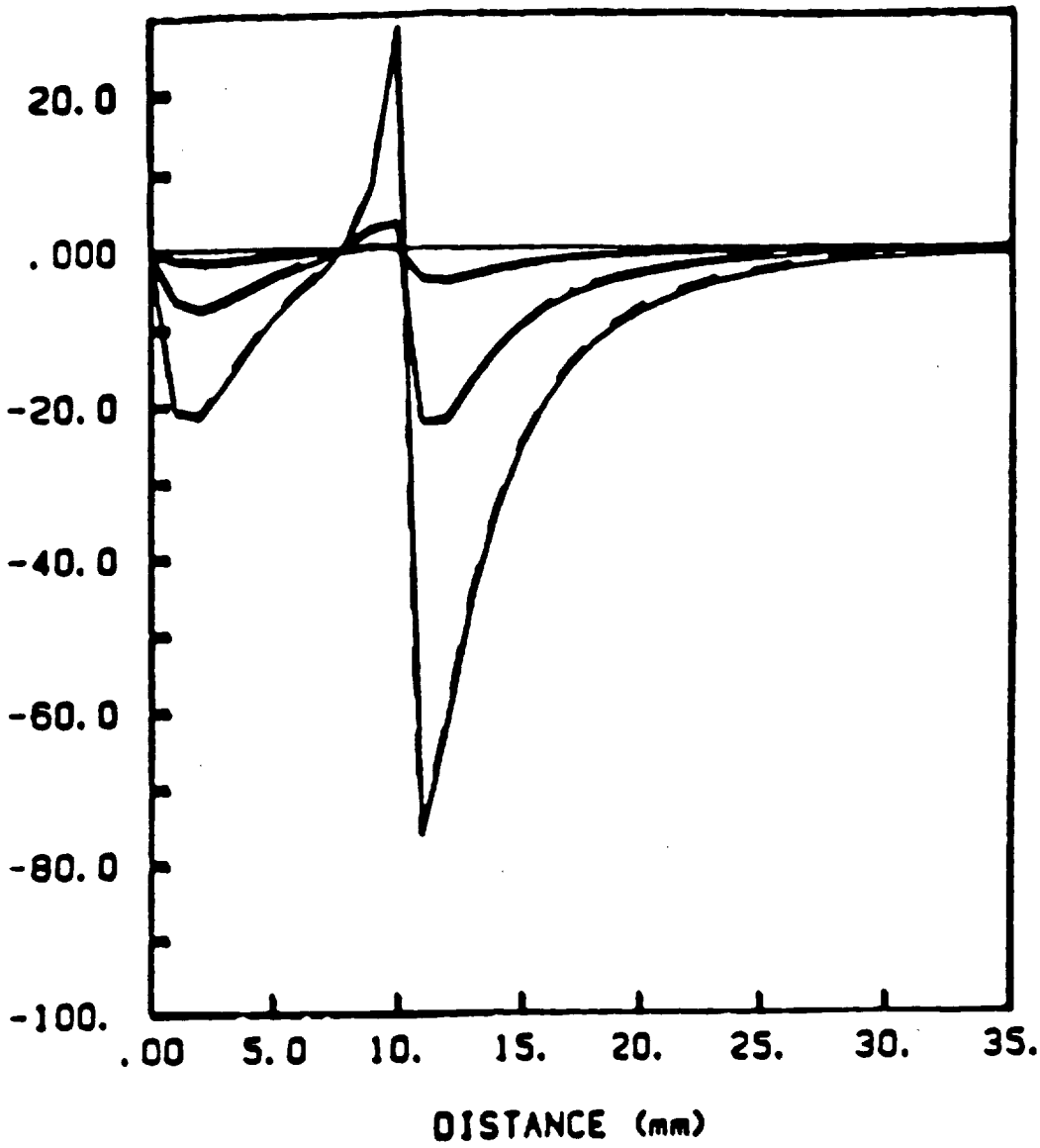

Figure 7. Radial temperature distributions relative to the centerline temperature for the Arc Furnace with a tungsten sample and stainless steel holder. Boundary conditions on the external surface of the holder were controlled at 10°C (dashed line) and 38°C (solid line).

deviation in the radical profile occurs on either side of the sample entrance into the stainless steel holder and quench region.

Figure 8, 9, and 10 and Figures 11, 12, and 13 show a similar plot to those discussed above but using water cooled aluminum and copper quench blocks/holders, respectively. Figures 8 and 11 show the axial center line profiles developed with the aluminum and copper holders. The maximum axial gradient calculated for these materials as holders was 349^{o}C/mm for the aluminum holder and 358^{o}C/mm for the copper holders. From an examination of the isotherms in Figures 9 and 12, both quench blocks will effectively cool the tungsten sample without melting the holder material. If one considers the influence of the cooling media in Figures 9 and 12, it becomes obvious that higher operating temperatures on the cooling media greatly improves the uniformity of the thermal gradients in the core of the sample. Figures 10 and 13 permit an analysis of the radial temperature profiles relative to the centerline temperature. This analysis shows that the aluminum holder will provide more uniform quench for directional solidification operations.

3.5 Objective 5. Arc Furnace Performance Verifications.

The fifth and final objective for research concerned the initial performance verification of the S. T. International Orbital Arc Welder. The arc welder power supply and 3" orbital head were purchased in September 1988. The 3" head was flight tested in November 1988. During this testing the "Home" switch

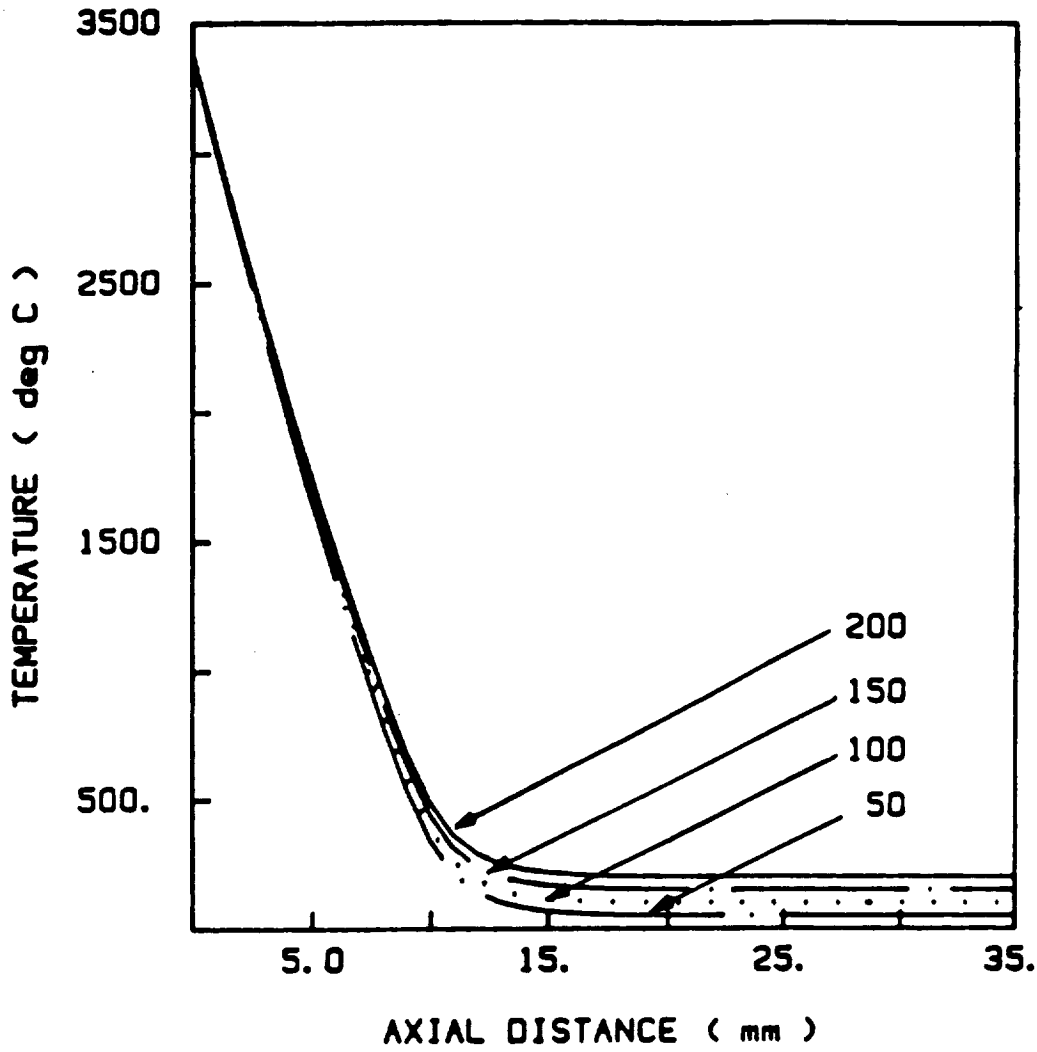

Figure 8. Centerline temperature profiles for different quench block temperatures for the tungsten\aluminum holder model.

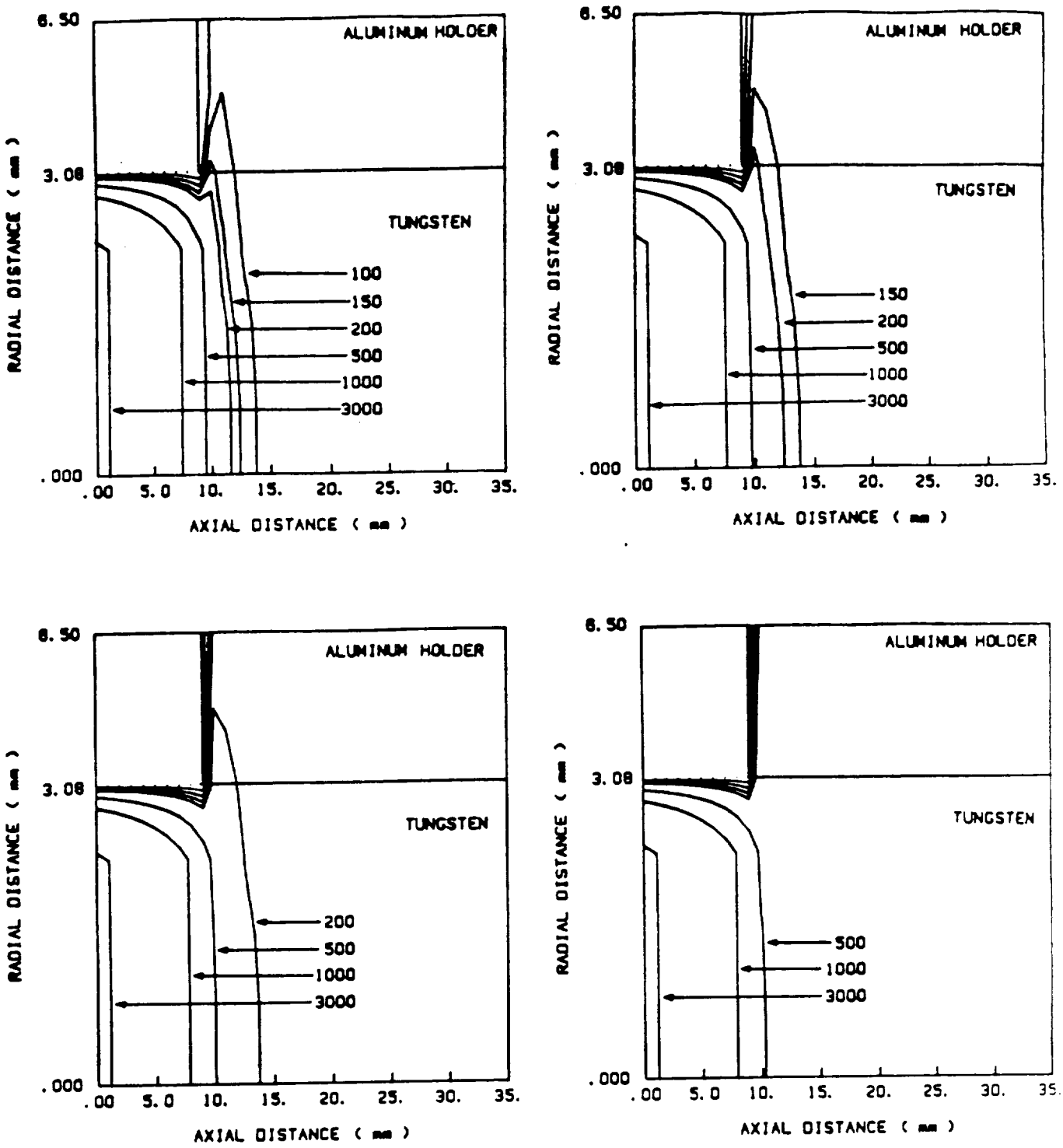

Figure 9. Contour plots obtained for the Arc Furnace with a tungsten sample and aluminum holder. Boundary conditions on the external surface of the holder were controlled at a) 50°C, b) 100°C, c) 150°C, and d) 200°C.

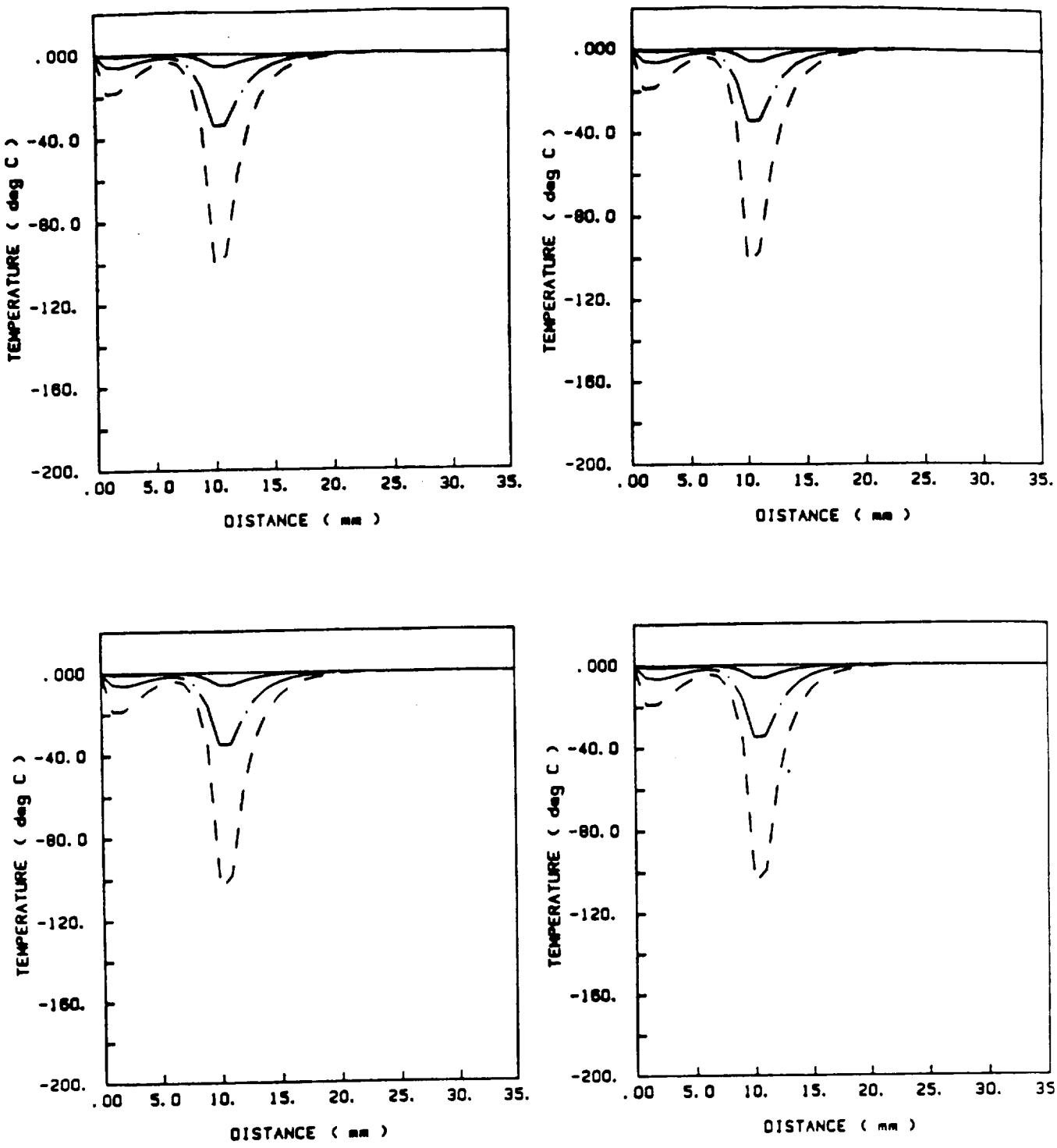

Figure 10. Radial temperature distributions relative to the centerline temperature for the Arc Furnace with a tungsten sample and aluminum holder. Boundary conditions on the external surface of the holder were controlled at a) 50°C, b) 100°C, c) 150°C, and d) 200°C.

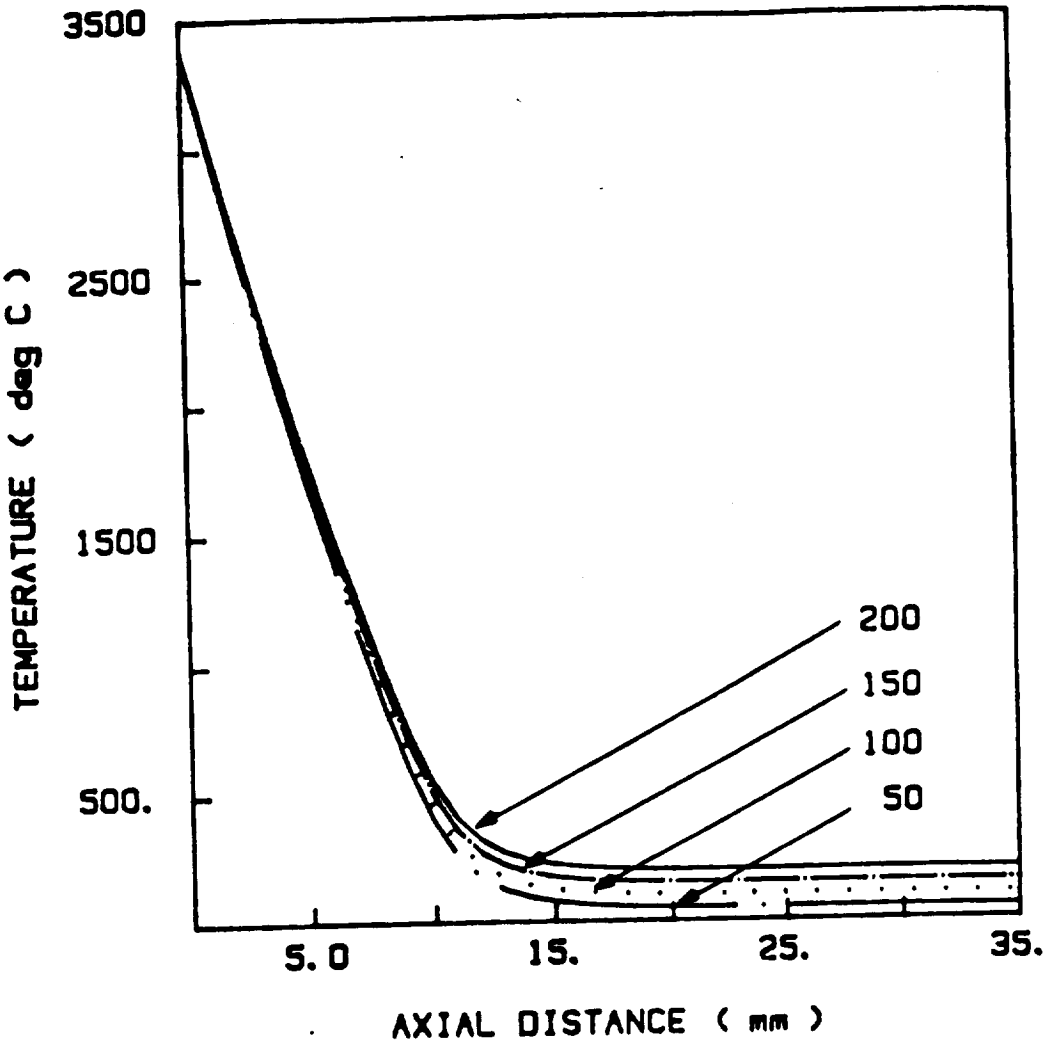

Figure 11. Centerline temperature profiles for different quench block temperatures for the tungsten\copper holder model.

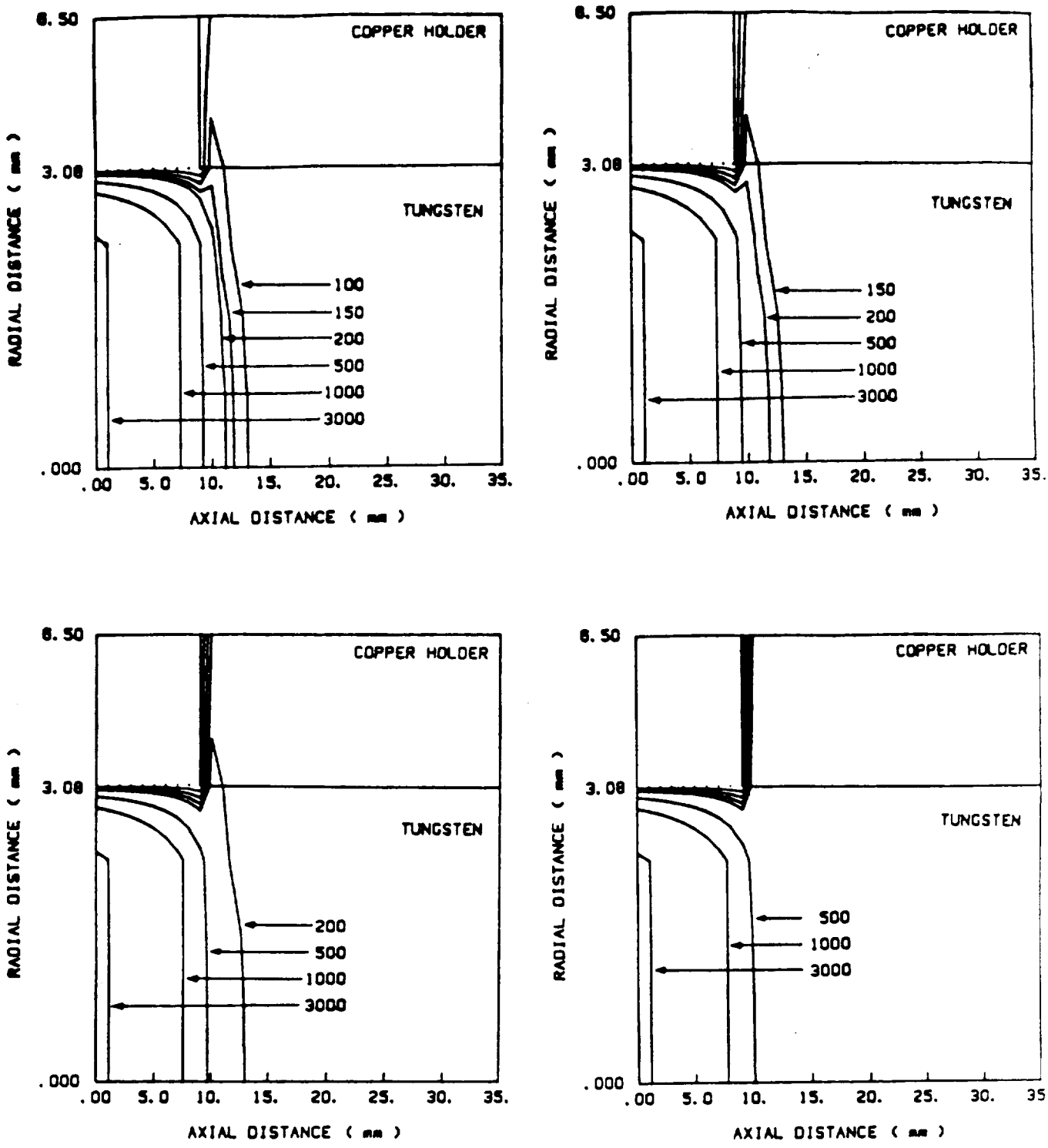

Figure 12. Contour plots obtained for the Arc Furnace with a tungsten sample and copper holder. Boundary conditions on the external surface of the holder were controlled at a) 50°C, b) 100°C, c) 150°C, and d) 200°C.

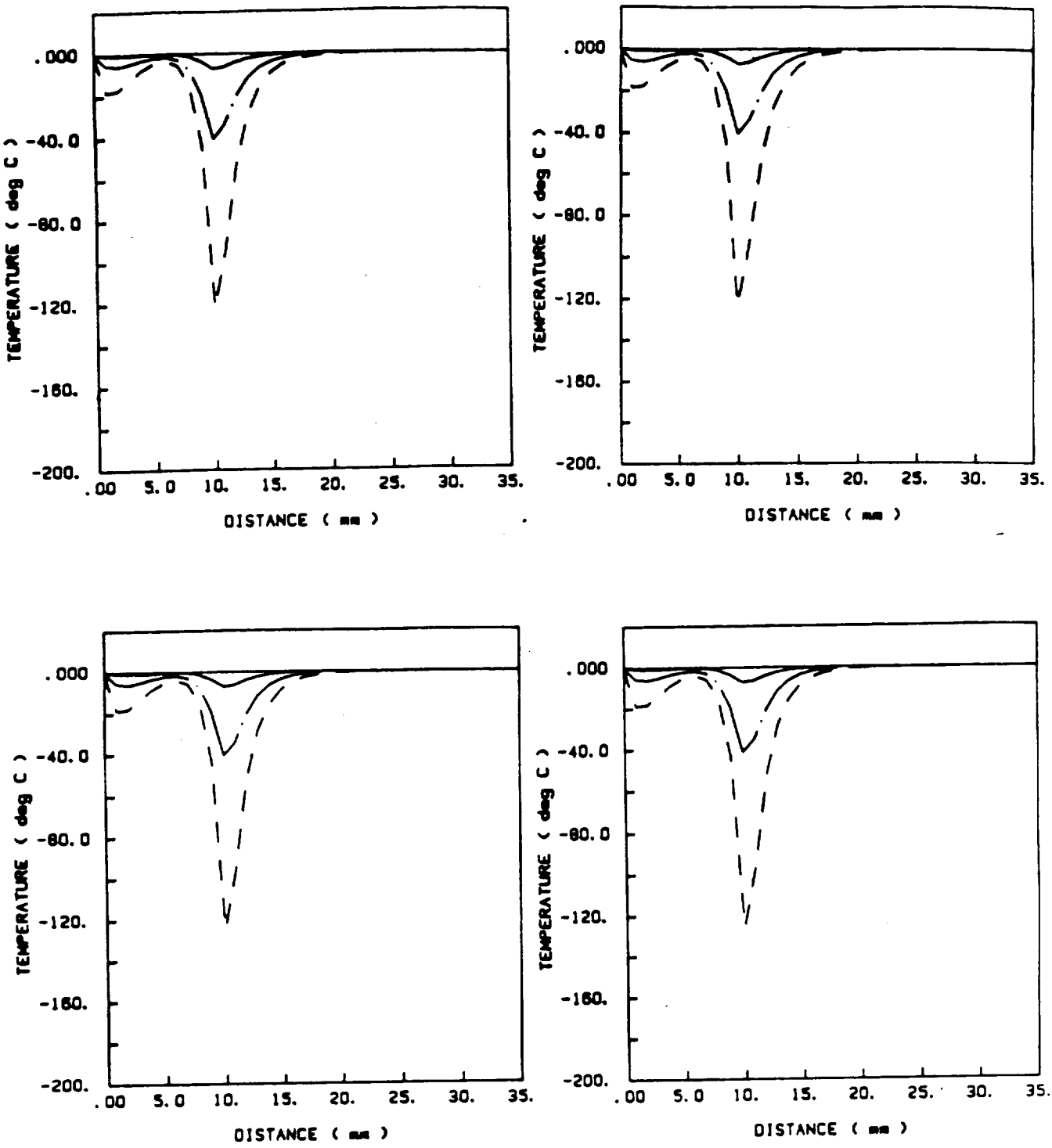

Figure 13. Radial temperature distributions relative to the centerline temperature for the Arc Furnace with a tungsten sample and copper holder. Boundary conditions on the external surface of the holder were controlled at a) 50°C, b) 100°C, c) 150°C, and d) 200°C.

in the head was found to be defective. The head was returned to the manufacturer for repair in December 1988. The manufacturer returned the 3" weld head in January 1989 where it was mated with the power supply for testing in the laboratory. These tests indicated that the power supply was not functional and it was also returned to the manufacturer for repair. The repaired unit was received in February 1989 and tests were performed to verify its performance. The unit passed all tests, welding 3" diameter stainless steel and aluminum tubing.

During the flight test of the 3" weld head, it was noticed that the temperature of the weld head body greatly exceeded past measurements with 1" weld head. Since the 3" head was ordered with a water-cooled feature, it was decided that a system was needed to control the head temperature during flight. The system had to be light, portable, and dependable. Such a system was designed as follows. The basic components needed to cool the head included; two Amtrol holding tanks, a Love Model 690-1 controller, a Hoke 115 volt AC solenoid valve, and associated fittings and tubing. The Amtrol holding tanks were selected because they contain bladders which can be pressurized for operation in microgravity. The cooling water is held in the upstream supply tank which is fitted with the solenoid valve and pressurized to 75 psia. Hot water is collected in a second tank which has its valve stem removed so that its bladder operates against a constant back pressure (15 psia). In operation the controller measures the weld head temperature using a type K thermocouple and compares it to the set point temperature. If the

temperature is higher than the set point, the solenoid valve is opened allowing pressurized water to pass through the head and into the collection tank. The unit was tested in February 1989 and performed as expected.

Additional research was directed at estimating the translation rate of the S. T. International Arc Furnace, the design of refractory lined collet for improved heat transfer, and development of a cooling system to handle the additional heating loads generated by the lined collet. Work on the ST International Arc furnace included the modification of an existing translation mechanism that allowed directional melting/solidification of two different samples. Samples of aluminum rod and thin walled stainless steel tubing were melted and/or heated while translating at various rates to investigate the translation speed and power required that would give consistent melting zones within the samples. In addition a keyboard, color monitor, and color video card were installed in the welder power supply to permit easy access to the weld parameters.

To evaluate the potential for the S. T. International weldhead to function in a directional solidification mode we performed the following experiments. The weldhead was installed on an existing jackscrew driven platform designed to move horizontally. The weldhead was translated using a variable speed DC drive motor connected to the fine thread jacking screw. Samples of either 1/2" O.D. aluminum rods or 1/2" O.D. with 1/16" wall stainless steel tubing were supported on both ends using an

aluminum support stand. The stand was connected to the positive terminal of the weldhead. Two inch O.D. aluminum collet lined with lava stone of 5/8" I.D were manufactured and served to both insulate the sample and contain the argon atmosphere needed during arcing operations. An existing color video card was exchanged for the monochrome video card used in the IBM-XT which is inside of the S.T. International power supply. A Zenith keyboard and color monitor were connected to the unit. Addition of these components, permitted more ready access of welding routines provided with the unit.

Preliminary tests were performed on stainless steel tubes at current levels ranging from 50 to 90 amps and translation rates of 0.1 to about 5 inch/min. At the highest translation rates and maximum power, the sample did not melt uniformly with the melted zone resembling a spiral. The best results were obtained for translation rates at or below 1 inch/min.

Tests were also performed on 1/2" O.D. solid aluminum rods at conditions similar to those previously discussed. The aluminum rod, having a greater thermal conductivity and heat capacity, required maximum currents and much slower translation rates than did the stainless steel samples. At a translation rate of 0.25 inch/min and a current of 90 amps the weld pool only extended half way into the sample. Since the sample was not preheated, this result suggests that aluminum and, perhaps, large rod samples in general, will require preheating prior to the arc melting.

4.0 CONCLUSIONS AND RECOMMENDATIONS

The major results of this research show that the current configuration of the ARTCOR Model 460-15 Bench Top Tubular Laboratory Research Furnace lack sufficient thermal controls to provide scientific temperature data and lacks dimensional stability to retail the zirconia element in a fixed location. Lack of element support on one end is an engineering problems that can be addressed with simple modifications of there design as shown by using the research version prepared during this research.

The controls problem is a larger problem that requires further research. The upgrade of the controller or the inclusion of a computer/controller combination that would permit feed-back control based on temperature measurements from either thermocouples or an optic pyrometer, and would greatly improve the research potential of the ARTCOR Model 460-15 zirconia furnace research for use with directional solidification in both unit gravity and eventually microgravity environment.

Control techniques should include a direct temperature feed-back technique. Analysis or calibration using a constant emmisivity optical pyrometer may not predict the processing temperature to within limitations placed on directional solidification standards. This conclusion is based on the spectral radiation models developed for a similar geometry. A possible control technique that uses an optical pyrometer incorporating spectral radiation within a numerical model to adjust the applied power may be possible based on the numerical

results. It is apparent from this work that solving the temperature measurement and controls problem is the key to advancing this furnace toward directional solidification operations.

Element failure was evidenced with the two elements purchased from the manufacturer. Though the manufacturer claims that the elements have long life our research did not support this claim. This is not to say that all zirconia elements will last a short time, it is possible that we received two elements from a bad batch, since an experimental element prepared by us without input from ARTCOR has operated successfully for over 37 hour without failure, even after ramped through a thermal gradient of over 45^{o}C/min from 900-1600^{o}C. Research with this element shows that the basic concepts of using a zirconia ceramic tube as a heating source are sound and deserving of further study for directional solidification operation under an air atmosphere.

Both furnace technologies show great potential to advance directional solidification to higher operating temperature. The Arc Furnace concept should be developed. The Zirconia Furnace needs to be further researched to correct the problem found during this research, before development.

5.0 REFERENCES

J. P. Holman, Heat Transfer, McGraw Hill, New York, N. Y., (1981).

R. M. Poorman, "Rapid Melt/Quench Furnace Using Commercially Available Hardware," NASA Technical Memorandum, George C. Marshall SpaceFlight Center, Marshall Space Flight Center, Al, March 1986.

6.0 **APPENDIX 1.** Experimental and Numerical Considerations in the Design of an Extreme Temperature Materials Processing Furnace.

EXPERIMENTAL AND NUMERICAL CONSIDERATIONS IN THE DESIGN OF AN EXTREME TEMPERATURE MATERIALS PROCESSING FURNACE

by

NASSOR A. SHABIBY

A THESIS

Submitted in partial fulfillment of the requirements
for the degree of
MASTER OF SCIENCE IN ENGINEERING
in
The Department of Chemical Engineering
of
The School of Graduate Studies
of
The University of Alabama in Huntsville

April 1991

FORM 8

THE UNIVERSITY OF ALABAMA IN HUNTSVILLE

School of Graduate Studies

THESIS/DISSERTATION APPROVAL FORM

(To be submitted by the student to the School of Graduate Studies with thesis copy [before reproduction], and with all signatures obtained.)

Name of Candidate Nassor A. Shabiby

Department: Chemical Engineering

Major Subject Materials Engineering

Degree Master of Science in Engineering

Title of Thesis/Dissertation: Experimental and Numerical Considerations in the Design of an Extreme Temperature Materials Processing Furnace.

Approved by:

Thesis/Dissertation Committee:

Chairman	4-29-91 Date		Date
	4-24-91 Date		Date
	4-24-91 Date		Date
Department Chairman	4-29-91 Date		
College Dean	4/29/91 Date	Dean, School of Graduate Studies	4/29/91 Date

ACKNOWLEDGMENTS

I wish to thank my advisor, Dr. James E. Smith, Jr., for his unwavering support and thoughtful advice during the period this research was being conducted. Without his sincere commitment, this thesis would not have been possible.

I would also like to thank my advisory committee members, Dr. C. P. Chen and Dr. T.J. Chung, for their patience and assistance during the preparation of this thesis.

Thanks and appreciation to the past and present members of our research group for their kindness, friendship and encouragement. I wish to particularly thank Steven Noojin, Dr. Kathleen Leonard, Scott Johnson, and Thomas Bond for the cooperation they extended to me as part of the research group. I wish to thank John G. Vandegrift for his help with the figures and overhead viewgraphs. I also wish to thank all the rest of the members in the present research group; John Cashon, Terri Morris, John Kress, and David Swafford.

Most importantly, I would like to express my gratitude to my entire family at home for their sacrifice and prayers during the period that I had been away from them.

Support from NASA and the University of Alabama in Huntsville, is gratefully acknowledged. Any opinions, findings, conclusions, or recommendations expressed in this thesis are those of the author and do not necessarily reflect the views of either NASA or the University of Alabama in Huntsville.

ABSTRACT

This study focuses on experimental and numerical considerations that are required in the design of high temperatures materials processing furnaces using zirconia heating elements.

The experimental study was performed using a commercial zirconia tubular research furnace. This furnace was evaluated and its application in microgravity experiments assessed. Based on this furnace a number of design improvements and modifications were suggested. A new zirconia heating element was designed, based on oxygen sensor technology and the results from numerical studies that were performed in this study. Improvements to the furnace were made and together with the newly designed elements received further study.

One and two dimensional conduction/radiation models for an alumina crucible in a zirconia heater/muffle tube enclosing a liquid iron sample were solved numerically. Variations in the crucible wall thickness were numerically examined. The results showed that the temperature profiles within the liquid iron sample were significantly affected by the crucible wall thicknesses.

Experimental and numerical studies were accomplished in parallel so that integration of these studies could produce a workable model for the furnace while extending the capabilities and understanding of the zirconia heating elements.

TABLE OF CONTENTS

LIST OF FIGURES

page

LIST OF SYMBOLS

$B_{n\lambda}$	radiosity defined in equation (2.14)
E_n	exponential integral function defined in equation (2.9)
$e_{b\lambda}$	Planck's function
I_λ	time rate of radiant energy per unit solid angle and per unit area normal to the radiant rays
k	thermal conductivity
n	refractive index
Q_R	radiation heat flux
q_λ	radiative flux (eqn. 2.30)
T	temperature (K)
ϵ	emissivity
τ	dimensionless distance in the radial direction (r/R)
θ	dimensionless temperature (T/T_{ref})
κ	absorptivity
μ	$\cos\theta$
σ_s	Stefan Boltzmann constant
η	dimensionless distance in the z direction (z/z_0)
Φ_i	radiation potential

Subscripts and Superscripts

+,-	positive and negative directions respectively
1,2	indicate directions
b	blackbody
opq	opaque case
R	radiation
λ	monochromatic property

CHAPTER 1

INTRODUCTION

This study focused on the development and design of a high temperature zirconia furnace. A zirconia tube was used as the main heating element. Normally zirconia is an insulator, but when heated to temperatures above 1000K it becomes conductive and thus can be used as a heating element in such furnaces. The thesis included experimental and numerical studies that were performed to understand the heat transfer interactions of the furnace. The study is limited to high temperature furnaces that used a zirconia ceramic heating element.

The furnace development was influenced by work presented in the literature and the numerical work performed in this study. Numerical modeling of a crucible wall enclosing a liquid iron sample with radiation/conduction were performed to study the various modes of heat transfer. The numerical work was performed to study parameters that could affect furnace performance. Among the factors needed to be studied in the design of an efficient furnace system were crucible wall thicknesses and the transparency of the ceramics used in the construction of the furnace.

In the design of high temperature materials processing furnaces, temperatures in the range of 1873K to 2273K (1600°C - 2000°C) are anticipated in the hot zones. At these high temperatures, ceramics used in the construction of critical furnace components, i.e. muffle tubes and crucibles, enter regions in which spectral radiation effects cannot be ignored if adequate control of the furnace is to be achieved by open

loop control techniques.

Models used in the open loop control must predict temperatures in the samples based on measurements made either at the furnace wall or exterior crucible surfaces, using either direct measurements or optical pyrometry. When spectral radiation properties as functions of wavelengths are considered, the wall assumes a diffuse boundary in which some radiative frequencies see an opaque surface at some frequencies and a semitransparent surface at other frequencies.

The scope of this thesis included a review of previous literature on furnace design and development, techniques that are available for the measurements of temperatures in semitransparent media, and the numerical techniques used in solving combined modes of heat transfer. To facilitate the understanding of combined modes of heat transfer and the numerical modeling of such processes, a review of the literature is given is section 1.1.

The experimental investigations that were performed in previous years and a review of the methods used to measure temperatures in semitransparent materials is given in section 1.3. The transparency of ceramics at high temperatures was a major consideration in the design of this furnace, therefore the absorption spectra of solids in general will be discussed in section 1.2.

1.1 ANALYSIS OF COMBINED MODES OF HEAT TRANSFER

This thesis focuses on how numerical studies could be used in conjunction with experimental work to calculate the temperature profiles that would closely resemble real experimental conditions. The formulation of the radiation/conduction models in this thesis will take into account the radiative properties as functions of wavelengths and

temperature. This should closely resemble the actual heat transfer processes within the alumina crucible and sample.

Energy transfer in solids is normally treated as if conduction were the only means of transport. This is an erroneous assumption when the temperatures are such that thermal radiation is significant and the material is partially or completely transparent to this radiation. Neglecting spectral radiative heat transfer can lead to incorrect conclusions and design failure.

Presently, our understanding of coupled conduction-radiation is based upon analysis with emphasis on gases rather than solids (Edwards and Matovosian, 1984). Unlike gases, where the conductive flux is small and may be justifiably neglected, conduction is always present in a solid. Additional phenomena which are not present in gaseous radiative transfer must also be considered. According to Kirchoff's laws, the emission of radiation is proportional to the square of the refractive index. Hence, emission plays a greater role in high index solids than gases whose index is approximately unity. There are significant differences between gaseous and solid spectral absorption coefficients. In contrast to gases whose absorption spectra are established by quantum and statistical mechanics, some of the absorption mechanisms of the solid state remain to be identified and one must of necessity turn to experimental data (Armaly and El-Baz, 1977).

Little experimental or analytical work directly applicable to solids at these extreme conditions has been reported. Difficulties with controlling the experimental conditions and accurate measurement of temperature at the required levels have curtailed experimental studies. For simplicity, analysis is commonly based on unrealistic property

models and typically concentrated on the radiation dominant situation. Simplified procedures for real materials such as those developed for the gray model (Olfe, 1968) are required so that the significance of the radiative transfer may be assessed.

There have been many previous studies in combined modes of heat transfer. Viskanta and Grosh (1962) solved a one-dimensional simultaneous conduction and radiation problem by reducing a non-linear integro-differential equation to a nonlinear integral equation. They then solved the integral equation iteratively and compared their results with Rosseland and Milne-Eddington approximate solutions. Anderson and others (1973) further investigated the heat transfer through a plane layer of a semitransparent solid experimentally and compared the results with the approximate techniques. Using a method similar to Viskanta and Grosh, Eryou and Glicksman (1958) compared the results with their experimentally measured one-dimensional temperature profiles and heat fluxes within a slab of molten glass. They reported agreements of measured values of within 5 K throughout the slab. Grief (1964) studied a one-dimensional energy transfer problem of an emitting, absorbing, and conducting gas. He considered the thermal conductivity and absorption coefficient as having power law dependence on temperature.

The calculation of radiative transfer in a cylindrical nonisothermal emitting-absorbing medium has attracted considerable attention in recent years, because of its important applications in many high temperature phenomena associated with planetary reentry, nuclear explosion, and industrial furnace designs (Kellet 1952, Kingrey,1976). The emerging field of materials processing and crystal growth will pose challenging problems in the area of combined heat transfer in

semitransparent materials. Various limits in radiation heat transfer problems have been investigated, depending on whether the dominant mode of transfer was conduction or radiation (Wang and Tien 1967).

Modest and Azad (1981) evaluated the radiative heat flux in an absorbing, emitting and linear-anisotropically scattering cylindrical media. Their study was limited to linear-anisotropy for two reasons. First, exact analytical solutions (Lick, 1965) are practically impossible to obtain for higher-order scattering phase functions. This is due to the fact that the azimuthal direction cannot be eliminated by integration as in the planar case, resulting in higher order integral equations in the radial and local direction coordinates. Secondly, the accuracy of a linear-anisotropic approximation to realistic scattering phase functions in the heat transfer applications without collimated irradiation had been already established.

The difficulty in exact calculation of multidimensional radiative transfer has prompted researchers to develop approximate schemes such as the mean-beam length method (Siegel and Howell, 1980), the zoning method, the differential approximation, and the Monte Carlo method (Steward and Cannon, 1971).

Chang and Smith (1970) analyzed the heat transfer in a conducting, emitting and absorbing medium bounded by two infinite coaxial cylindrical surfaces, for both transient and steady states. They formulated the problem in two differential equations (one for the radiation potential and the other for the temperature) using quasi-steady simplification and Eddington's first approximation for radiative transfer. They found that for highly emissive surfaces, the interaction of radiation with conduction has a negligible effect on the

total heat flux. Ho and Ozisik (1988) used the Galerkin method to obtain an exact solution to the radiation part of the problem, and a finite difference scheme to solve the conduction part. They solved a steady state conduction and radiation heat transfer for an absorbing, emitting and isotropically scattering two dimensional rectangular enclosure. They examined the effects of the conduction-to-radiation parameter, the single scattering albedo, and the aspect ratio on the temperature distribution. They considered the boundary surfaces to be black and subjected to a constant temperature on one surface and zero temperature on others.

A modified finite difference approach to the problem of transient combined conduction and radiation in an absorbing and emitting annular medium was presented by Gordaninejad and Francis (1984). They studied two different boundary conditions; the first one was a step change in temperature on both inner and outer surfaces, while the second type of boundary condition was a step flux in the inner surface. The solution was shown to closely represent the exact solution for the case of pure conduction. Fernandes and Francis (1982) solved a transient combined conduction and radiation in a gray absorbing, emitting, and scattering medium of cylindrical geometry, using the Galerkin finite element method. The results were compared with exact solutions for the extreme cases, i.e., pure conduction and radiative equilibrium.

Some experimental investigations and methods that can be used in such studies are reviewed in the section 1.3.

In the following section, a detailed description of the absorption spectra for solids, including some ceramics, will be discussed.

1.2 ABSORPTION SPECTRA OF SOLIDS

In order to understand the semitransparent nature of solids, the nature of the absorption spectra of solids with respect to spectral radiation at high temperatures needs to be analyzed.

Radiative transfer analysis requires the spectral absorption coefficient which may be obtained from either theoretical models or experimental data. For gases the absorption spectra are well known and have been reduced to workable models for energy transfer processes (Edwards, 1984). Such is not the case for the liquid and solid phases where the energy levels are largely determined by the intermolecular binding and proximity of molecules. Since these two factors are determined by the composition and molecular arrangement as well as a number of other factors, the absorption spectrum can no longer be obtained from the structure of an isolated molecule and its collisions with others. Rather, the entire molecular structure, which may take a variety of forms, must be considered to accurately predict the spectral absorption coefficient of a solid or liquid.

The optical properties of solids are thoroughly discussed in the literature. All of these are devoted to the interpretation of the optical properties from the crystallographic structure and spectrographic analysis. Since this area is properly left to the expertise of the solid-state physicist the intent here is not to delve into the details of absorption but rather to examine some representative data for possible simplifications and generalizations which may be used for energy transfer purposes. Representative spectral data for the range in which thermal radiation is important at temperatures normally encountered are presented in Figure 1.1.

Common to most materials is a strongly absorbing, broad lattice vibration band as represented by the inserted data of Gottlieb (1960). Over the majority of this band the absorption coefficient is quite large (10^3 to 10^5 per cm) and the solid is effectively opaque. In the visible and near infrared ranges these materials become transparent eliminating any interaction between the material and radiation except for reflection and refraction. For the purposes of thermal radiation transfer, only the semitransparent absorption edge influences the temperature of the medium. As with any generalizations there are exceptions such as type II diamond which has a narrow weak band that must be considered in its entirety.

Many of the semitransparent regions might be treated empirically by an expression of the form $K_\nu = a\,\nu^{-b}$ which is the same as that for a gaseous ionization edge (Nelson and Crosbie, 1970). Lithium fluoride is a good example of this empirical fit. Other materials have more complex spectra as, for example, synthetic sapphire and silicon. These anomalies can be attributed to several resonant modes. Since no general correlation can be found which fits any but a limited class of materials, experimental data must be correlated separately.

The spectral absorption coefficient also has a dependence on temperature. For lattice vibrations the temperature effects are only apparent in the band center (Gottlieb, 1960). To avoid fracturing a solid the temperature gradients must be minimal, thereby restricting the temperature range normally encountered in practice.

It can be concluded that for computational purposes a piecewise approximation appears to be appropriate for correlating complex spectra. Workable comprehensive theoretical models for nonlinear spectral

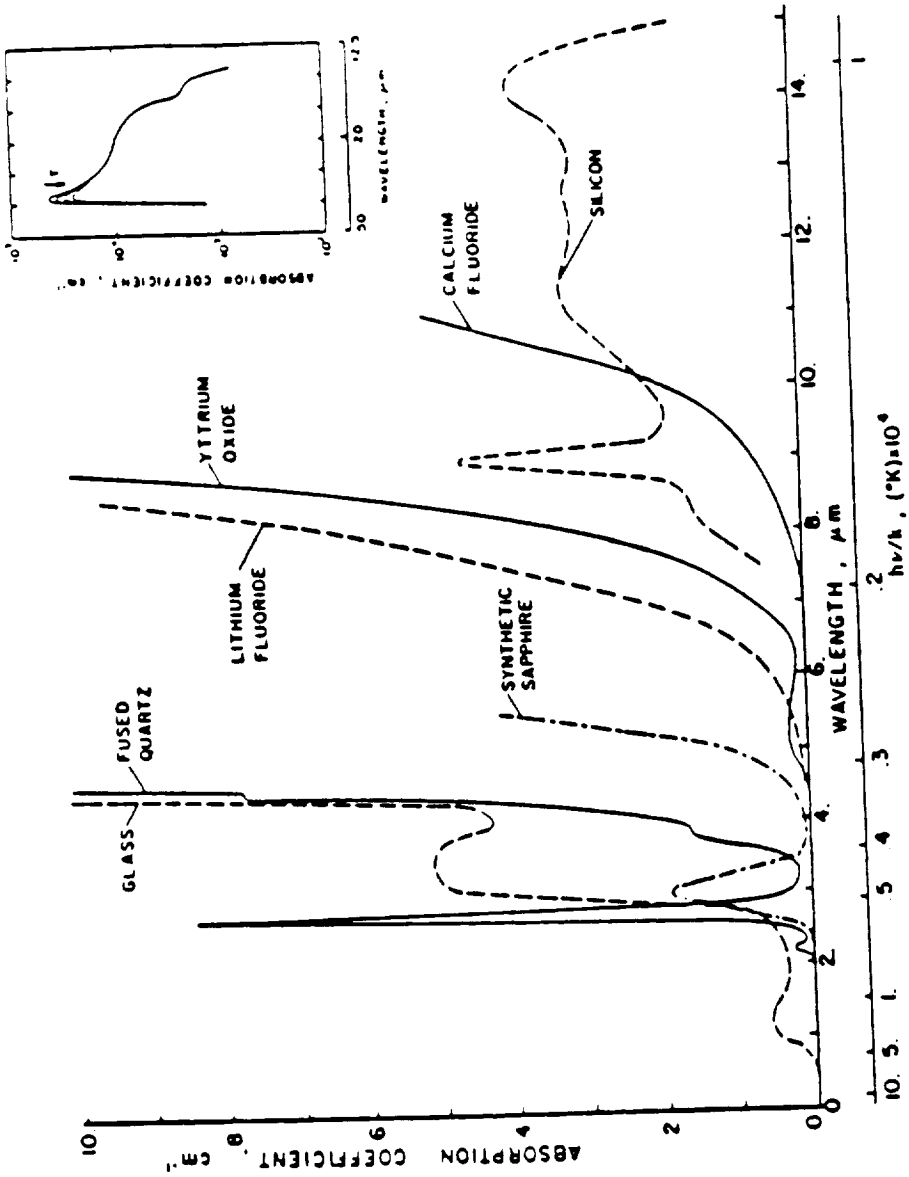

Figure 1.1 Absorption Spectra of Typical Semitransparent Solids

behaviors do not appear to be available for all but a few semi-transparent solids.

In conjunction with a heat transfer numerical model, an optical pyrometer can be used to calculate a temperature profile that would closely resemble real experimental conditions in a furnace. The temperature profile can then be used in the feedback control of the furnace temperature. High temperatures materials processing furnaces that are used for zone refining and other processes, depend on accurate control of their temperatures for successful processes.

The formulation of the numerical model which uses the spectral properties for the materials is discussed in chapter 2.

1.3 EXPERIMENTAL INVESTIGATIONS AND METHODS

A long range goal of this research is to show that it is possible to deduce an accurate temperature profile from measurements made by an optical pyrometer if these measurements could be used in conjunction with a heat transfer model of the crucible.

Many applications are encountered in applied physics and engineering where it is necessary to measure the temperature distribution within a semitransparent material at high temperature. Examples of such materials are combustion products in a combustion chamber, glass when solid or molten, crystals, plasmas, etc. It is difficult to measure the temperature distribution of such materials. Probes cannot be readily used because they disturb the temperature measurements and radiation fields, and thus produce erroneous results. Also probes must be specially designed for high temperature applications to keep them from melting; for example pulsating thermocouples for combustion applications. An alternative approach is to remotely measure

the radiation field emerging from the medium and recover the temperature distribution from these data (Chupp and Viskanta, 1974). This is possible because the emerging radiation field from a semitransparent medium is a function of the temperature distribution. For the limiting case of opaque materials, the remote sensing approach reduces to conventional pyrometry and only a surface temperature is recovered.

Thermal remote sensing specifically involves using a spectral sensor (spectrometer or monochrometer with detector, radiometer with filters, etc.). This equipment is expensive and may not be required if accurate modeling of the semitransparent materials can be achieved.

A number of experiments have been conducted for gaseous, liquid and solid materials with radiative transfer. Many of those are of an applied nature undertaken for purposes other than identifying the role of radiative transfer and its coupling with other energy transfer modes. Since the experimental methods developed in these works are applicable to a more fundamental objective, they are included in this study. Most of the techniques which will be discussed are applicable to all materials and are independent of the material phase. Therefore this review will not concentrate on the phase of the material. The different types of techniques, their limitations, and applications in temperature measurements will be discussed in the following sections.

1.3.1 Thermometry Methods

Several investigators have applied conventional thermocouple and resistance thermometer probes for the measurement of temperature with significant radiative transfer. The presence of the probe alters the temperature field by partial blockage of the radiation, conduction along the probe, probe mount and leads, and the absorption and reemission of

radiant energy by the probe. Since all of these errors depend on the physical size of the probe, they can be minimized by appropriate design.

Nishimura and others (1968), examined the validity of a gray analysis for simultaneous energy transfer in glass. It was found that this model failed to predict the experimental results. It is of interest to note that the gray assumption overpredicts the temperature for a solid whereas it underpredicts that of a gas. This behavior can be attributed to the fact that solids have but a few regions of high spectral bandpasses whereas gases are transparent over a large portion of the spectrum. Fowle and others (1969), experimentally studied the unsteady heat transfer through glass and measured the surface temperatures with thin-film gold resistance thermometers.

The effect of subsurface temperature gradients on the total emittance of a translucent solid was examined by Cox (1963) using small blackbody cavities drilled into the specimen normal to the gradient. Internal temperature measurements were made by focusing an optical pyrometer on the aperture of the cavities. The validity of this approach is questionable since the cavities appreciably disturb the radiation and conduction fields.

1.3.2 Optical Methods

Optical interference methods which have been widely used in heat transfer studies eliminate several errors since no external probes are introduced into the material. Also, they have the advantage that the entire field may be observed instantaneously. The earliest application of an interferometric technique to a situation in which radiation is significant appears to be that of Gill and Goody (1964), who measured the critical Rayleigh number of a model atmosphere heated from below.

A Michelson interferometer which passes the beam through the test medium twice was used to obtain the temperature distribution. The investigators were very meticulous in the design of the experiment and error analysis although the correlation with analysis is poor because of the statistical nature of the convective instabilities. No account of the refractive error which the Michelson interferometer accentuates was given.

For solids the temperature field may be indirectly measured with photoelastic optical methods (Veduta and Leontivich, 1967), which measure the thermal stress. This approach has had little application because of the limited accuracy inherent in correlating the birefringence patterns and temperature.

The variation with temperature in the transmittance of molten glass at 0.6328 μm was employed by Eryou and Glicksman (1972). This method is more practical than an interferometer in that it is simpler to use and less sensitive to external error sources such as vibration and convection. Since the transmittance as a function of temperature is in many cases unknown, elaborate calibration techniques were required.

1.3.3 Inversion Methods

The inference of the internal temperature from measurements of radiant energy emerging from the surface (inversion) has the advantage that no probes or external stimulus need be applied to disturb the fields. The earliest attempt using inversion techniques to measure the temperature was made by Beattie and Coen (1960). They recognized that the spectral radiation emitted from a semitransparent medium is dependent on the internal as well as surface emission. A pyrometer capable of remotely measuring the emitted radiation in two wavelength

bands, a semitransparent band to measure a weighted internal temperature and an opaque band to measure the surface temperature, were developed.

The logical extension is to increase the number of spectral bands in order to resolve the entire temperature profile. This extended approach has been of considerable interest for astrophysical and meteorological applications. For the atmosphere which can be modeled as a plane layer, the emergent radiation is a weighted integration of the local composition and temperature. Inferring the temperature then requires the inversion of this integral equation.

In chapter 3 experimental investigations that were performed using a commercially available ARTCOR Model 460-15 Bench Top Tubular Laboratory Research Furnace are discussed. The study also considers combined mode spectral radiation-conduction modeling of semitransparent materials using finite differencing techniques.

In chapter 4, the results are discussed, with conclusions given in chapter 5.

CHAPTER 2

FORMULATION AND ANALYSIS OF SPECTRAL RADIATION EFFECTS IN A ZIRCONIA FURNACE

The understanding of the heat transfer processes within an alumina crucible containing a liquid iron sample is an integral part in the design of this furnace. Heat transfer modeling at these very high temperatures is complicated by the semitransparent nature of the materials. The interaction between conduction and radiation within the crucible wall also needs to be understood for an efficient design of the crucible wall thicknesses.

In this chapter a general steady state analysis of coupled conduction/radiation heat transfer analysis through semi-transparent media will be developed. In section 2.1 a one-dimensional spectral radiation/conduction model in a semi-transparent material was developed for a zirconia furnace, operating at 1873K (1600^{o}C), with an alumina crucible containing molten iron. This model was developed to understand how the variations in the radiative functions affected the temperature profiles within the system.

The one dimensional radiation conduction model was able to predict the temperature profiles within the alumina crucible wall. The model was also used to verify the solution techniques that were used. The model could not predict how the variations in wall thicknesses influenced the temperature profiles within the crucible wall. Therefore in order to solve this problem a two dimensional model had to be developed. In section 2.2 a two dimensional spectral model for the semitransparent material was developed.

Both models included variable radiation properties namely, transmissivity, emissivity, and absorptivity all as functions of temperature and wavelengths. Numerical results for the temperature profiles were obtained using finite difference techniques.

2.1 ONE DIMENSIONAL ANALYSIS

A one dimensional spectral radiation heat transfer model for a semitransparent alumina crucible containing liquid iron sample was developed. The radiation/conduction model included emissivity, transmissivity, reflectivity, and absorptivity that are both functions of wavelengths and temperatures, as discussed in section 2.1.2.

2.1.1 One Dimensional Physical Model

Figure 2.1 shows the cross section of a cylindrical alumina crucible containing liquid iron and enclosed by a heated furnace wall. The furnace wall temperature is controlled so that the outside surface of the alumina crucible wall (a) is maintained at 1873K (1600°C). The problem is modeled in one dimension as shown in Figure 2.2. In Figure 2.2, region II, the space between the muffle tube and the alumina crucible, was assumed to be at vacuum. The alumina crucible is considered to be an absorbing, emitting, and isotropic scattering media, with both conduction and radiation taking place. The alumina crucible will be considered as semitransparent in some regions of wavelengths as dictated by its transmissivity (case 1) and compared to a totally opaque wall (case 2) which will be used as a reference condition. Thermal conductivity will vary with temperature and the modeling reflects this. Radiation properties will be considered to vary with both temperature and wavelength. Finally, in

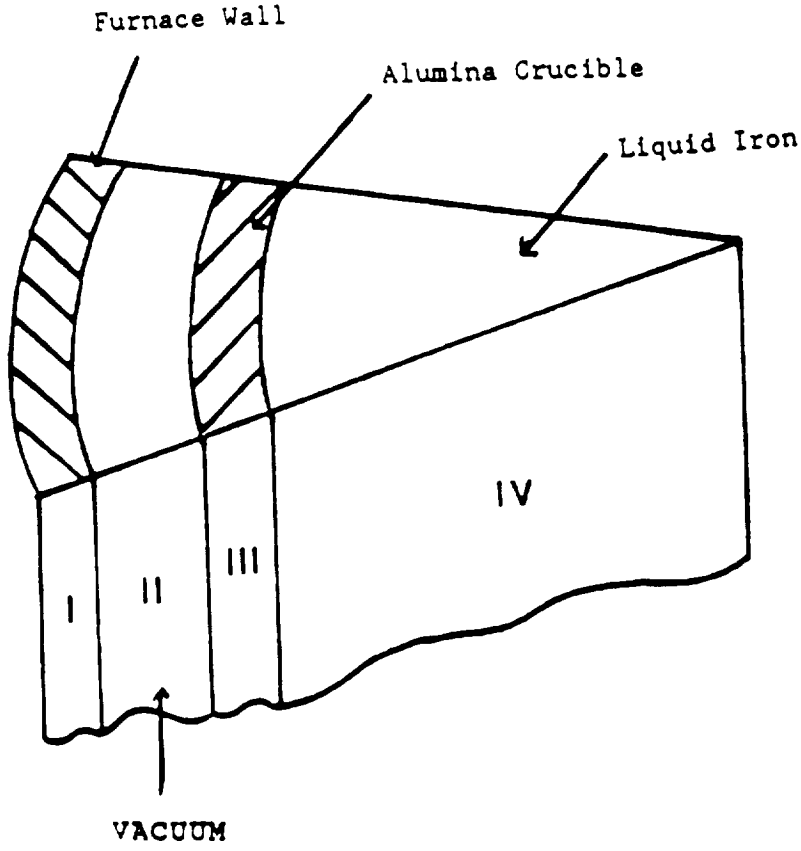

Figure 2.1 A Cross Section of a Cylindrical Alumina Crucible Containing Liquid Iron and Enclosed by a Heated Furnace Wall.

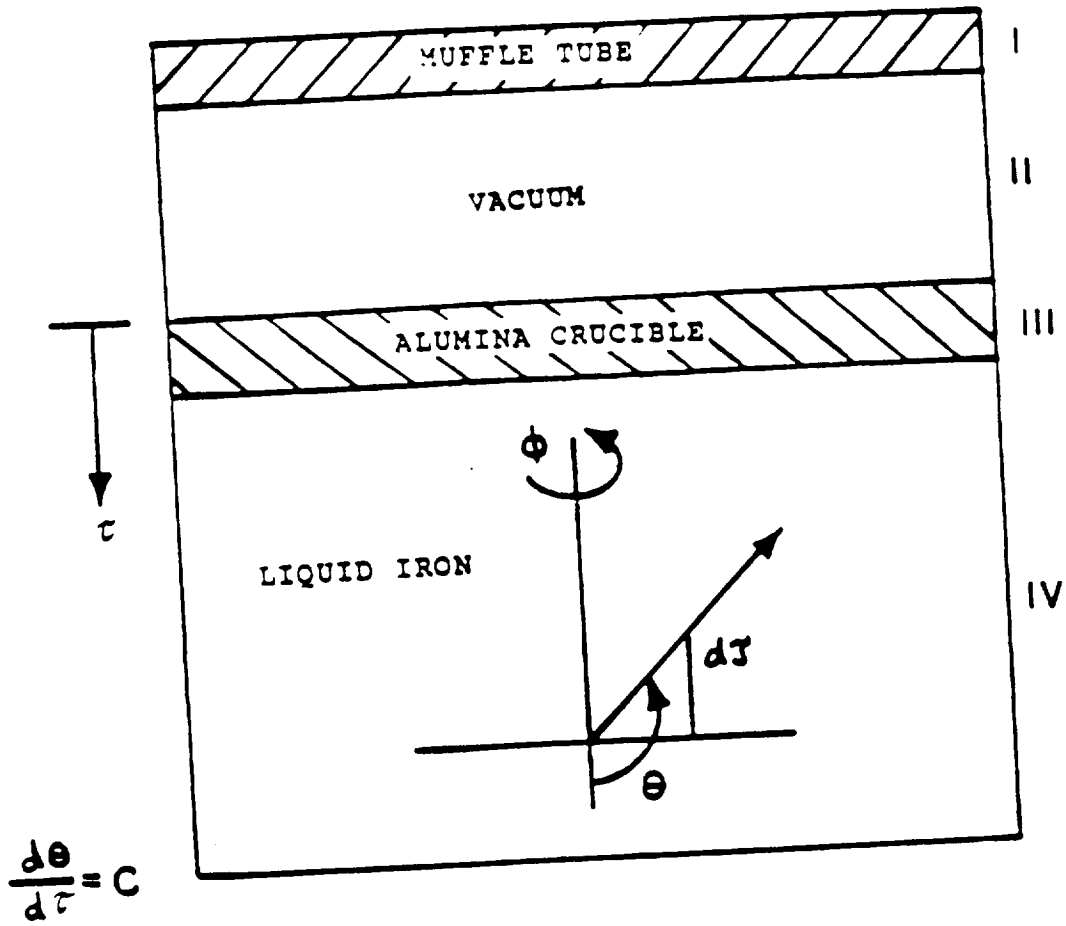

Figure 2.2 One Dimensional Representation of the Model to be Solved. τ is Dimensionless Distance.

region IV, we assumed liquid iron with conduction in the radial direction. Convection effects were ignored in the liquid iron sample as it is assumed the unit will operate in microgravity. Finite difference techniques were employed to solve this problem using the coordinate system shown in Figure 2.2 and discussed in section 2.1.3.

2.1.2 Physical Properties

This section details the various radiative and physical properties of alumina and liquid iron sample. The spectral radiative property functions were obtained by correlating materials property data using high order polynomials. The objective was to develop a combined radiation and conduction heat transfer model for an alumina crucible in thermal contact with a molten iron sample in order to demonstrate the importance of spectral modeling.

Figure 2.3 shows the emissivity of alumina as a function of temperature, while Figure 2.4 shows the emissivity as a function of wavelength at 1873K. Figure 2.5 shows the transmissivity of alumina as a function of wavelength over the range of 1873 to 1973K. Note that at 1873K approximately 80% of the transmitted energy for alumina occurs between 2 to 6 microns. It is for this reason that transmissivity cannot be ignored in high temperature radiation problems. The thermal conductivity of alumina as shown in Figure 2.6 changes by almost 7% from 1773 to 1873K. Finally, Figure 2.7 shows the thermal conductivity for liquid iron, which changes by about 30% of its value at 1773K to its value at 2000K. This represents a significant error if it were to be assumed constant over the temperature range examined here, Toulokian (1967).

This study considers all the radiative properties, namely

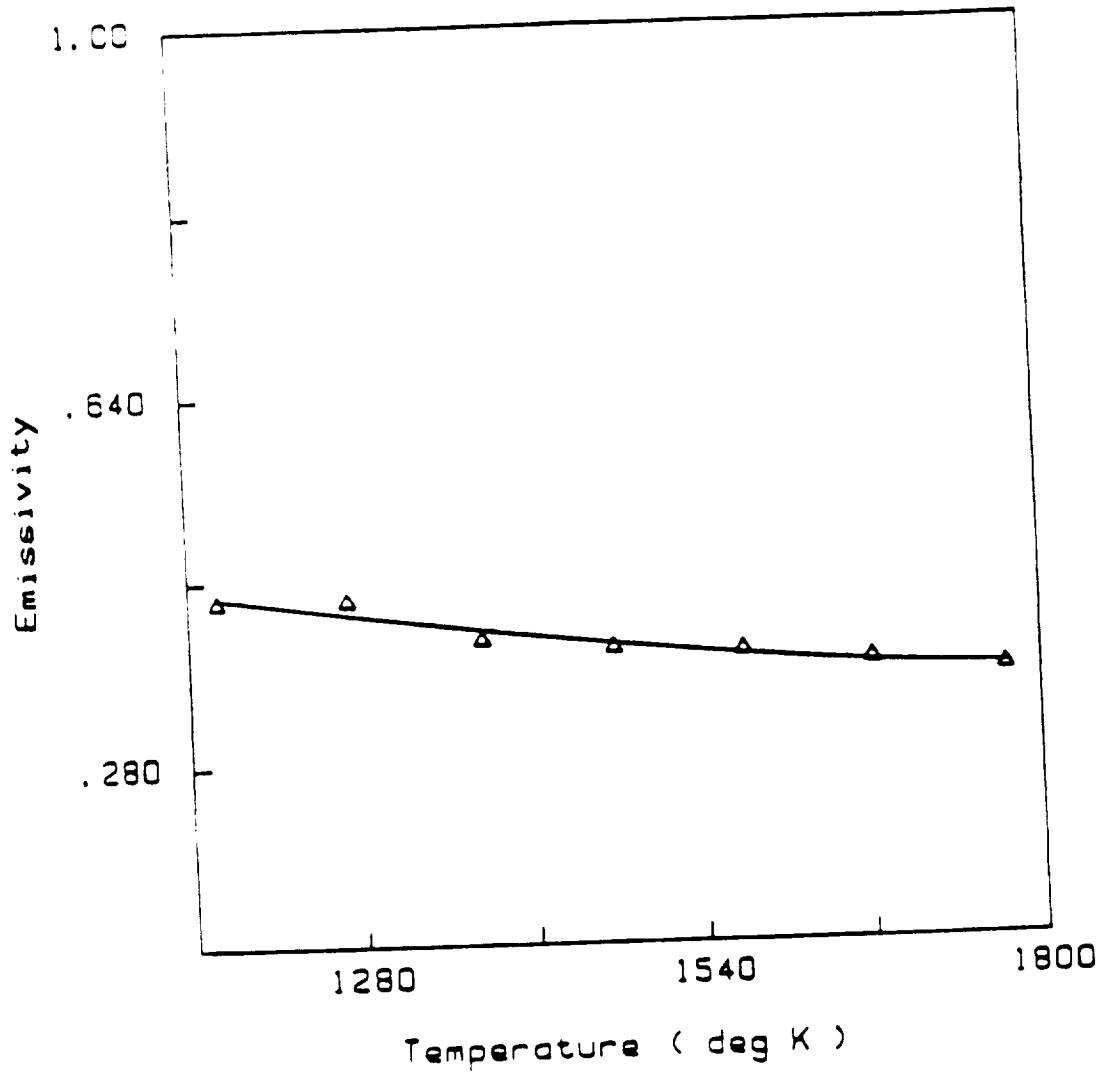

Figure 2.3 Emissivity of Alumina as a Function of Temperature

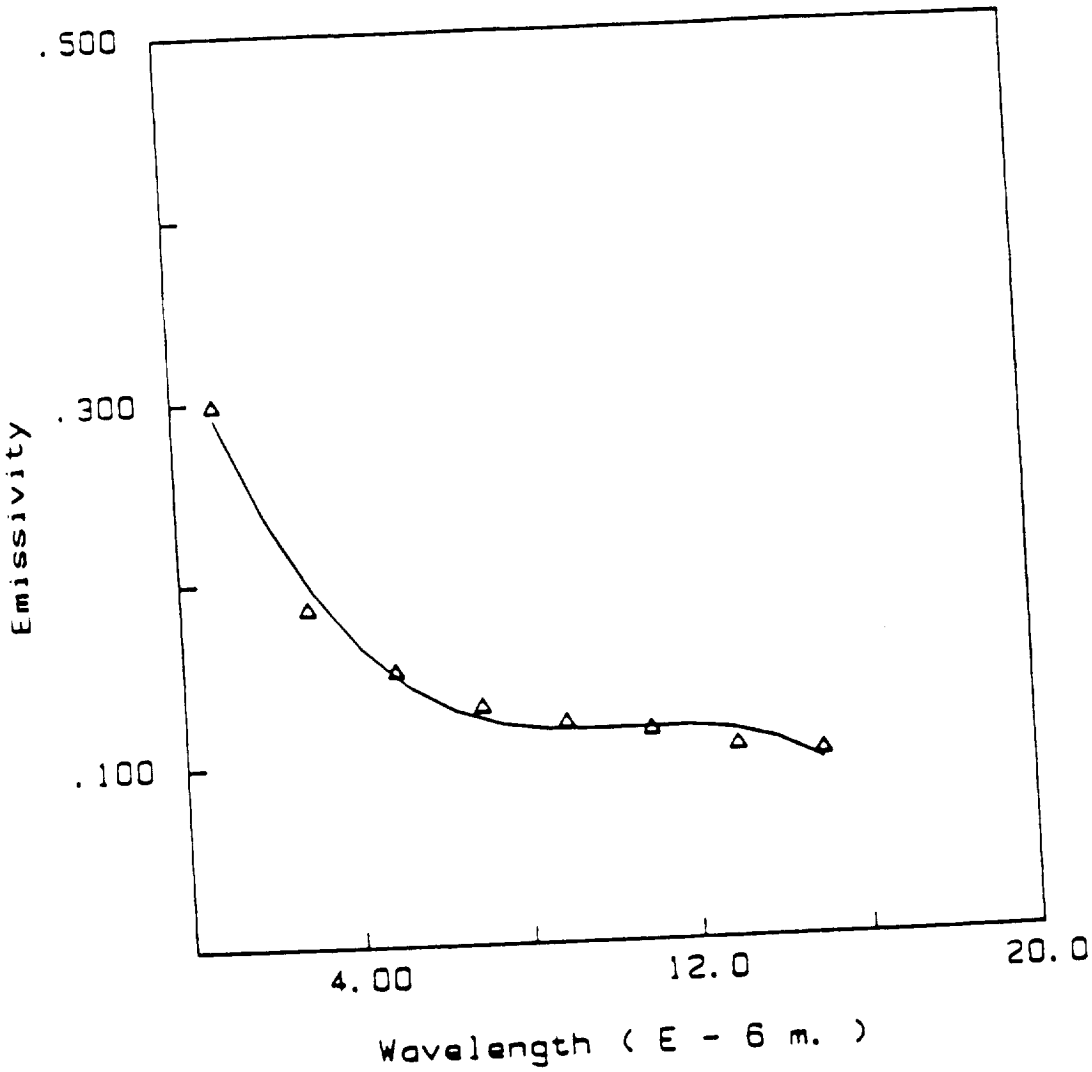

Figure 2.4 Emissivity of Alumina as a Function of Wavelenght at 1873K.

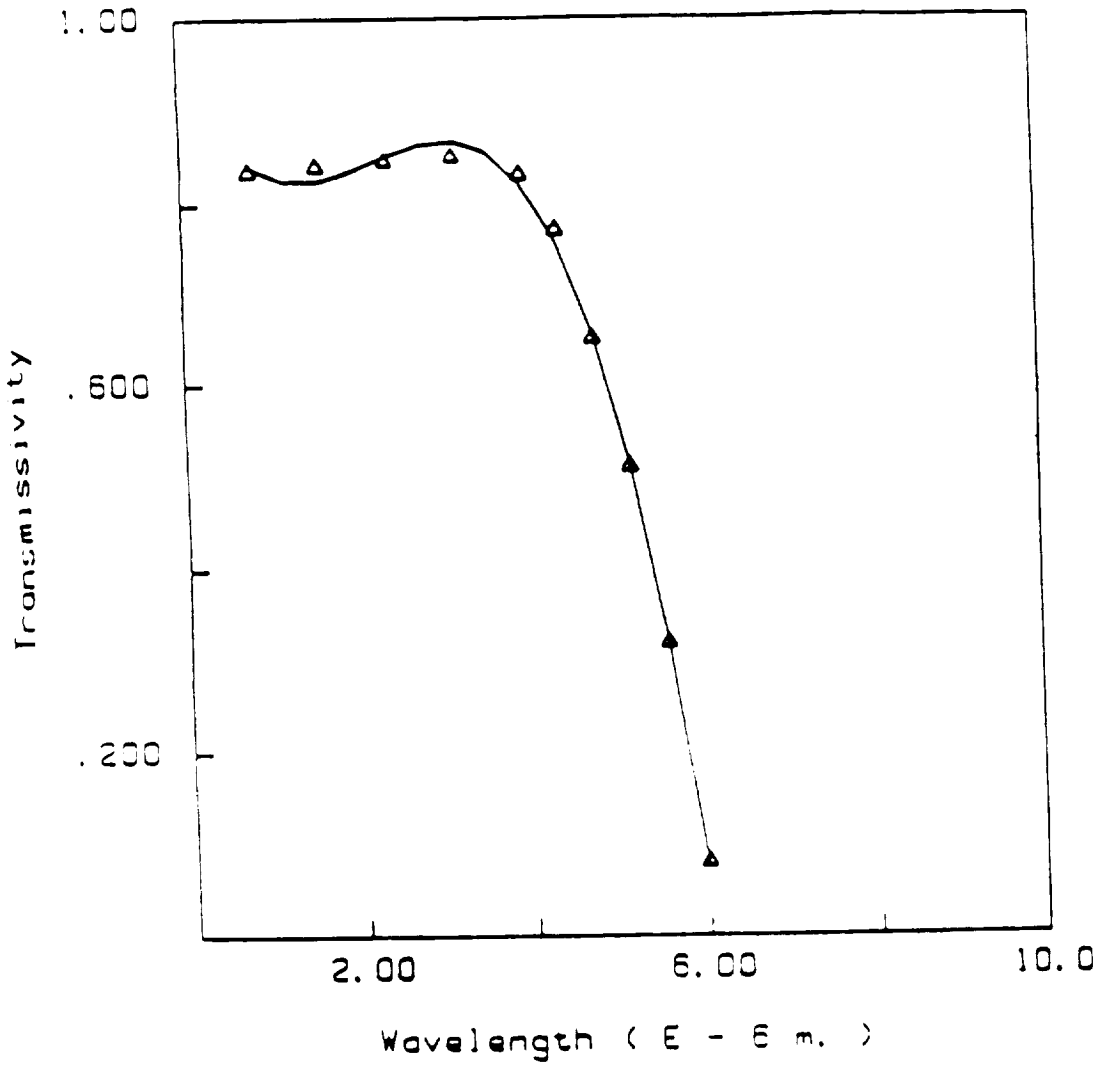

Figure 2.5 Transmissivity of Alumina as a Function of Wavelenght over the range of 1873 - 1973K.

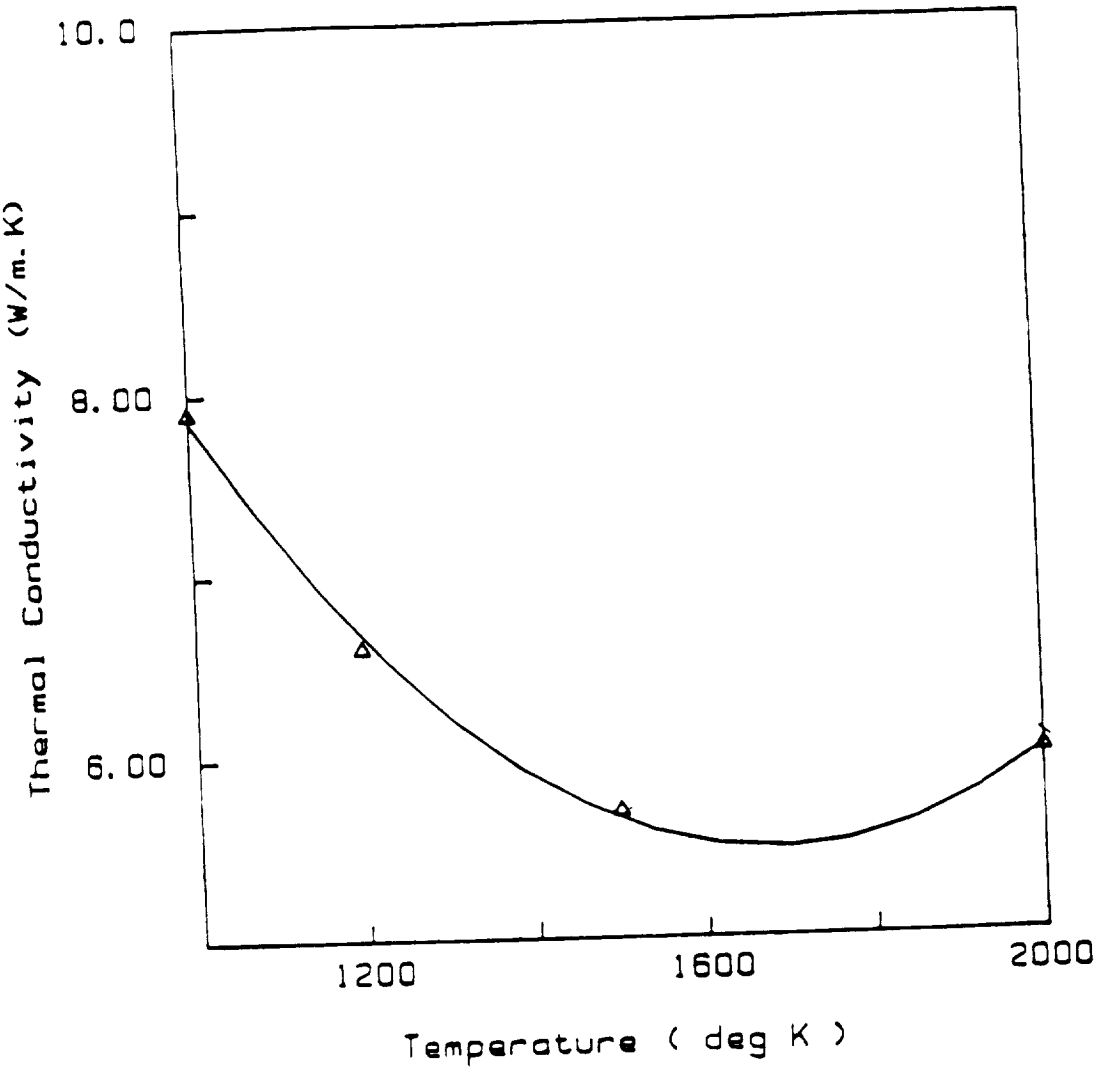

Figure 2.6 Thermal Conductivity of Alumina as a Function of Temperature.

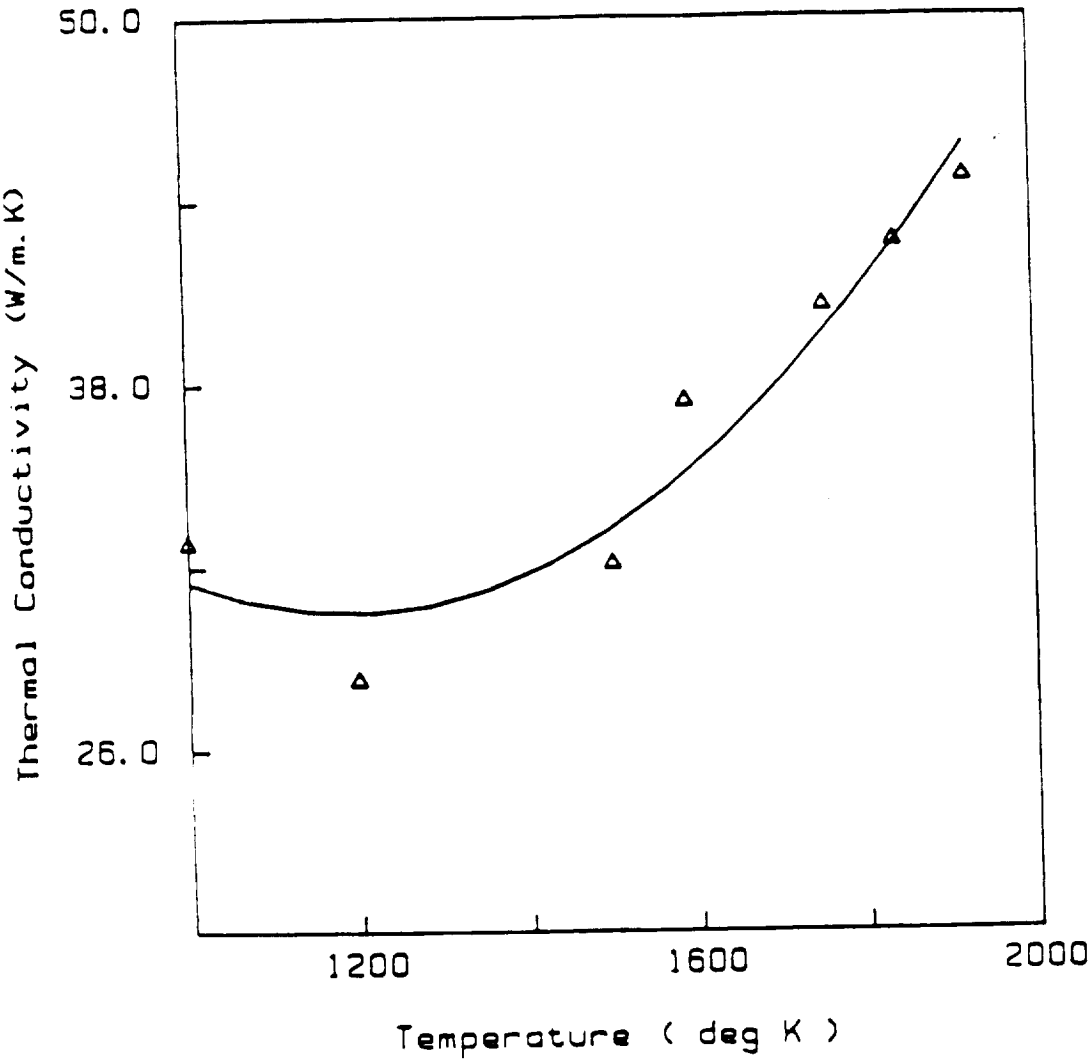

Figure 2.7 Thermal Conductivity of Liquid Iron as a Function of Temperature.

transmissivity, absorptivity, and emissivity as functions of both wavelengths and temperatures. This is important since at these such high temperatures (1773 - 2273K) the radiation properties vary due the transparency of the ceramic. Therefore the transparency of ceramics at these high temperatures is important in model development and must be included if we are to advance high temperature furnace technology.

2.1.3 Governing Equations and Boundary Conditions

Since only conduction is considered in region IV (see Figure 2.2), the thermal gradient in region IV will only be a function of the heat flux established in region III. Thus, the conduction in region IV will be determined from the heat flux at the interface (b) after the results in region III are converged to a solution. That is, we shall solve the conduction and radiation within the alumina crucible by considering the interface with the liquid iron as a boundary condition with constant heat flux at steady state.

The boundary conditions at the surface of the alumina crucible for the two cases studied were as follows. For the semitransparent crucible (case 1) we have emission, absorbed irradiation, and molecular energy transfer between the interface and the heated furnace wall, thus the energy balance is as given in equation (2.1):

$$-k \left.\frac{dT}{dx}\right|_{x=0} = h_1[T_1 - T_0] + \epsilon_{opq}\left[e_{b\lambda opq}(T_1) - e_{b\lambda opq}(T_0)\right] \qquad (2.1)$$

For the opaque reference condition (case 2), the temperature at the surface of the crucible is considered constant at 1873 K.

At steady state in the absence of internal heat sources,

conservation of energy requires that

$$\frac{d}{dx}\left[-k(T)\frac{dT}{dx}\right] + Q_R(x) = 0 \tag{2.2}$$

be satisfied. This implies that the sum of the conductive and radiative flux must equal the constant heat flux. The radiative flux over the entire range of wavelengths is therefore

$$Q_R(x) = 2\pi \int_0^\infty \left\{ \int_0^1 I^+_\lambda(x)\mu d\mu - \int_0^{-1} I^-_\lambda(x)\mu d\mu \right\} d\lambda \tag{2.3}$$

where $I^+_\lambda(x)$ and $I^-_\lambda(x)$ are the spectral intensity of radiation in the forward ($\mu > 0$) and backward ($\mu < 0$) directions, respectively. As a result of internal emission of radiation, the intensity is coupled to the temperature distribution in the solid. Now consider the equations of transfer and following the work of Sparrow and Cess (1970), we have

$$\mu \frac{dI^+_\lambda}{dx} = K_\lambda \left[\frac{\epsilon_{b\lambda}(x)}{\pi} - I^+_\lambda \right] \tag{2.4a}$$

$$\mu \frac{dI^-_\lambda}{dx} = K_\lambda \left[\frac{\epsilon_{b\lambda}(x)}{\pi} - I^-_\lambda \right] \tag{2.4b}$$

for $0 < \mu \leq 1$. Note that I^+_λ corresponds to positive values of μ whereas I^-_λ is associated with negative values of μ.

For the time being let the boundary conditions for equations (2.4a) and (2.4b) be

$$I^{+}_{\lambda}(\tau_{\lambda}, \mu) = I^{+}_{\lambda}(0, \mu), \qquad \tau_{\lambda} = 0 \tag{2.5a}$$

$$I^{-}_{\lambda}(\tau_{\lambda}, \mu) = I^{-}_{\lambda}(\tau_{0\lambda}, \mu), \qquad \tau_{\lambda} = \tau_{0\lambda} \tag{2.5b}$$

by defining

$$\tau_{\lambda} = \int_{0}^{x} \kappa_{\lambda}(x)dx \tag{2.6}$$

called the optical thickness. By using either an integrating factor or the method of variation of parameters, the solutions to equations (2.4a) and (2.4b) are found to be

$$I^{+}_{\lambda}(\tau_{\lambda}, \mu) = I^{+}_{\lambda}(0)e^{-\tau_{\lambda}/\mu} + 1/\pi \int_{0}^{t_{\lambda}} [\kappa_{\lambda} e_{b\lambda}(t)]e^{-(\tau_{\lambda}-t)/\mu}\, dt/\mu$$

$$0 \leq \mu \leq 1 \tag{2.7a}$$

$$I^{-}_{\lambda}(\tau_{\lambda}, \mu) = I^{-}_{\lambda}(\tau_{0\lambda})e^{(\tau_{0\lambda}-\tau_{\lambda})/\mu} - 1/\pi \int_{t_{\lambda}}^{t_{0\lambda}} [\kappa_{\lambda} e_{b\lambda}(t)]e^{-(\tau_{\lambda}-t)/\mu}\, dt/\mu$$

$$-1 \leq \mu \leq 0 \tag{2.7b}$$

Equation (2.7) describes the radiation field in terms of the temperature field within the medium through Planck's constant $e_{b\lambda}$.

Substituting equations (2.7a) and (2.7b) into equation (2.3), the expression for the one-dimensional total radiation flux becomes

$$Q_R(\tau_\lambda) = \int_0^\infty \Big(2\pi \int_0^1 I^+_\lambda\,(0,\,\mu) e^{-\tau/\mu}\,\mu\,d\mu - \int_0^1 I^-_\lambda\,(\tau_{0\lambda},-\mu) e^{-(\tau_{0\lambda}-\tau_\lambda)/\mu}\,\mu\,d\mu + 2\int_0^{t_\lambda} \kappa_\lambda e_{b\lambda}(t) E_1(\tau_\lambda - t)\,dt - 2\int_{t_\lambda}^{\tau_{0\lambda}} \kappa_\lambda e_{b\lambda}(t) E_2(t - \tau_\lambda)\,dt \Big) d\lambda \qquad (2.8)$$

where

$$E_n(\tau) = \int_0^1 \mu^{n-2} e^{-\tau/\mu}\,d\mu = \int_1^\infty e^{-\tau/\mu_\mu - n}\,d\mu \qquad (2.9)$$

are the exponential integral functions. Differentiating equation (2.8) we get

$$dQ_R(\tau_\lambda)/d\tau_\lambda = \int_0^\infty \Big(4\kappa_\lambda e_{b\lambda}(\tau_\lambda) - 2\pi \Big[\int_0^1 I^+_\lambda\,(0,\,\mu) e^{-\tau_\lambda/\mu}\,d\mu + \int_0^1 I^-_\lambda\,(\tau_{0\lambda},-\mu) e^{-(\tau_{0\lambda}-\tau_\lambda)/\mu}\,d\mu \Big] - 2\int_0^{\tau_{0\lambda}} \kappa_\lambda e_{b\lambda}(t) E_1(\tau_\lambda - t)\,dt \Big) d\lambda \qquad (2.10)$$

Equation (2.10) therefore describes the divergence of the radiation term in the energy equation (2.2).

Substituting equation (2.10) into the conservation of energy equation (2.2) we get

$$d/dx[k(dT/dx)] = -\int_0^{\infty} \{ 4\kappa_\lambda e_{b\lambda}(\tau_\lambda) - 2\pi[\int_0^1 I^+_\lambda (0, \mu)e^{-\tau_\lambda/\mu} \, d\mu$$

$$+ \int_0^1 I^-_\lambda (\tau_{0\lambda}, -\mu)e^{-(\tau_{0\lambda}-\tau_\lambda)/\mu} \, d\mu]$$

$$- 2\int_0^{\tau_{0\lambda}} [\kappa_\lambda e_{b\lambda}(t)E_1(|\tau_\lambda - t|)dt) \, d\lambda \qquad (2.11)$$

Assuming diffuse surfaces, the intensities may be expressed in terms of radiosities by the following

$$I^+_\lambda(0,\mu) = B_{1\lambda}/\pi \, , \quad \text{and} \quad I^-_\lambda(\tau_{0\lambda},\mu) = B_{2\lambda}/\pi \qquad (2.12)$$

Substituting equation (2.12) into equation (2.11)

$$d/dx[k(dT/dx)] = -\int_0^{\infty} \{ 4\kappa_\lambda e_{b\lambda}(\tau) - 2B_{1\lambda}E_2(\tau_\lambda)$$

$$+ 2B_{2\lambda}E_2(\tau_{0\lambda} - \tau_\lambda)$$

$$- 2\int_0^{\tau_{0\lambda}} [\kappa_\lambda e_{b\lambda}(t)E_1(|\tau_\lambda - t|)dt) \, d\lambda \qquad (2.13)$$

where the radiosities $B_{n\lambda}$'s are defined by

$$B_{1\lambda} = \epsilon_{1\lambda}e_{b1\lambda} + 2(1 - \epsilon_{1\lambda}) (B_{2\lambda}E_3(\tau_{0\lambda})$$

$$+ \int_0^{\tau_{0\lambda}} \kappa_\lambda e_{b\lambda}(t)E_2(t)dt) \qquad (2.14a)$$

$$B_{2\lambda} = \epsilon_{2\lambda} e_{b2\lambda} + 2(1 - \epsilon_{2\lambda}) \left(B_{1\lambda} E_3(\tau_{0\lambda}) + \int_0^{t_{0\lambda}} \kappa_\lambda e_{b\lambda}(t) E_2(\tau_{0\lambda} - t)dt \right) \tag{2.14b}$$

where solving for $B_{2\lambda}$ we get

$$B_{2\lambda} = \frac{2(1 - \epsilon_{2\lambda})E_3(\tau_{0\lambda})}{2E_3(1 - \epsilon_{1\lambda}) + \epsilon_{2\lambda} e_{b2\lambda}} \left(\cdot \epsilon_{1\lambda} e_{b1\lambda} \right.$$
$$\cdot \; 2(1 - \epsilon_{1\lambda}) \int_0^{t_{0\lambda}} \left(\kappa_\lambda e_{b\lambda}(t) E_2(t)dt \right.$$
$$\left. \left. \cdot \; 1/E_3(\tau_{0\lambda}) \int_0^{t_{0\lambda}} \kappa_\lambda e_{b\lambda}(t) E_2(\tau_{0\lambda} - t)dt \right) \right) \tag{2.15}$$

Using dimensionless variables previously defined

$$\tau_\lambda = \int_0^x \kappa_\lambda(x)dx \qquad \theta = T/T_0 \tag{2.16}$$

equation (2.13) becomes

$$\kappa^2_\lambda T_0 \; d/d\tau [\, k \, (d\theta/d\tau) \,] = \int_0^\infty \left(4\kappa_\lambda \epsilon \sigma \theta^4 T_0^4 - 2B_{1\lambda} E_2(\tau_\lambda) \right.$$
$$+ 2B_{2\lambda} E_2(\tau_{0\lambda} - \tau_\lambda)$$
$$\left. - 2 \int_0^{t_{0\lambda}} \kappa_\lambda \epsilon \sigma \theta^4 T_0^4 E_1(|\tau_\lambda - t|)dt \right) d\lambda \tag{2.17}$$

In equation (2.17), the first term on the right-hand side represents the emission from the medium at τ_λ, the second two terms represent the radiation absorbed at point τ_λ, and the fourth term represents

the emission from all the other points in the medium absorbed at point r_λ.

2.1.4 Numerical Formulation

A finite difference technique was used to solve equation (2.17), as [A][θ] = [B]. The coefficient matrix [A] was composed of the conduction terms with variable thermal conductivities, while the force vector [B] was composed of the right-hand side of equation (2.17) multiplied by $T_o^3\sigma/\kappa_\lambda$. Since the thermal conductivity varies with temperature, we can write the left-hand side of equation (2.17) as

$$dq/dr = \text{R.H.S. of eqn (2.17)} \tag{2.18}$$

where $q = -k\, d\theta/dr$.

The finite difference formula for the above equation is

$$[k(\theta_{n+1/2})(\theta_{n+1} - \theta_n) - k(\theta_{n-1/2})(\theta_n - \theta_{n-1})]/h^2 = \text{R.H.S. of eqn (2.17)} \tag{2.19}$$

By defining $k(\theta_{n+1/2}) = 0.5(k_n + k_{n+1})$, our coefficient matrix consists of

$$a_{n,\,n-1} = 0.5(k_{n-1} + k_n)/h^2 \tag{2.20a}$$

$$a_{n,\,n} = -(0.5k_{n-1} + k_n + 0.5k_{n+1})/h^2 \tag{2.20b}$$

$$a_{n,\,n+1} = 0.5(k_n + k_{n+1})/h^2 \tag{2.20c}$$

Equation (2.18) contains the variable radiation properties. Notice the double integral; one with respect to λ, while the other was with respect to distance (which is a function of temperature along the medium). Therefore the radiation properties were integrated using simpson's rule for a range of wavelength between 2.0E-6 and 6.0E-6 m. and then a three point gaussian quadrature was used to integrate across the nodes for temperature variations. The values at each node formed the force vector. The problem was posed for two cases.

Case (1) was the transparent case. In this case, the boundary condition b_1 was determined by integrating opaque variables $(\epsilon[e_{b\lambda}(T_1)] \cdot e_{b\lambda}(T_0))_{opq}$ over the range of wavelenghts (see equation 2.1), where T_1 was determined by iteration.

Case (2) was the opaque case. In this case the boundary condition was fixed, i.e. b_1 = 1873K (θ = 1).

For both cases the second boundary condition was that $d\theta/dr$ was assumed constant.

After the solution to region III converged to within 0.005 in r, the crucible/metal boundary, θ_{nd}, was then used as a boundary condition to solve the conduction within region IV (liquid iron region). The flux at the crucible/metal boundary was then tested for convergence between regions III and IV. If these fluxes did not converge to a difference of less then 0.05 then the whole iteration is repeated by adjusting the initial guess for temperature profile within the alumina crucible.

2.2 TWO DIMENSIONAL ANALYSIS

The one dimensional model developed to estimate the thermal profiles within an alumina crucible, having semitransparent radiation

properties, was found to be insufficient to study the effects of variations in crucible wall thicknesses. Variations of temperature profiles within the crucible wall are required to determine the optimum crucible wall thickness for samples containing molten iron.

To solve this problem, a two-dimensional model was developed to improve the overall understanding of heat transfer interactions occurring within the zirconia furnace. The two-dimensional analysis more closely models both the spectral radiation and conduction occurring within the zirconia furnace. This model was used to determine the temperature profiles within the crucible wall and the liquid iron sample. The knowledge of the temperature profiles is important in the design of this furnace, since, as will be shown, the location of the maximum in the temperature profile was a function of the crucible wall thickness.

An important requirement in the design of an efficient furnace is that the maximum temperature location be at a minimum distance from the crucible/liquid iron interface, resulting in higher temperatures within the sample. If the maximum temperature within the crucible wall occurs near the crucible/liquid iron interface then the crucible wall can basically be neglected during control of the zirconia furnace.

In this study, as with the one dimensional model, we have considered all the radiative properties, namely transmissivity, absorptivity, and emissivity as functions of both wavelengths and temperatures.

2.2.1 Two Dimensional Physical Model

The model considered here is shown in Figure 2.8. A heating

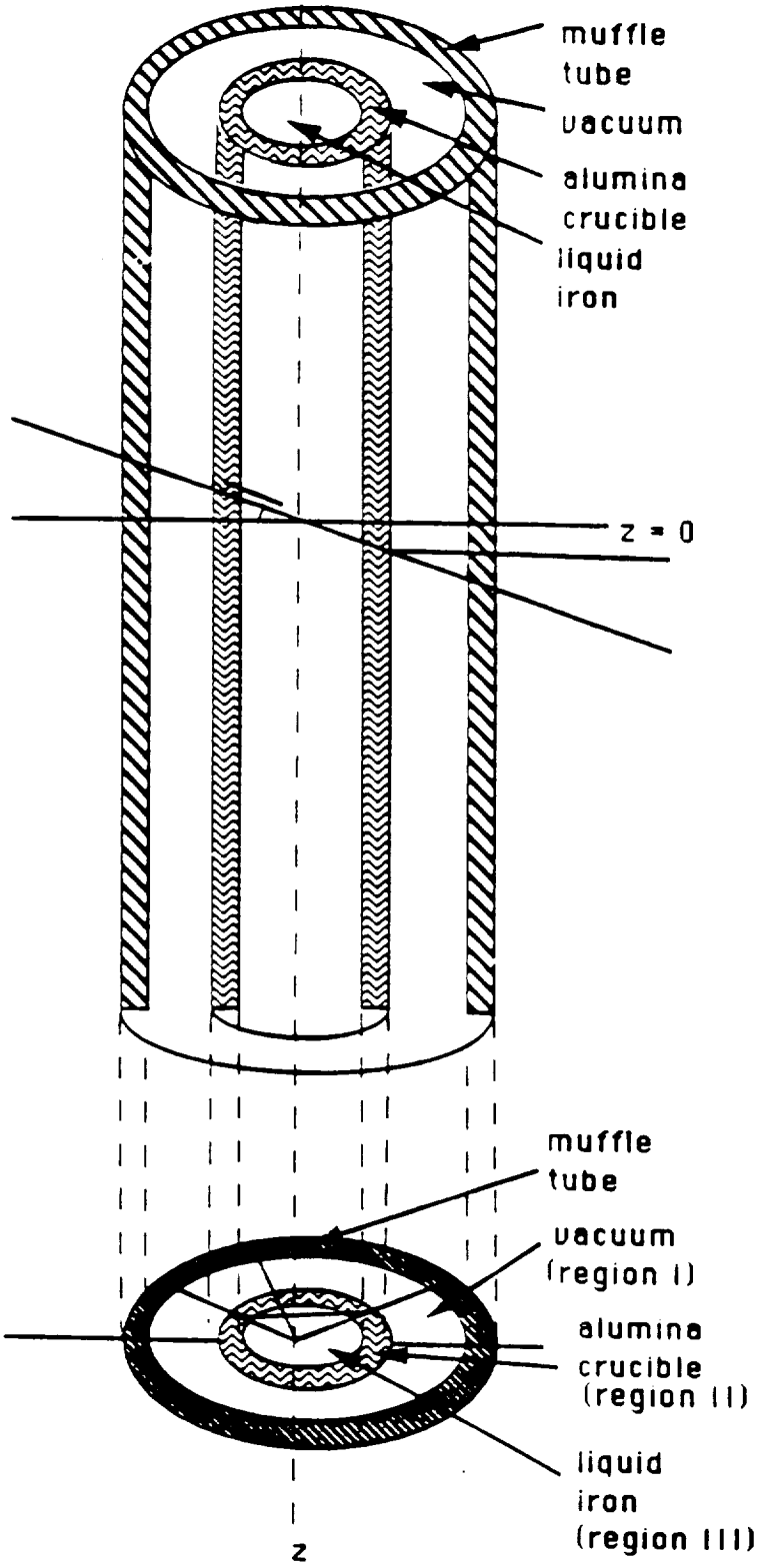

Figure 2.8 An outline of the alumina crucible containing liquid iron and enclosed by a heated furnace wall.

element/muffle tube, hereto referred as the heating element, encloses an alumina crucible wall containing a liquid iron sample. The heating element, made of yttrium stabilized zirconia, acts as an isothermal radiant source of energy. The alumina crucible will be considered opaque for certain frequencies and semitransparent for other regions of the radiation spectrum. Heat will be transmitted through the crucible wall by radiation and conduction, while in the liquid iron sample conduction is considered as the main mode of energy transfer. The effects of the spectral radiation to conduction parameters on the temperature profiles in the crucible wall were presented by Viskanta and Anderson (1975). They showed that radiation is the dominating factor in the energy transfer within the alumina crucible wall at these temperature ranges.

Spectral radiant energy will be transferred from the zirconia heating element radially into the alumina crucible wall through a vacuum. To evaluate this radiant transfer, the emission spectrum for zirconia was used. The energy will be further transferred into the liquid metal in both the radial and axial directions. The cooling of the liquid iron sample is encountered at both the top and bottom of the sample. Therefore, it was assumed that the heat flux at both ends was equivalent.

As shown in Figure 2.8, region I is a vacuum between the zirconia heating element and the alumina crucible wall. Region II is the crucible wall made of alumina. In this region both radiation and conduction are assumed to take place. Region III is the liquid iron sample. In this region conduction will be considered as the major source of heat transfer.

2.2.2 Governing Equations

At steady state in the absence of internal heat sources, conservation of energy requires that

$$-\nabla \cdot (\nabla T) + \nabla \cdot Q_R = 0 \qquad (2.21)$$

be satisfied. This implies that the sum of the conductive and radiative fluxes must equal the total heat flux. For an annular geometry with cylindrical symmetry, equation (2.21) in cylindrical coordinates becomes

$$-\{1/r\ \partial/\partial r(k\ \partial T/\partial r)\} - \partial/\partial z(k\ \partial T/\partial z) + \partial Q_R/\partial r = 0 \qquad (2.22)$$

where the first two terms represent conduction in the radial and axial directions respectively. The second term represents the radiation in the radial direction. To partially simplify the analysis, radiation is assumed negligible in the axial direction, within the crucible wall. Also in the liquid iron, only conduction is considered to be the dominating mode of heat transfer.

Using dimensionless variables defined as follows

$$r = \int_0^{\infty} \kappa_\lambda r d\lambda \qquad (2.23)$$

$$\theta = T/T_{ref} \qquad (2.24)$$

$$\eta = z/z_0 \qquad (2.25)$$

equation (2.22) becomes

$$\frac{1}{r}\frac{\partial}{\partial r}\left(k\frac{\partial\theta}{\partial r}\right) + \frac{1}{\kappa^3 z^2_0}\frac{\partial}{\partial\eta}\left(\frac{\partial\theta}{\partial\eta}\right) = \frac{1}{N}\frac{\partial Q_R(r)}{\partial r} \qquad (2.26)$$

where we define the radiation conduction parameter N as follows

$$N = \kappa^2/4\sigma_s T^3_{ref} \qquad (2.27)$$

The transport equation, using the coordinates shown in Figure 2.8 for a material with refractive index n, is given by

$$dI_\lambda/dr = -\beta_\lambda I_\lambda + \kappa_\lambda n^2 I_{b\lambda} + \sigma_\lambda G_\lambda(r)/4\pi \qquad (2.28)$$

where I_λ, the intensity and is composed of I^+ and I^- which are dependent on the direction of radiation, and $G_\lambda(r)$ is the integrated intensity defined below.

$$G_\lambda(r) = 2\int_0^{\pi/2}\int_0^{2\pi} I_\lambda \cos\alpha\, d\gamma\, d\alpha \qquad (2.29)$$

Therefore, the net radiative flux directed radially inward is given by

$$q_\lambda(r) = 2\int_0^{\pi/2}\int_0^{2\pi} I_\lambda \cos^2\alpha\cos\gamma\, d\gamma\, d\alpha \qquad (2.30)$$

From the above equation (2.30), the expression for the radiative flux directed inward in nondimensional form is

$$Q_R(r) = 4r_1/\pi r \int_0^{\pi/2} \int_0^{\sin^{-1}(r_0/r_1)} (\Phi_1^+(r,\alpha,\beta) - \Phi_1^-(r,\alpha,\beta)) \cos^2\alpha \cos\beta \, d\beta \, d\alpha$$

$$+ 4r_1/\pi r \int_0^{\pi/2} \int_{\sin^{-1}(r_0/r_1)}^{\sin^{-1}(r/r_1)} (\Phi_2^+(r,\alpha,\beta) - \Phi_2^-(r,\alpha,\beta)) \cos^2\alpha \cos\beta \, d\beta \, d\alpha \qquad (2.31)$$

where Φ is the nondimensionalized radiation potential defined as

$$\Phi = \pi I / n^2 \sigma_s T^4_{ref} \qquad (2.32)$$

and I is the intensity of radiation.

Substituting equation (2.31) into equation (2.26) gives the final form of the governing equation.

2.2.3 Boundary Conditions

Again, we will consider two kinds of boundary conditions. First, case (1), we shall assume that the surface of the crucible is opaque. Secondly, case (2), this same surface will be considered as semitransparent for some regions of radiation wavelengths. The other boundary condition for both cases will be a zero heat flux at the center of the liquid iron sample. This assumption is justified by the cylindrical symmetry of the model.

Since the model now has two separate regions where heat transfer is being considered, that is region II and III, there exists another restriction at the interface of the crucible wall and the liquid iron sample. At this interface between the crucible and the liquid iron sample, we shall assume that the temperature is continuous, thus the heat fluxes on both sides will be identically matched. This assumption is justified by the fact that the crucible wall and the liquid iron sample are in thermal contact. If we assume

zero contact resistance, then the temperatures at both sides of the interface are equal.

For case (1), the opaque case, the temperature at the crucible external wall will be calculated from the radiating zirconia element. This implies that at the boundary $r = 1$ will be fixed at a known temperature. For the semitransparent case (2), the boundary condition at the surface of the wall is given below

$$-k\partial\theta/\partial r\Big|_{r=R} - \epsilon_{opq}[e_{b\lambda opq}(T_1) - e_{b\lambda opq}(T_0)] = 0 \qquad (2.33)$$

When we consider the interface, as mentioned earlier, the temperatures at the crucible side and the temperature on the liquid iron side have to be identical. Therefore we can write

$$T_{crucible} = T_{iron} \quad \text{at} \quad T = T_{interface} \qquad (2.34)$$

For both cases the boundary condition at the center of the liquid metal sample is that the temperature gradient is zero. Thus we have at $r = 0$,

$$d\theta/dr = 0 \qquad (2.35)$$

Now for the iron sample we have two more boundary conditions for the axial (z) direction. Using the coordinate system applied to the model (see Figure 2.8), at the center of the sample, ($\eta = 0$), we have

$$d\theta/d\eta = 0 \qquad (2.36)$$

while at each end of the crucible wall ($\eta = 1, -1$), we have

$$d\theta/d\eta = 0.5Q_R \tag{2.37a}$$

$$d\theta/d\eta = -0.5Q_R \tag{2.37b}$$

Equations (2.26) and (2.28) together with the boundary conditions are the final equations needed to solve the problem.

2.2.4 Numerical Formulation

A finite difference formulation of the energy equation (2.26) is given by [A] [θ] = [radiation terms]. The coefficient matrix [A] consists of the following

$$a_{n-1,m} = k_{n-1/2}/g^2\tau_m \tag{2.38a}$$

$$a_{n,m} = (-k_{n+1/2} - k_{n-1/2})/g^2\tau_m + (k_{n+1/2} - k_{n-1/2})/h^2\kappa^3 z^2{}_0 \tag{2.38b}$$

$$a_{n+1,m} = k_{n+1/2}/g^2\tau_m \tag{2.38c}$$

$$a_{n,m-1} = -k_{n-1/2}/h^2\kappa^3 z^2{}_0 \tag{2.38d}$$

$$a_{n,m+1} = k_{n+1/2}/h^2\kappa^3 z^2{}_0 \tag{2.38e}$$

where $k_{n+1/2}$ is defined as $0.5(k_n + k_{n+1})$ and $k_{n-1/2}$ is defined as $0.5(k_{n-1} + k_n)$ with k_n being the thermal conductivity at temperature θ_n, $g = \Delta\tau$ and $h = \Delta\eta$.

The left hand side coefficient matrix represents the conduction terms (equation 2.26), while the right hand side represents the integral radiation terms in equation (2.31). The finite difference equations for the conduction part included two spatial variables, namely r and η in the radial and axial directions respectively. For the crucible wall, the integrals on the right hand side of equation (2.26) were calculated in the following manner. For an assumed temperatures, the integrals were calculated using simpson's method for the range of wavelengths given between each of the nodes. This provided the total radiation properties at those nodes. Since this problems represents a double integration of complex mathematics, simpson's rule was first used to integrate over discrete wavelengths to reduce the problem to a single integral of sums of the integrated wavelengths, which were further integrated using a three point gaussian quadrature. This calculation provided the elements for the force vector at each of the nodes. For this force vector the temperature was assumed linear between the nodes.

An implicit method was used to solve the equations in region II (the crucible wall), and the flux and temperature leaving the end node of the wall was used to start the calculations in region III (the iron sample). When both the solutions converged, a test was performed to compare the fluxes at the interface. When the thermal fluxes were within the prescribed error of 10^{-2} the profiles were assumed to converge.

The results for both the one and two dimensional models are discussed in chapter 4. The model results were used in conjunction with experimental results to modify the zirconia furnace heating

element. Appendix (B) and (C) show the computer code developed to solve this problem.

CHAPTER 3

EXPERIMENTS AND PROCEDURES

This thesis addressed improvements in the design of high temperature furnaces that use zirconia ceramic heating elements. The goal was to adapt, improve, and redesign a zirconia furnace for use in materials processing experiments. This chapter will discuss the experimental apparatuses and procedures used to examine both a commercially available zirconia furnace and a furnace developed during this research.

Both furnaces, used a zirconia heating element that can operate continuously at temperatures above 1873K (1600°C) and can reach limits of 2273K (2000°C). The above temperature limits were based on the mechanical deterioration of the elements and insulating ceramics, the atmospheric air operating environment and electrical damage resulting from current flow within the zirconia heating element as the resistance decreased with increasing temperature. As mentioned earlier, the zirconia element is basically an insulator at temperatures below 1073K (800°C) but becomes a conductor above this temperature. As the temperature is increased, the resistance of the zirconia element is reduced as will be shown in later sections.

The major components for each furnace consisted of a main furnace assembly and a number of auxiliary systems that are necessary to perform the experiments. Section 3.1 describes in detail both the commercial and research furnaces and auxiliary

subsystems. The auxiliary subsystems included such items as temperature measurement devices, control and power supply system, and fluid delivery systems. This section also highlights the design improvements that were made in the furnace arrangement to include an alumina crucible assembly.

To develop this furnace for eventual application to directional materials solidification, several experiments had to be designed to verify its performance. Initial experiments were performed using an ARTCOR model 460-15 Bench Top Tubular Laboratory Research Furnace. This furnace will be referred to as the commercial zirconia furnace (CZF). The commercial furnace and its associated auxiliary subsystems are discussed in sections 3.1.1 and 3.1.2, respectively. The procedures for this furnace are discussed in section 3.2.1. Using the CZF, preliminary experiments were accomplished to evaluate its performance. Results from this furnace formed a basis on which new designs and procedural modifications were made which ultimately led to an improved furnace. This improved furnace will be referred to as the research zirconia furnace (RZF). The equipment and procedures used with the research furnace are detailed in sections 3.1.4 and 3.2.2.

A parallel study was performed on the numerical modeling of semitransparent materials heat transfer. The study assisted in the overall understanding of the heat transfer within the zirconia furnace, of the drawbacks of optical pyrometry and the thermal profiles within the crucible wall. The information obtained from the numerical model was used to select the internal components of the furnace that is detailed in section 3.1.3.

3.1 DESCRIPTION OF EXPERIMENTS

This section describes the furnace assembly. A description of the ARTCOR Model 460-15 is given in section 3.1.1 and modifications to the furnace assembly are then discussed in section 3.1.3. This section also describes the various components of the experimental setup for the two sets of experiments, set #1 and #2. The setup for the commercial zirconia furnace experiments (set #1) are given in section 3.1.2 while the setup for the research zirconia furnace experiments (set #2) are given in section 3.1.4.

A number of auxiliary modules had to be integrated into the experiment so that successful investigations could be accomplished. An infrared pyrometer (Omega type OS-1000-HT), with a water jacket, was included for temperature measurements. Specifications of the pyrometer are given in Appendix A. A stand was required to support the furnace, optical pyrometer, and ventilator. The stand was designed to protect the furnace from vibrations and was fitted with clamps to hold accessories needed during the experiments.

Additional procedures were developed after thorough investigation of the commercial furnace operations.

3.1.1 The Commercial Furnace Assembly

The furnace assembly is the core of the experimental set up. Figure 3.1 shows the commercial furnace arrangement for the ARTCOR model 460-15 bench top tubular laboratory research furnace. The main heater element is a zirconia tube. The zirconia acts as a conducting material at high temperatures, thus acting as a heater. Lead wires are attached to the zirconia tube at the top and bottom.

The zirconia heating element is loosely held in place by two

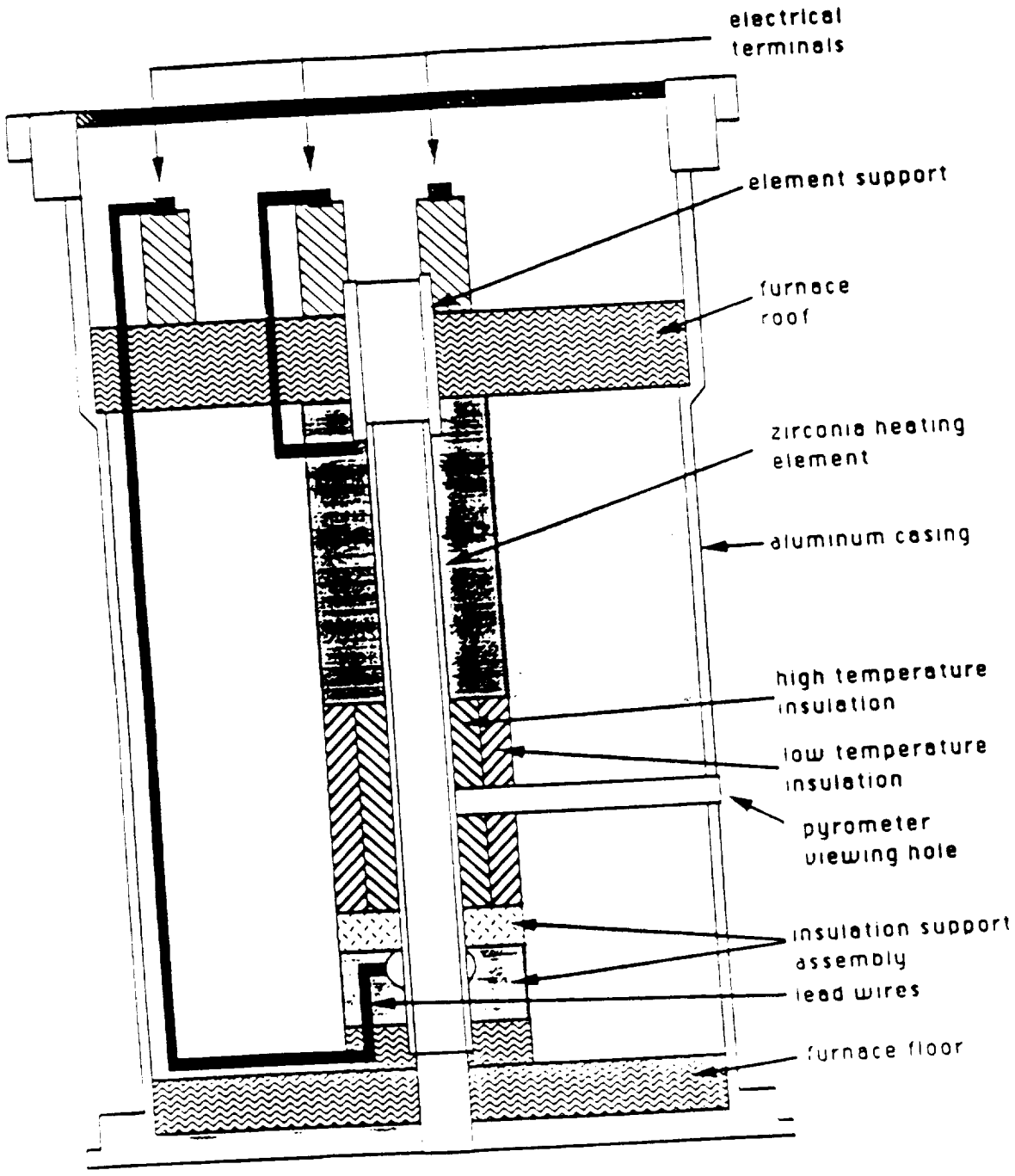

Figure 3.1 Furnace Arrangement for the ARTCOR Model 460-15 Bench Top Tubular Laboratory Research Furnace for Experiment Set #1

heater element supports; an upper support, and a lower support. Both supports are made of low density alumina ceramic tubing. At the middle of the zirconia element is an insulation assembly. The insulation cylindrical blocks consist of high and low temperature zirconia insulating blocks. These insulating blocks are held in place by highly porous ceramic rings, labeled the insulation support assembly (see Figure 3.1). The above forms the main heating element assembly.

The zirconia heating element and the insulating blocks, including all the support rings, are contained in a preheater module. The preheater also acts as an insulator after the zirconia main heater element has ignited. The assembly also consists of a pressed kaolin top and bottom and an outside casing made of anodized aluminum.

Electrical terminals that feed the current to both the preheater and the zirconia main heater element exit from the top of the assembly. The furnace assembly is attached to its control and power box by two protruding pipes. The whole assembly sits on a pressed ceramic board.

3.1.2 Experimental Layout for Commercial Furnace

The experimental layout consists of the furnace arrangement, temperature measurement devices, the fluid delivery systems, and the control and power supply. The furnace assembly is the major equipment for this experiment and has been detailed above. In order to adapt the furnace to material processing experiments, a number of auxiliary systems were installed. This section will discuss these auxiliary systems. The experimental layout is shown in

Figure 3.2. This set up was used to perform experiment set #1.

For the initial experiments two temperature measurement devices were installed to permit temperature measurements on the commercial unit. A type K thermocouple with a digital display was used to monitor the centerline temperature within the heating element. An infrared pyrometer was needed to monitor the temperature of the furnace via a viewing hole provided with the unit. This pyrometer measured the temperature of the element using an average emissive power of the element, therefore the emissivity of the zirconia had to be manually adjusted in the pyrometer electronics package to reference the pyrometer. A goal of the numerical portion of this research addresses the accuracy of using an "average" emissivity. A second goal of this research was to correlate the pyrometer readings and numerical results with those of the centerline temperatures within the alumina crucible.

The fluid delivery system cooled the pyrometer at high operating temperatures. The pyrometer was equipped with a water-cooled jacket around its inlet lens. The water temperature in the jacket was normally kept around 10 K above room temperature.

The control and power supply to the main heater and preheater formed the fourth subsystem. An Eurotherm controller (Model 818P) was used to supply the power to the heating elements by switching the channels allocated to the preheater and main heater elements. This switching presented some problems in the furnace operation, as will be discussed in later sections.

As discussed above, the ARTCOR Model 460-15 zirconia furnace was equipped with the necessary auxiliary systems so that an

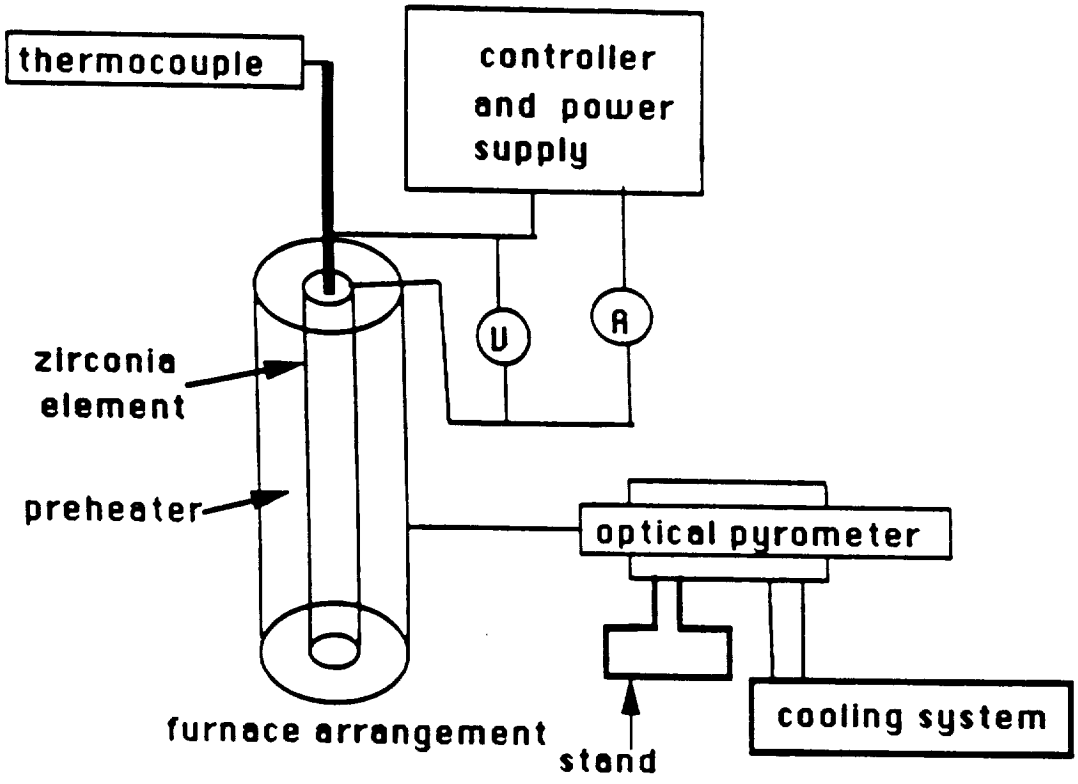

Figure 3.2 Layout of the Experiment including the Auxiliary Systems for Experiment Set #1.

evaluation on its performance could be made. As modifications were made to the commercial furnace assembly, further modifications to the auxiliary systems were needed. These changes formed the setup for the zirconia research furnace experiments (set #2). This set up is discussed in following sections.

3.1.3 The Research Furnace Assembly

The design changes in the furnace assembly are shown in Figure 3.3. To adapt the furnace for materials processing experiments, alumina crucibles and supporting ceramics were installed. These components were used to form the muffle tube and support small diameter crucibles which could be filled with pure component metals with known melting points. These experiments were designed to calibrate the optical pyrometer, evaluate the pyrometer in closed loop control schemes, and test the numerical models developed for semitransparent alumina crucibles which were discussed in chapter 2.

One part of the commercial furnace was redesigned. The roof of the furnace was redesigned from a 1" thick by 6" diameter yttria stabilized zirconia blank to partially restrain the element in both the radial and axial directions. This restraint would be needed to operate the furnace in a microgravity environment. The redesigned part also decreased heat losses from the top of the furnace while supporting and stabilizing the main heating element.

The main heating element, was replaced by an experimental yttria stabilized zirconia heating element. This new element is discussed in section 3.2.4. A type K thermocouple was installed between the main heater and preheater to accommodate a preheater

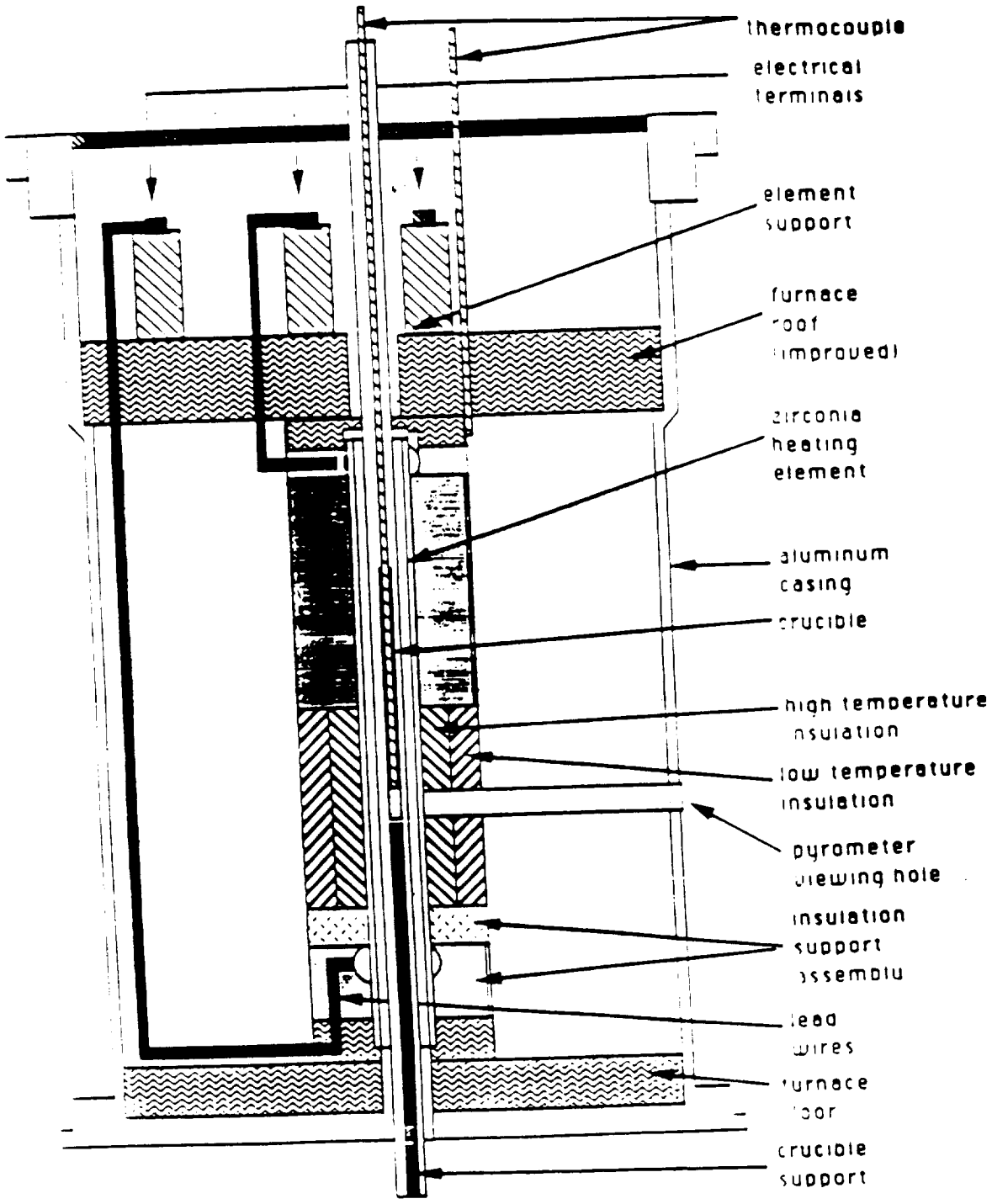

Figure 3.3 Furnace arrangement for the ARTCOR Model 460-15 Bench Top Tubular Laboratory Research Furnace for Experiment Set #2

power supply arrangement as discussed in section 3.1.2.

Alumina crucibles and supporting ceramics were used to form a muffle tube and support small diameter crucibles which could be filled with pure component metals with known melting points. These experiments were designed to resemble process conditions that exist in materials processing environments. In addition a type S thermocouple with electronic readout was added to measure the centerline temperature immediately adjacent to the viewing hole.

With the furnace equipped as shown in Figure 3.3, experiments were performed to compare the thermocouple (centerline) temperature measurements to the optical pyrometer readings from the external wall of the zirconia furnace.

3.1.4 Experimental Layout for the Research Furnace

Figure 3.4 shows the experimental layout of the research furnace and its auxiliary systems. This setup was used to perform the experiment set #2. In addition to the pyrometer, a type S thermocouple with a digital display was installed to monitor the centerline temperature in the crucible. These measurements were needed to correlate the pyrometer readings with the centerline temperatures.

In addition to the cooling water, the fluid delivery system also consisted of argon purge gas. Argon was used as a purge gas with a flow rate of 25 cm^3/min. using a HOKE (Model 1335G4B) precision micrometering valve.

For these set of experiments (set #2), a Valley Forge linear programmer was used to control power to the preheater. This controller ramped the preheater voltage based on a temperature

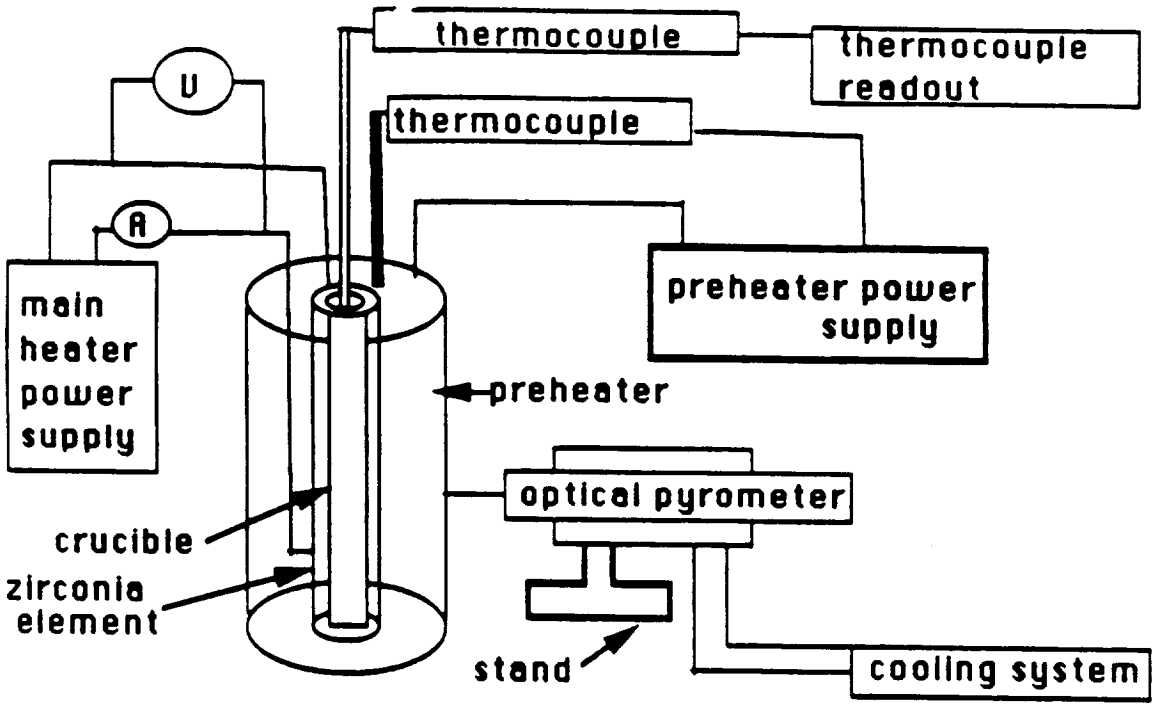

furnace arrangement

Figure 3.4 Layout of the Experiment including the Auxiliary Systems for Experiment Set #2.

measurement from a type K thermocouple. The specification for this thermocouple are given in Appendix A. The thermocouple was inserted between the preheater and the zirconia heating element and was manually removed once the zirconia ignition was achieved. The zirconia main heater element was connected to a variable transformer through a current meter. The transformer was calibrated using a voltmeter.

The following section discusses procedures used to examine both furnaces.

3.2 EXPERIMENTAL PROCEDURES

In this section, the experimental procedures required to verify the performance of the ARTCOR Model 460-15 Tubular Research Furnace are discussed. The procedures were devised to accomplish several objectives. Initial experiments were designed to characterize the performance of the furnace. These experiments are described in section 3.2.1. The results from these experiments gave indications of the areas for which improvements could be made. Auxiliary equipment had to be integrated into the experimental set up to permit further investigations.

There were three major design improvements that were considered in this study. The first was the improvement of the furnace components for future use in microgravity experiments discussed in section 3.1.2. The containment of the furnace components would be required for microgravity use. It should be noted that free convection was used to cool the furnace casing. Since the furnace ends were open to the atmosphere, one recognized that free convection and radiation losses would play major roles in

the furnace power consumption. Attempts to utilize this furnace for materials processing would require correction of these limitations.

Secondly, the new zirconia heater elements were designed, based on oxygen sensor technology. Improvements on these elements were concentrated on their ability to carry higher currents loads. The wall thickness of the alumina was deduced from the numerical studies that were performed. A detailed procedure for the construction of these elements is given in section 3.2.3.

In section 3.2.2 experiments were designed to study the temperature and heat transfer characteristics of the research furnace. The correlation between the optical pyrometer measurements and centerline temperatures were studied and for the two experimental setups.

In the following section a general view of the normal operation of the furnace is given.

3.2.1 Commercial Furnace Operation

In this section, the normal furnace operation as shown in Figures 3.2 is reviewed.

In this set of experiments, the power supply to the preheater and main heater were controlled by a preprogrammed Eurotherm Model 818P controller. The controller was preprogrammed to perform specific functions before the start of the experiment. Initially, the controller turned the preheater on at 20% applied power. It later ramped the applied power to 40% at a rate of 1% per minute. The preheater was then held at 40% power for a specified time to allow the main heating element to reach its conducting temperature. The controller would then switch the power supply from

the preheater to the main heating element. The power to the main heater was then ramped to a preset value and held for a specified time.

After the given time, the controller would ramp down the power to the main heating element at a rate of 1% per minute until shut off. Before the next start up of the furnace, the controller was initialized and, if desired, reprogrammed to go through the routine again.

As discussed in section 3.1.2 above, the furnace was controlled by % power to the zirconia main heating element. The temperature measurements for the furnace constitute a crucial role in determining its performance in materials processing. Since accurate process temperatures are required in various materials processing experiments, correlation between the pyrometer readings and the centerline temperatures of the furnace needed to be studied. Also a correlation between the % power to the element and the temperature of the element was an important task in determining the performance of this furnace.

The controller was programmed to power the main heater element at 15% to 30% applied power and the temperature responses of the element studied. The goal was to partially calibrate the furnace temperature as a function of applied power. The temperatures measured for different applied power outputs to the main heater element are given in Figure 3.1.

To measure the temperature profile using a pyrometer, a special mount to accurately position a high temperature optical pyrometer to measure wall temperatures in the zirconia furnace was

installed. This mount provided a very precise positioning of the pyrometer for consistent temperature measurements. A small viewing port was provided by the manufacturer at the side of the furnace for direct viewing of the zirconia heating element with the pyrometer.

Axial variations in temperature could also be used to characterize a furnace. To investigate the axial centerline temperature gradient, the furnace was held at applied powers of 20% and 30%. The temperature was allowed to stabilize before the readings were taken along the centerline of the furnace tube.

In order to investigate how the furnace responded to gradual increases in power input, the furnace was ramped at a rate of 1% per minute and the temperature recorded. This experiment was performed to evaluate the temperature overshoot which indicates the robustness of the controller.

The commercial furnace system (see Figure 3.2) was equipped with an ammeter and voltmeter to measure currents and voltages applied to both the preheater and main heater at different power settings. This experimental setup was designed to study the actual power consumed. The unit was ramped from 50-70% applied power following recommended procedures. Additionally, separate experiments were conducted at 50, 60, and 70% applied power.

3.2.2 Research Furnace Operation

For the second set of experiments, the research furnace was equipped with two independent power sources as shown in Figure 3.4. The preheater was powered by a Valley Forge linear programmer at the rate of 3°C per minute, to about 800°C. The preheater was then

held isothermally for about an hour. A variable transformer then powered the main heating element through a current meter. When the zirconia main heating element ignited, as evidenced by the current meter, the power to the preheater was disconnected.

One may deduce that for set #1, the zirconia element may not ignite if the setting for the preheater power and soak time were not sufficient to bring the zirconia element to its conduction temperature. In set #2, the preheater power was kept on for as long as the zirconia element had not ignited (monitored by an ammeter), thus assuring the ignition of the zirconia heating element in each experimental run.

During shutdown, the power to the heating element was reduced at a rate of 2% per minute to shut off.

With the furnace equipped as shown in Figure 3.2, experiments were performed to compare the thermocouple (centerline) temperature measurements to the optical pyrometer viewing the exterior wall of the heating elements.

3.2.3 Construction of Zirconia Furnace Heating Elements

During this research, experiments were performed on the two zirconia elements available for study. Both elements cracked and failed after only limited intermittent use. A possible reason for the cracking failure may be the periodic use of the furnace in a humid environment. Experimental evidence presented in following sections suggested that moisture may have absorbed into the elements when the furnace was not in use.

To study the effects of moisture on the life span of the heater elements, a number of elements, in addition to the two

obtained from the manufacturer, were required. Due to the high costs of elements, experimental zirconia elements, based on oxygen sensor technology, were designed and the various components ordered. One of these experimental elements was used in controlled experiments to determine the initial lifetime. Others will be used to determine the effects of moisture.

The improved elements were designed and manufactured from high purity zirconia tubes with 0.00635 m (1/4 inches) platinum bands on each end. These zirconia tubes were manufactured by McDanel Refractory Company. The zirconia elements were designed with inside diameters of 0.0142 m (0.56 inches) and lengths of 0.1143 m (4.5 inches). This larger inside diameter was selected so that different alumina crucibles based on the numerical model predictions (discussed in chapter 2) could be studied in an effort to design a crucible with an optimum wall thickness.

Platinum-10% rhodium wire measuring 1000 feet in length with a 0.003 inch diameter, was manufactured by the Englehard Corporation. This wire was cut into 80 2-ft. strands and twisted to form the lead wires for the zirconia heating element. The number of strands needed was calculated based on the current loads expected during the operation of the furnace. The length of the lead wires were established to accommodate the construction of about five additional heater elements. The lead wires can be reused to construct other elements by cutting off the portion that was attached to the spent zirconia heating element, thus resulting in a decreased construction cost per element.

The wires were attached to the zirconia heating element to

form a current carrying junction between the zirconia heater element and the lead wires using a special approach. The junction was then cured several times using a Watlow furnace. The element was initially cured at 110°C. The temperature was then increased at a rate of 5°C per minute to 225°C and held at that temperature for another hour. This operation ensured that trapped gases would diffuse out of the junction. The temperature was then raised to 525°C at the rate of 5°C per minute and held there for about one hour. At this stage all the gases and moisture were removed. The temperature was raised to 1025°C and held for another hour. The power was removed from this well insulated furnace and the system allowed to cool undisturbed overnight. The element was installed in the furnace cavity and operated following the procedures outlined in section 3.2.2.

In the following chapter the results of the experiments and the numerical modeling are discussed.

CHAPTER 4

RESULTS AND DISCUSSION

To verify the performance of the ARTCOR Model 460-15 furnace, several experiments had to be performed. The commercial furnace was initially analyzed using a number of experiments to determine its operating parameters. The furnace components were then analyzed and redeveloped as needed to improve the furnace's performance. The auxiliary systems were included to adapt the furnace for future use in materials processing experiments. A major development of this study was in the design of the main zirconia heating element which was developed based partially on results from the numerical modeling.

Investigations on the heat transfer within the zirconia furnace and alumina crucibles were further enhanced by the numerical analyses performed in this study. Integration of these numerical and experimental studies is necessary if the furnace is to be used for materials processing experiments.

The numerical results will be discussed in section 4.1. The experimental results for both the commercial furnace and the research furnace will be discussed in section 4.2.

4.1 ANALYTICAL AND NUMERICAL RESULTS

4.1.1 One Dimensional Analysis

To evaluate the model, several analyses were performed following the works of Viskanta and Grosh (1962), with fixed thermal boundaries, while varying the conduction/radiation

parameter $N = T_o^3 * \sigma / K$. For this analysis, as N approaches 0 one solves a purely radiation problem, while as N approaches infinity one solves a purely conductive problem. Figures 4.1, 4.2 and 4.3 show the temperature profiles which would be generated within a 1mm thick alumina crucible at various value of N and fixed temperature differences. For this analysis only the crucible wall was considered. Figure 4.1 shows the results for an extreme temperature difference of 1713K (1440°C). This figure shows that at large temperature differences, materials with very high semitransparent properties would be required to distort the thermal profile within the crucible. Basically, this analysis is representative of a radiation problem with constant emissivity followed by conduction to the other boundary. At lower temperature differences, Figures 4.2 and 4.3, radiation effects within the material begin to take effect and only small changes in the materials conduction/radiation parameter produce large gradients within the sample.

The above analysis was undertaken to verify literature results, as it would require actual variations in the crucible material of construction to vary the conduction-radiation parameter. The alumina crucible modeled here is a component of an actual furnace and is made of high purity alumina. At the furnace operating temperature, the crucible has almost a constant value for N. The numerical problem addressed in this study was principally concerned with temperature measurements of an alumina crucible using an optical pyrometer and prediction of the thermal profile within a liquid iron sample based on these measurements. Refer to Figure 2.2 to review the system being analyzed. Optical pyrometers

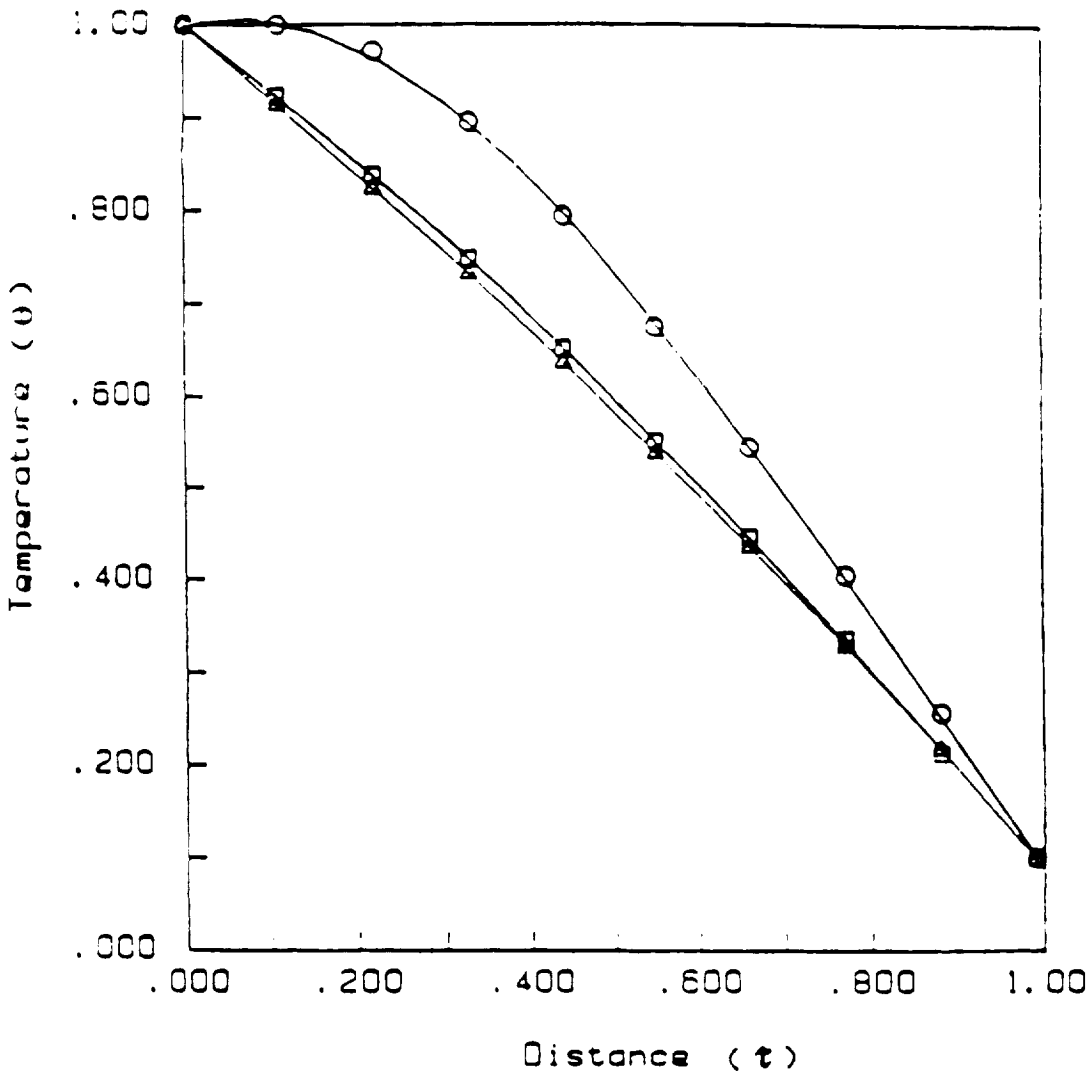

Figure 4.1 Variation of dimensionless temperature with distance for different ratios of conduction to radiation. Boundary temperatures are T_o = 1873K, T_b = 433K. ○ is for n = 0.0001, □ is for n = 0.001, △ is for n = 1.0.

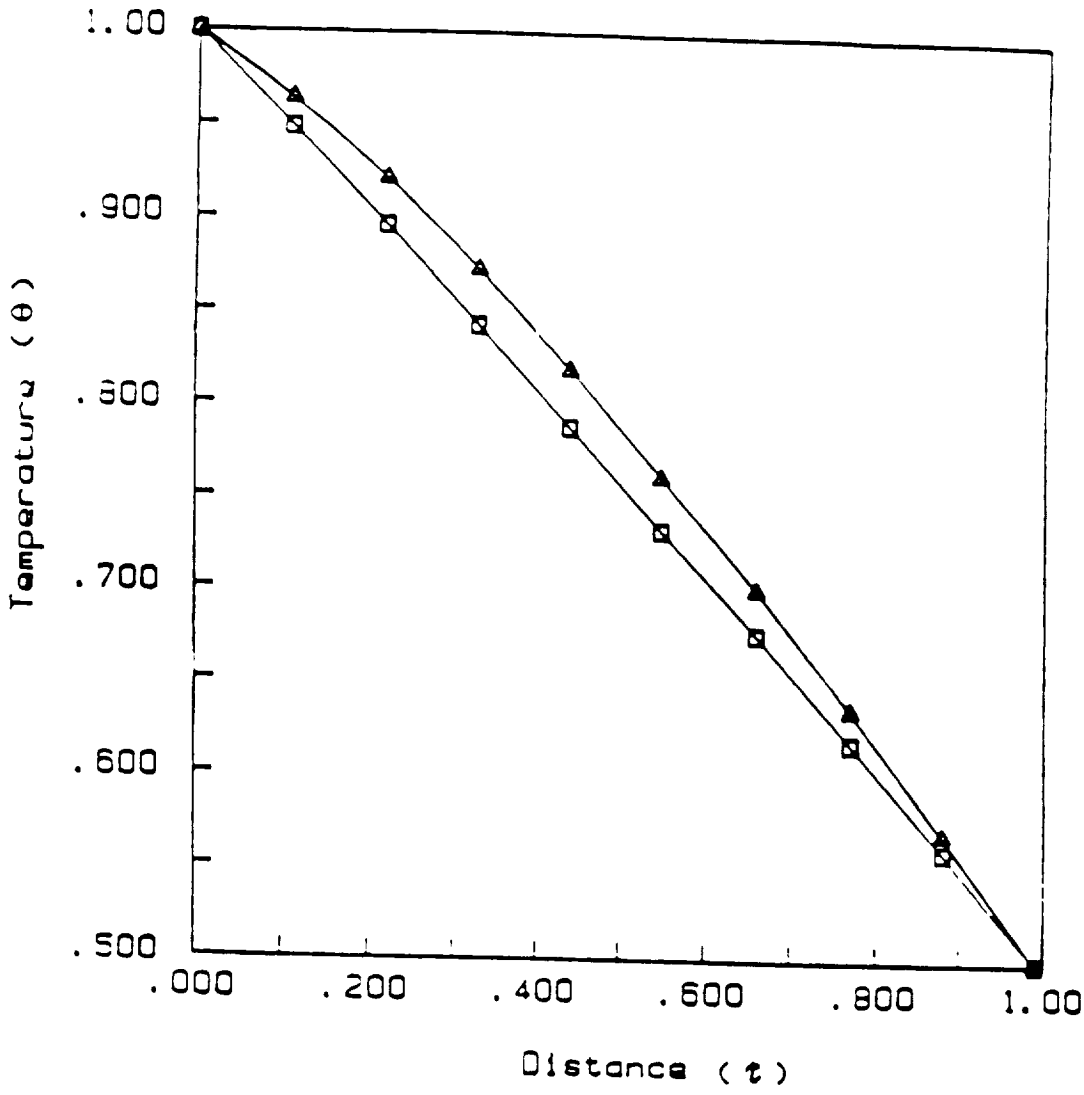

Figure 4.2 Variation of dimensionless temperature with distance for different ratios of conduction to radiation. Boundary temperatures are T_o = 1873K, T_b = 1073K. Δ is for n = 0.001, □ is for n = 1.0.

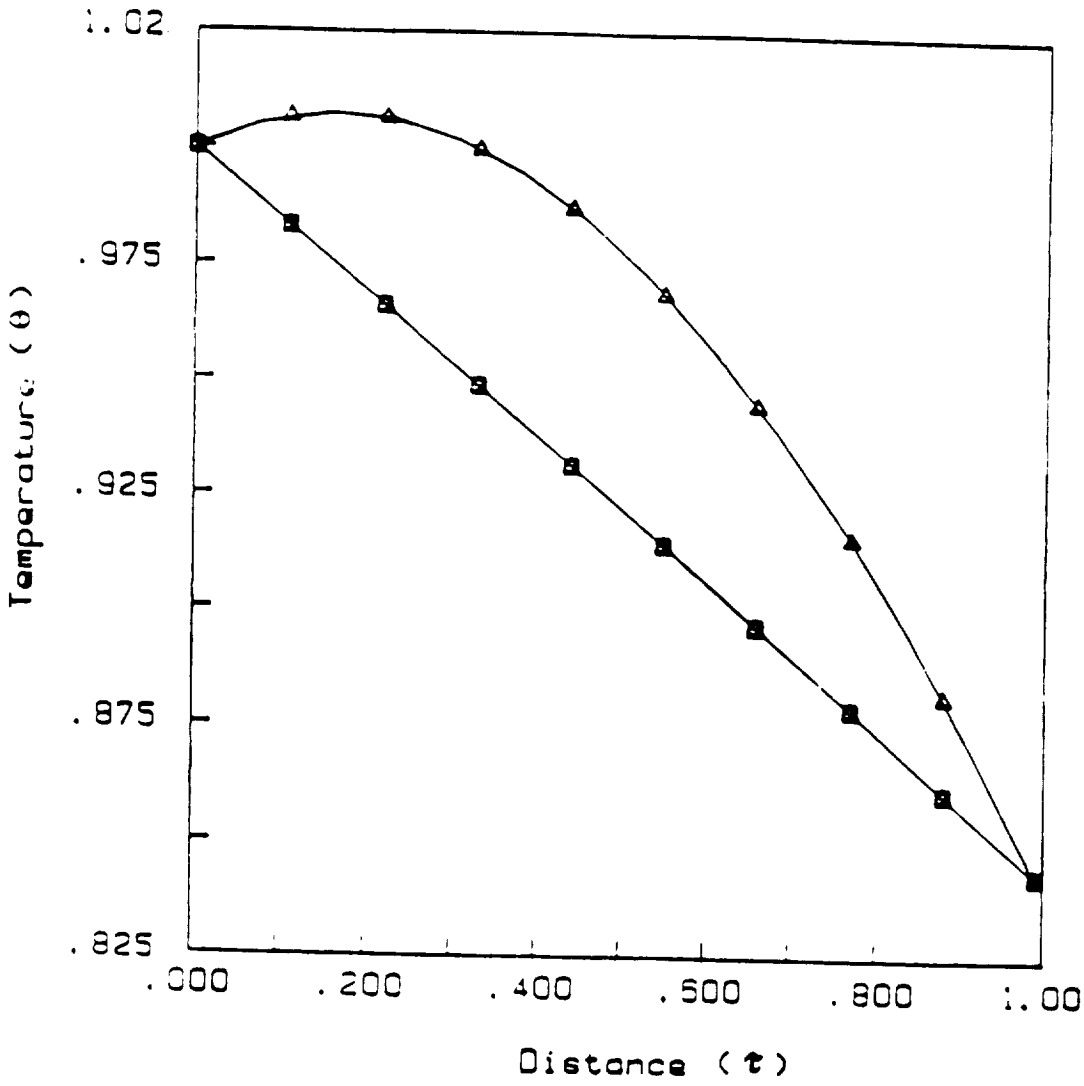

Figure 4.3 Variation of dimensionless temperature with distance for different ratios of conduction to radiation. Boundary temperatures are T_o = 1873K, T_b = 1673K. Δ is for n = 0.001, □ is for n = 1.0.

generally require an average emissivity value to calculate surface temperatures, and thus an opaque boundary is assumed. In Figure 4.4, is shown a comparison of an opaque alumina crucible with an average emissivity with heat transferred within the system purely by conduction, to the model developed in this study for a semitransparent material with the heat flux matched at the crucible/liquid metal interface. In Figure 4.4, this interface is located at radial distance of 1 mm. Since an optical pyrometer assumes an opaque boundary, it would over estimate the wall temperature by about 5°C. If one used the opaque model for open loop control, they would calculate a sample temperature 2-3°C lower than that of the semitransparent model. The semitransparent model (Figure 4.4) shows the expected hot spot within the crucible wall. This hot spot results from the various depths to which given frequencies of radiation can penetrate before being absorbed by the material. The degree to which the profile within the crucible influences the gradient within the liquid iron is a function of crucible thickness. Here a 1 mm crucible was assumed. Figure 4.4 suggest a possible solution for high temperature furnace control problems, ones in which direct temperature measurement techniques are impossible to employ due to material constraints. A combined approach would correct the optical pyrometer's temperature measurement using a semitransparent model to predict, in real time, the temperature profile within the sample. Thus, the power to the furnace element would be adjusted after a computer calculation of the predicted temperature versus the set point temperature was made. It should be noted that opaque boundary is commonly used to

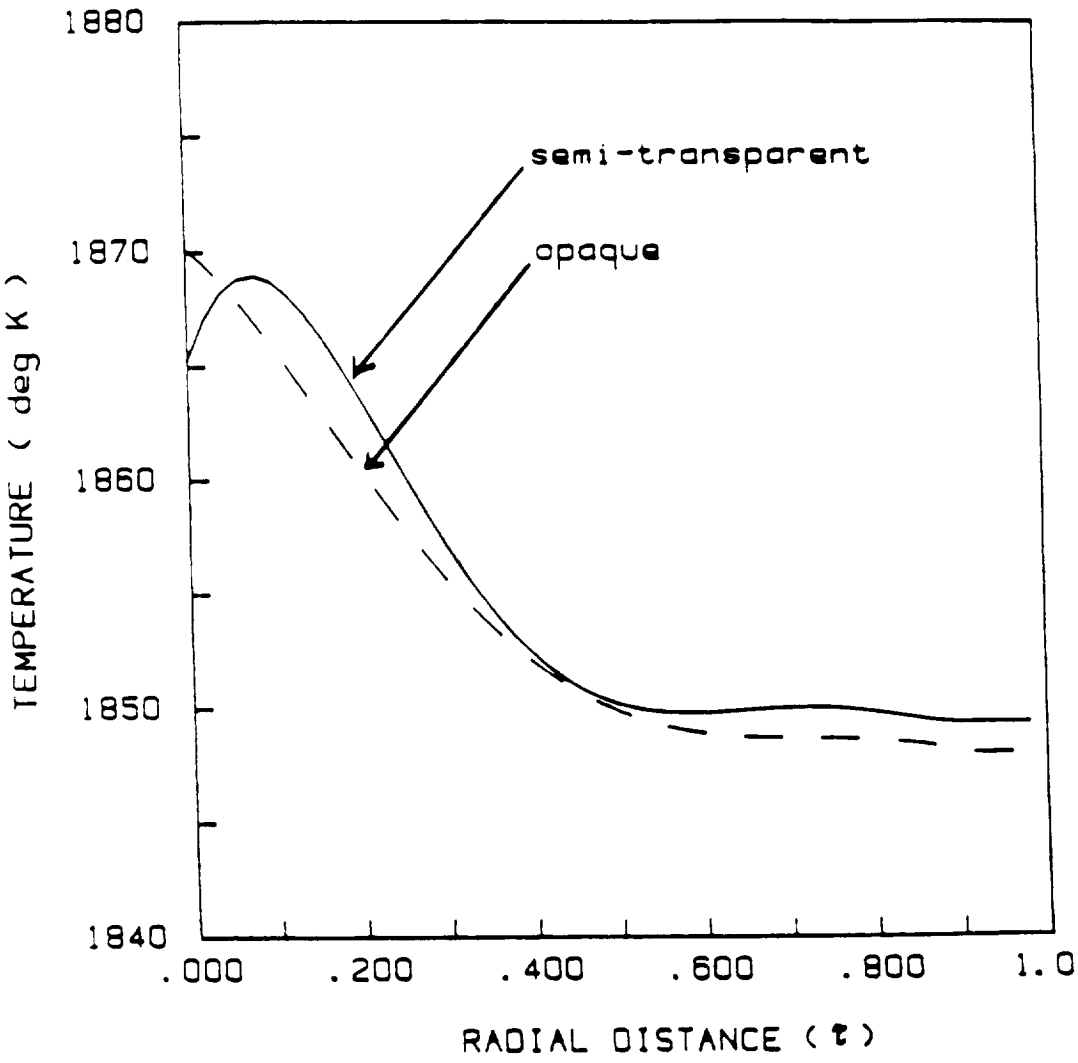

Figure 4.4 Temperature profiles for the Alumina Crucible and Liquid Iron Sample. ——— represents the profile for the semitransparent case while — — — represents the profile for the opaque assumption.

solve combined conduction/radiation problems in computer programs such as SINDA (Smith 1971). The one dimensional model failed to predict the thermal profiles within crucible walls as a function of crucible thicknesses, therefore a two dimensional model was required.

4.1.2 Two Dimensional Analysis

One of the main objectives of the two-dimensional analysis was to examine the effect of the variation in temperature profiles within crucible walls of varying thickness, with the heating element at a constant temperature of 1600°C. The results are shown in Figure 4.5 for different values on N (the radiation-conduction parameter). Here N is proportional to the ratio of crucible to liquid iron thicknesses, namely 1:3, 1:1, and 4:1. Therefore the variations in temperature profiles are a result of the total heat capacities of the crucibles and the heat dissipation in the axial direction within the liquid iron sample. Since heat is dissipated from both the top and bottom of the sample, the temperature profiles towards the ends will be more pronounced than the profiles within the center of the model.

When the relative thicknesses for the alumina crucible and the liquid iron samples are the same (see Figure 4.6) it was noticed that conduction in the liquid iron is strongly influenced by the thermal profile developed within the crucible wall. Notice that as the crucible wall gets thinner, the thermal profile increases to a maximum almost at the liquid iron interface. This suggests that an optical pyrometer observing the crucible wall would be largely measuring the temperature of the liquid iron surface.

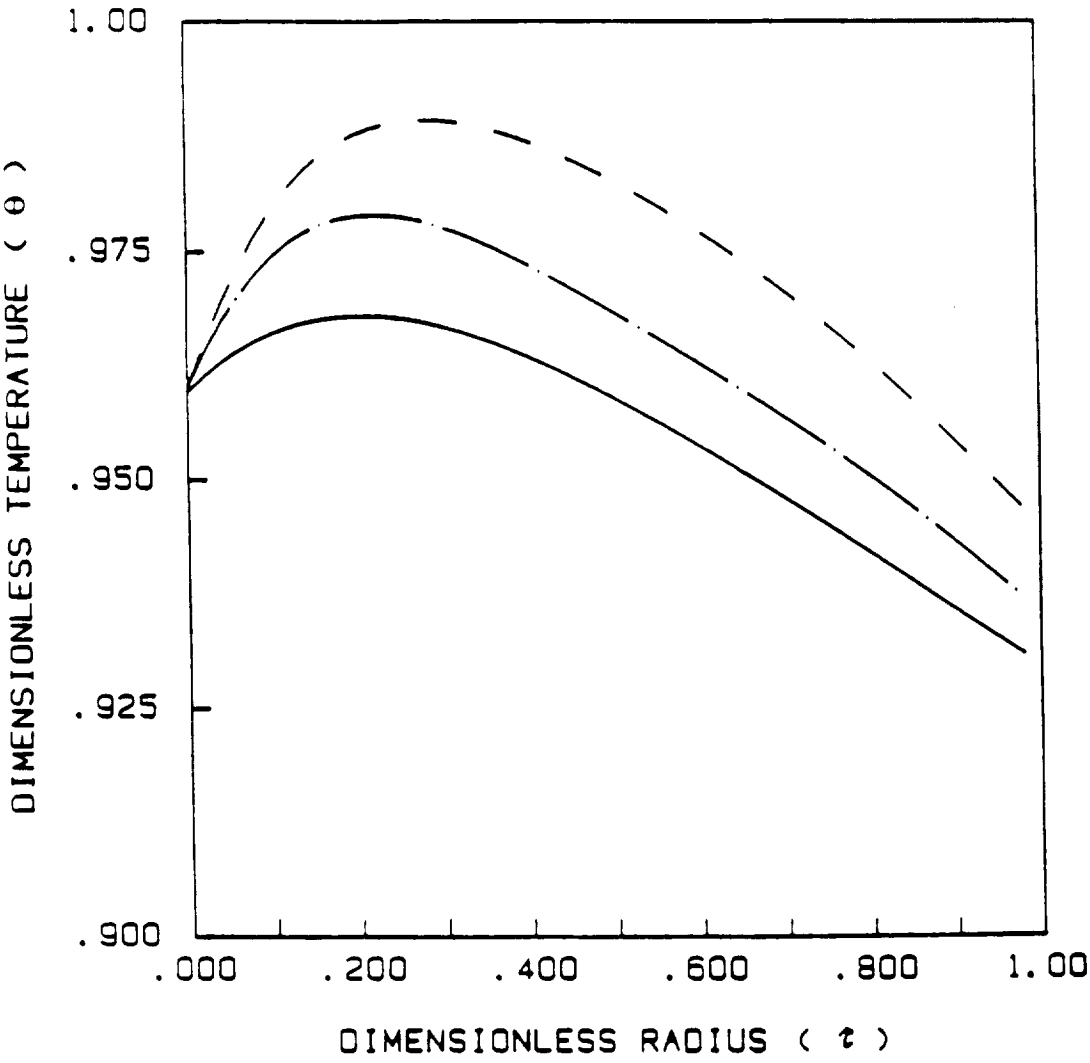

Figure 4.5 Variation of dimensionless temperature with radial distance for varying crucible thicknesses. (– – –) is for 1:3, (–•–) is for 1:1, (——) is for 4:1 ratio for crucible to iron sample.

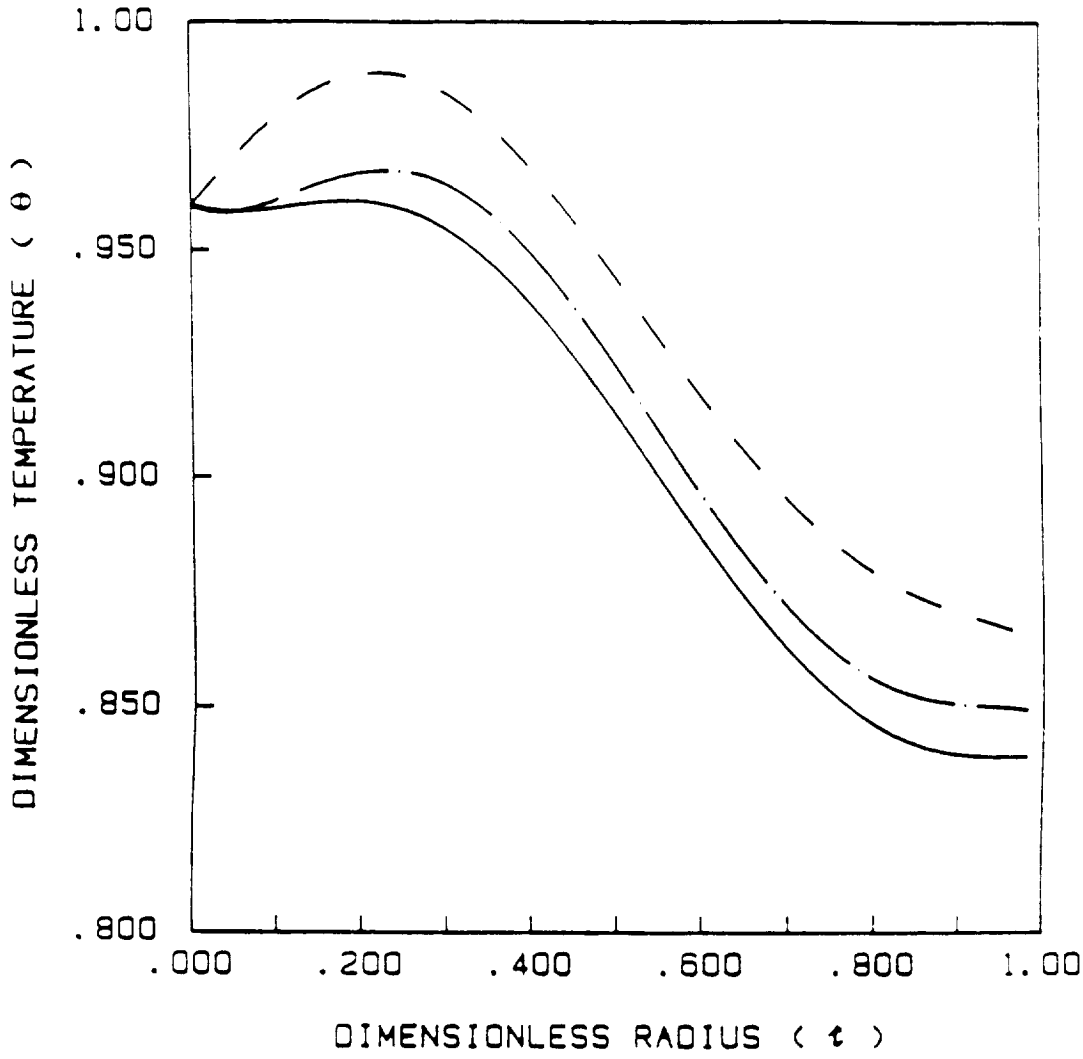

Figure 4.6 Variation of dimensionless temperature with radial distance for varying distances in the r direction. (- - -) is for η=0.75, (—·—) is for η=0.5, (——) is for η=0.25. Ratio of crucible to iron is 1:1.

In Figure 4.7, the ratio of the crucible wall thickness to that of the iron sample is 1:3. The temperature at the crucible/iron interface is much greater than for the previous cases. This is desirable since for a given power to the furnace, one would like to achieve a high temperature at the liquid iron interface while ignoring the crucible wall. This means that the radiative effects within the crucible are minimized with respect to the bulk sample.

4.2 EXPERIMENTAL OBSERVATIONS

In section 4.2.1 the results from the experiments performed and the problems encountered while using the commercial zirconia furnace are discussed. The experiments performed using the research furnace, including the design improvements are discussed in section 4.2.2.

4.2.1 Commercial Furnace

The initial experiments were designed to study the heat transfer characteristics of the commercial furnace. Figure 4.8 shows the centerline temperatures measured 1 inch from the bottom of the furnace by a thermocouple. These temperatures were matched to the pyrometer readings by increasing the input power to the furnace. The results are given in Figure 4.9. The results show a factor of two for the power requirements.

Figure 4.10 shows the measured axial temperature profile for 20% applied power, while Figure 4.11 shows the results at 30% applied power. Axial gradients of approximately 523K (250°C) per inch were determined for both figures. Temperatures were found to be higher at the furnace top than at equivalent distances from the

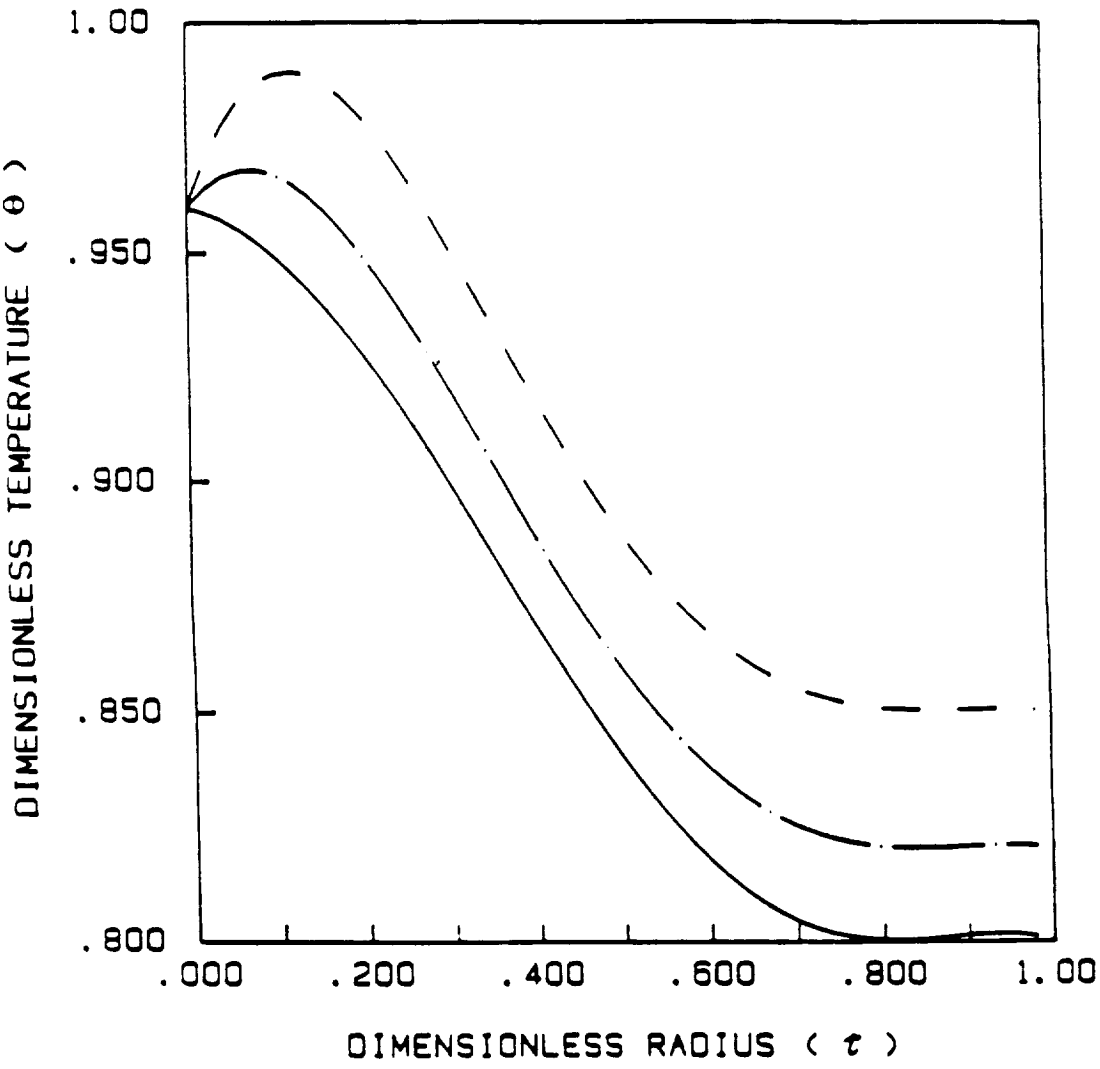

Figure 4.7 Variation of dimensionless temperature with radial distance for varying distances in the r direction. (- - -) is for η=0.75, (-·-) is for η=0.5, (——) is for η=0.25. Ratio of crucible to iron is 1:3.....

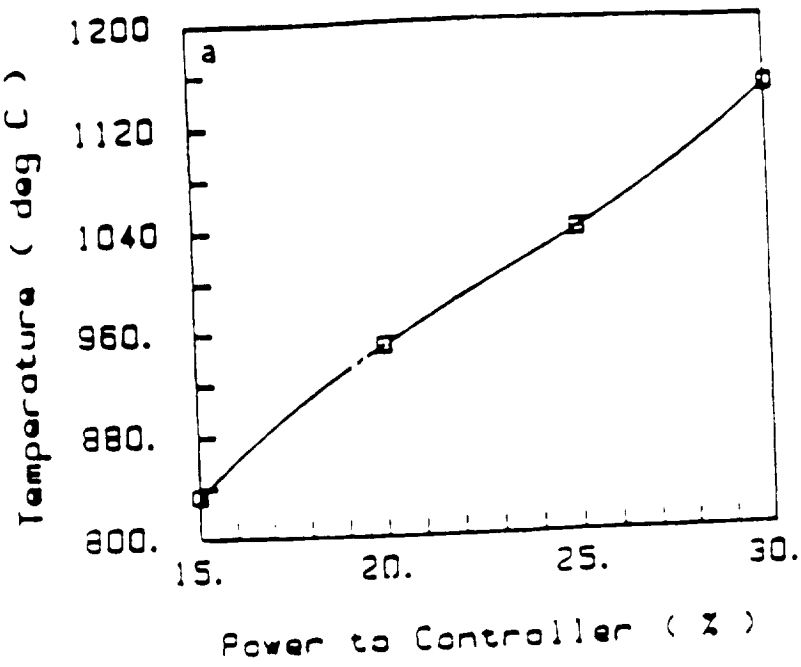

Figure 4.8 Temperature as a function of Applied Power for the ARTCOR Model 460-15 Furnace as Measured by a Thermocouple immersed along the Centerline of the Furnace.

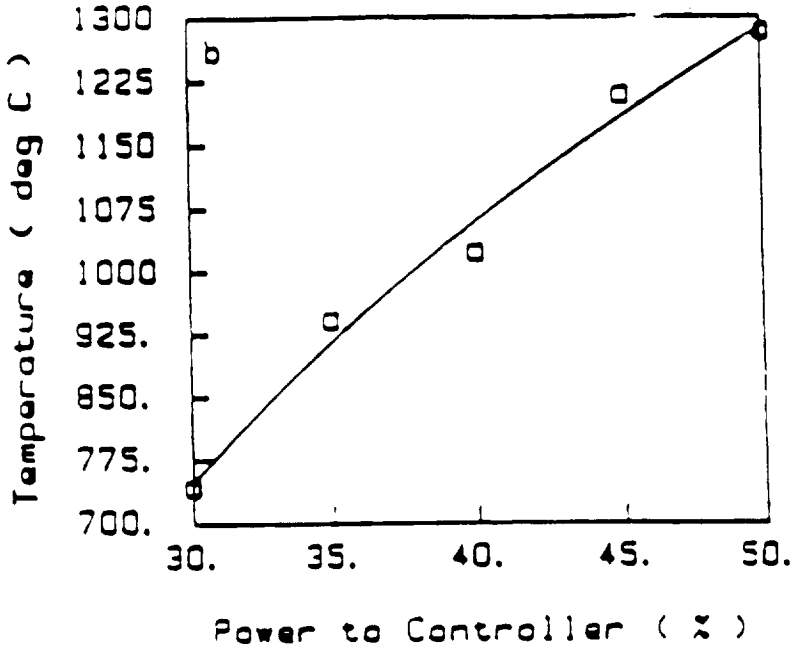

Figure 4.9 Temperature as a function of Applied Power for the ARTCOR Model 460-15 Furnace as Measured by a Water-Cooled OS-1000-HT Optical Pyrometer.

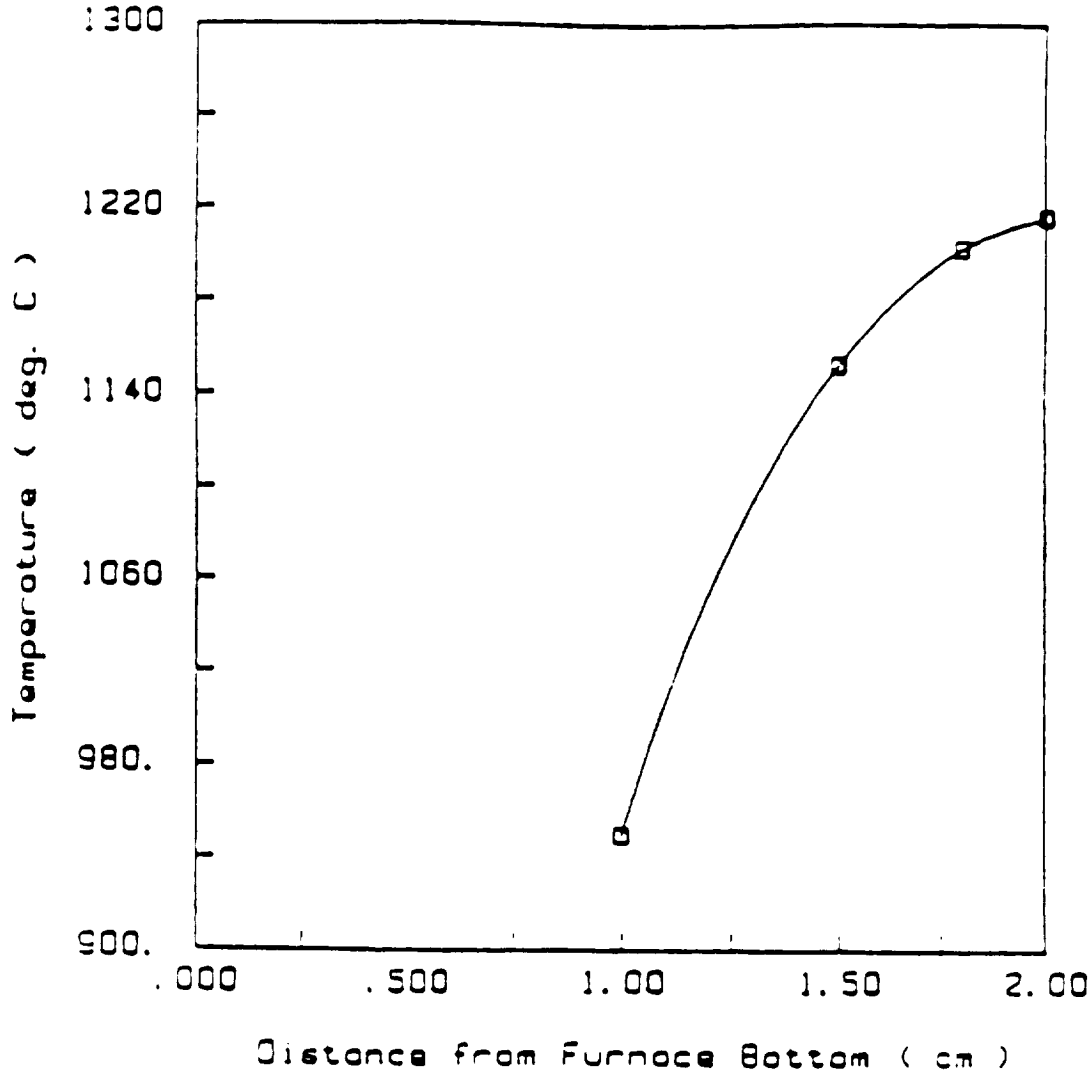

Figure 4.10 Axial Temperature Profile for the ARTCOR Model 460-15 Furnace at 20% Applied Power on the Controller.

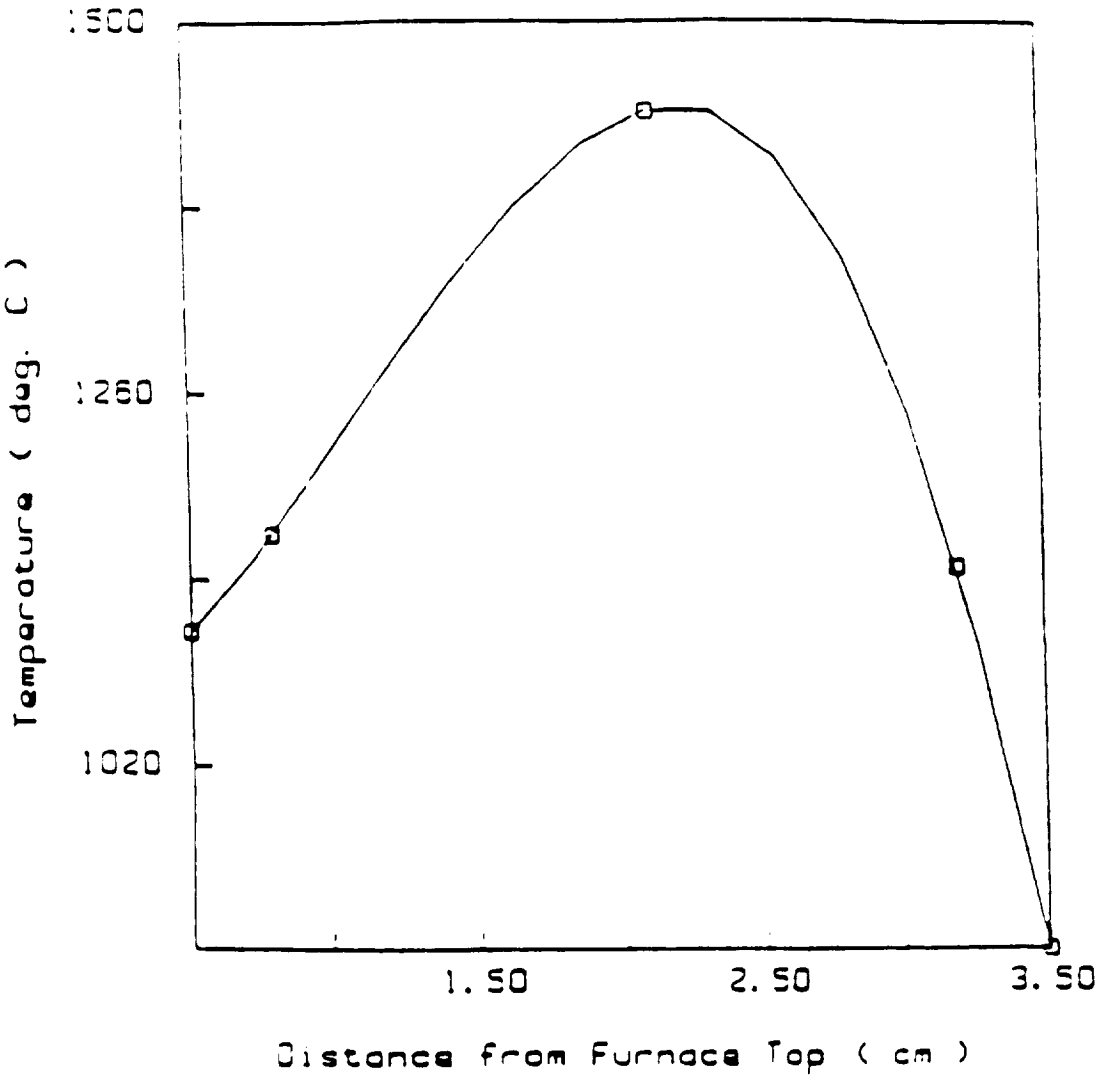

Figure 4.11 Axial Temperature Profile for the ARTCOR Model 460-15 Furnace at 30% Applied Power on the Controller.

furnace bottom as would be expected for a freely convecting medium.

Figure 4.12 shows the temperature response to a gradual increase in power at the rate of 1% per minute. It was found that the ratio of the increase in temperature to the applied power was approximately 1:15. A temperature overshoot of about 473ΔK (200°ΔC) was recorded.

After numerous experimental runs of the ARTCOR Model 460-15 Research Furnace, several problems were encountered. When the furnace was left for 48 hours or more, the main element would not ignite using the normal procedure of preheater setting of 40% applied power for 0.6 hours. It may be that the main heater element had a tendency to adsorb water vapor from the atmosphere, thus requiring a higher input of power by the preheater in successive runs.

The commercial furnace (shown in Figure 3.2) would not operate above a 50% power settings using the two commercial elements. The current and voltage achieved at 50% applied power were 3.7 amps and 80.0 volts, respectively. Identical current and voltage results were obtained at 60 and 70% applied power on the controller. Thus, a maximum power had been achieved for the commercial element.

Two commercial elements were used during a portion of this study. Both the elements failed prematurely compared to the manufacturer's suggested lifetime. The first zirconia element lasted for a total of 15 hours at main heater power settings varying from 15% to 50% applied power. The power setting of 50% corresponds to about 4 amps and 80 volts across the element, or 320

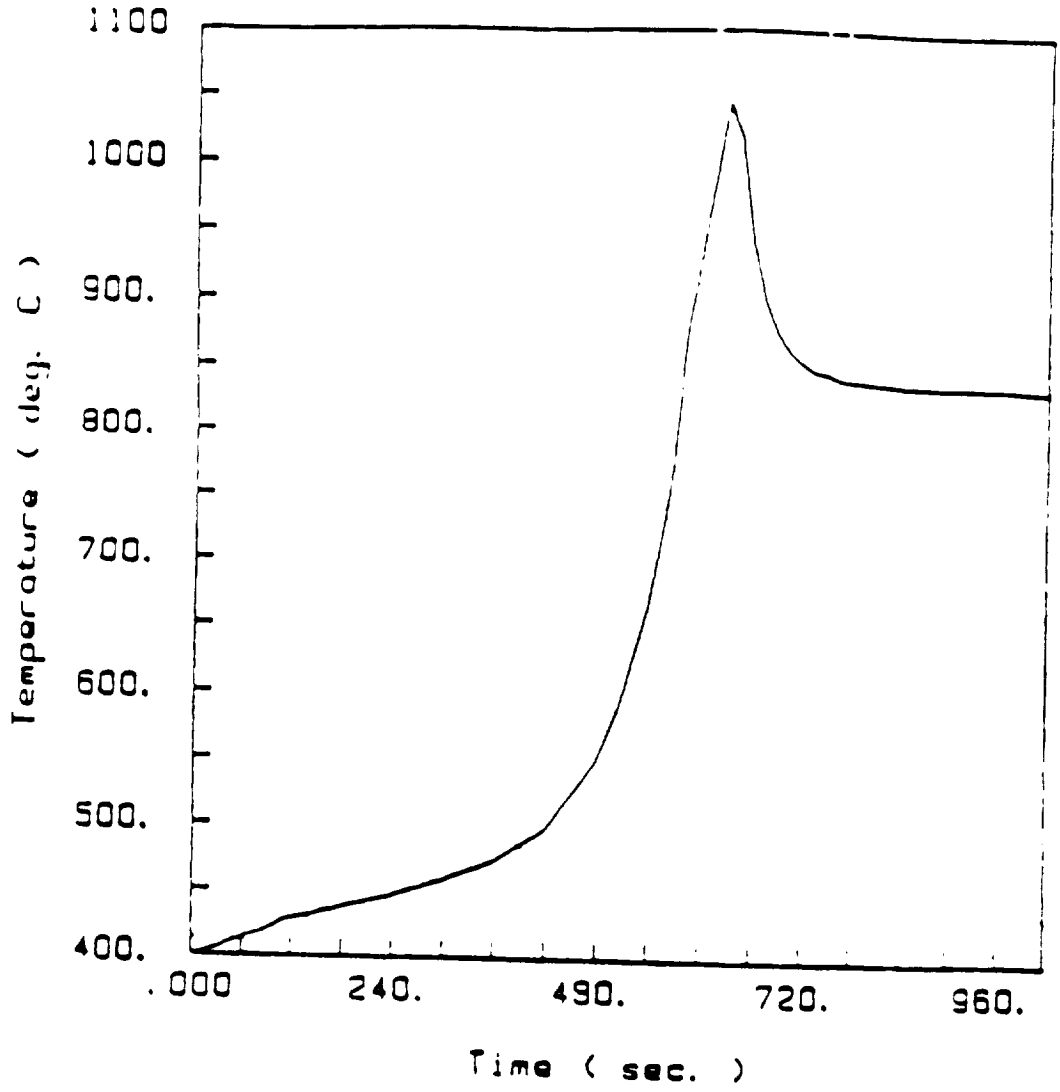

Figure 4.12 Temperature Response for the ARTCOR Model 460-15 Furnace to a Linear Applied Power Increase at a rate of 1% per minute. Final Applied Power was 15%.

watts. The second element was initially started using a 43% preheater power for 0.8 hour. This procedure was able to start the main heater element, but may have been the cause of its shorter lifetime as will be explained later. This element lasted for a total of only 3 hours at main element powers of 40% to 50%.

Figure 4.13 is a photograph of the two zirconia main heater elements. Element 1 is the shorter of the two elements shown. Under a microscope, both elements showed defects that appeared as glassy regions with a channeled structure at the points where the cracks could have initiated. Both cracks seemed to have initiated in the hottest zone of the furnace.

A possible explanation for the difference in lifetime between the two elements studied, may be that the first element received a slow cure while the second received a much faster cure. Slow curing may have removed water from the ceramic and further sintered the ceramic, providing greater strength. Additionally, preheating at 1073 - 1173K (800 - 900°C) may have partially annealed the ceramic thereby reducing stresses within the element.

Another possible explanation could be that the element, relative to its final operating condition, may be partially green. The elements may contain trace water within the matrix. Element #2 received both a rapid cure and a higher applied power than element #1. Perhaps element #1 had sufficient time for the water to diffuse through the nonporous zirconia matrix prior to heating at a lower power setting.

Pure water may act as an insulator if trapped within the zirconia element. Water trapped within the matrix at the high

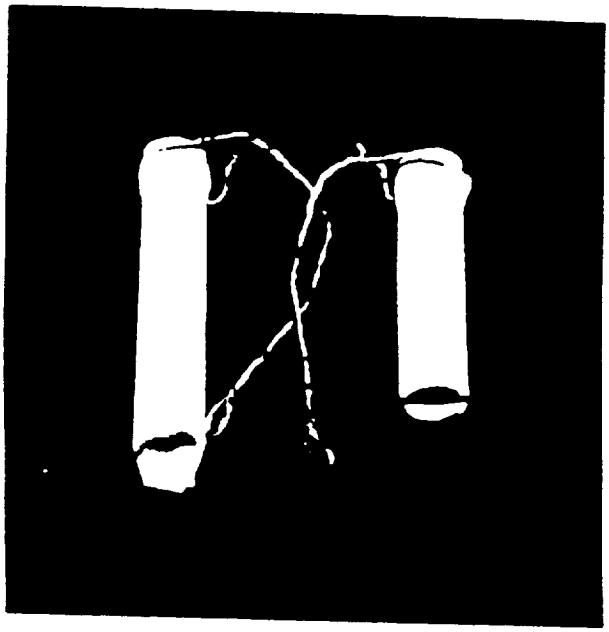

Figure 4.13 Zirconia Main Heating Elements. Element #1 is the shorter of the two elements which lasted a total of 15 hours, while element #2 lasted only 3 hours.

operating temperatures of the zirconia main heating element would convert to steam within the matrix resulting in an extremely high local pressure gradient. Element #2 may have been manufactured at the same time as element #1 and was stored locally for about 8 months. During this time it may have accumulated additional moisture from the atmosphere. Water is again suggested in the extra power required to heat the elements after sitting in a humid environment. This is partially supported by the microscopic investigation discussed above.

If we assume that water adsorbed into the element, it needed to be evaporated prior to ignition. This may have caused a pressure gradient within the element which resulted in a high stress distribution that lead to cracks and ultimate failure of the element.

After the preliminary studies were performed using the commercial heating elements and the results analyzed as above, the study focused on efforts to design improved zirconia elements and furnace component parts.

4.2.2 Research Zirconia Furnace

In order to analyze why the element's lifetime was shorter than expected, several controlled experiments needed to be performed; therefore a more economical design of the furnace elements for research was required.

In an effort to reduce the cost of replacement elements and to study the elements in greater detail, preliminary studies were performed on techniques to design new experimental elements, that reduced the cost and performed as required. There were two basic

components to the main heating element. These were basically 2 high temperature high current lead wires and a high density high purity piece zirconia tubing.

The new main heater elements, were manufactured from high purity zirconia tubes with 1/4 inch platinum bands on each end. Platinum bands were added to permit better contact between the zirconia tube and the platinum-rhodium lead wires. The method of attachment of the wires to the platinum band was devised based on oxygen sensors technology. The lead wires, composed of 90% platinum - 10% rhodium alloy, were selected to carry the required current at the maximum operating conditions. The Pt band/paste combination provided a good electrical connection to the zirconia element.

The experimental runs were designed to study several aspects of the new zirconia heating elements. These newly developed elements (with layout shown in Figure 3.4) were powered to values of 70% power at currents of 6.0 amps and voltages of 80 volts. In this set of experiments (set #2), the furnace was equipped with two independent power supplies, one to power the preheater and the other to power the main heater element. This configuration eliminated the uncertainties in igniting the main zirconia heater element, that were caused by the element not reaching its conduction temperature (1073K).

Figures 4.14 and 4.15 show the results of one of these experiment. In Figure 4.14 is shown the current history from the element operated at a constant voltage of 98 VAC. Notice that the current rises as a function of time due to the fact that as the element heats its resistance continually decreases (Figure 4.15)

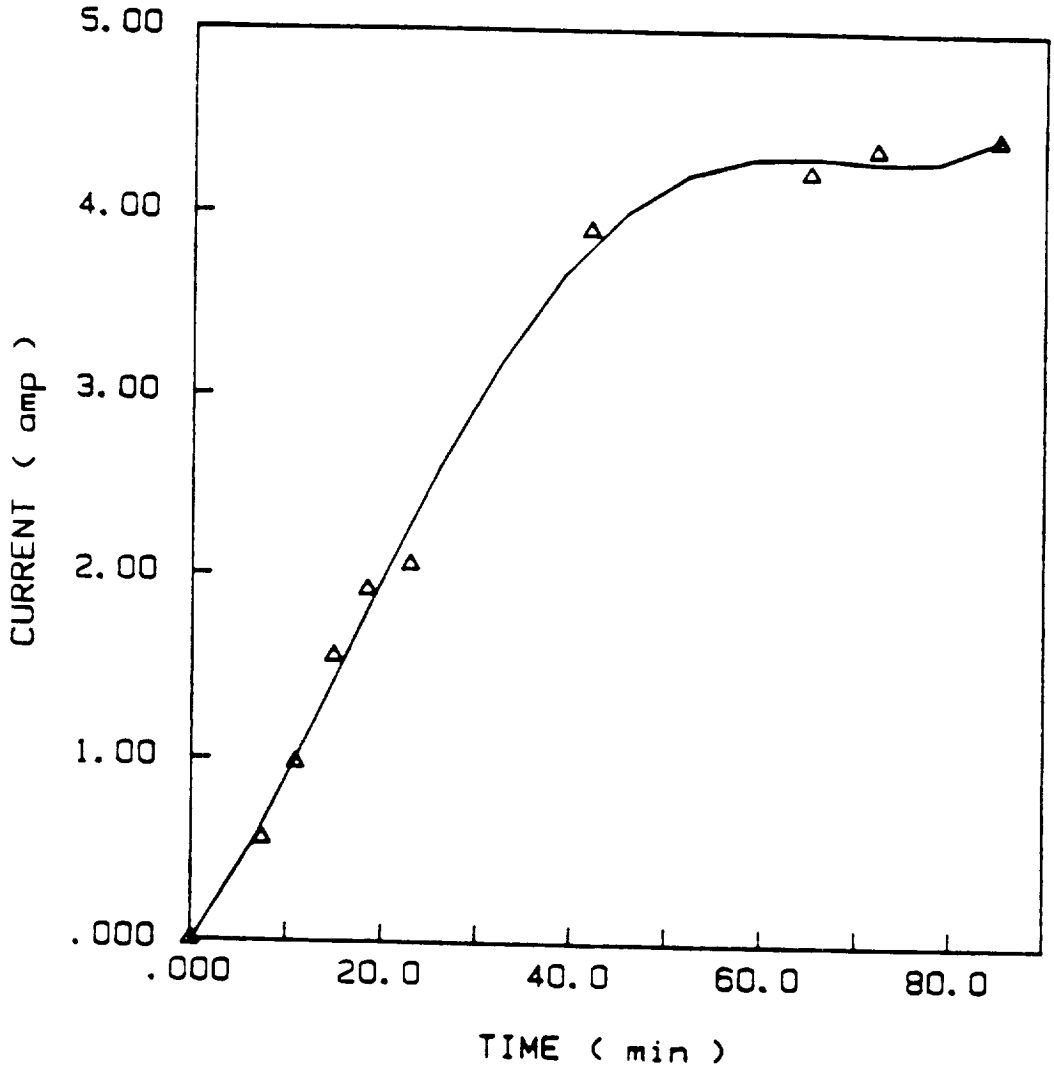

Figure 4.14 Variation of Current with Time for a Constant Voltage of 98 VAC.

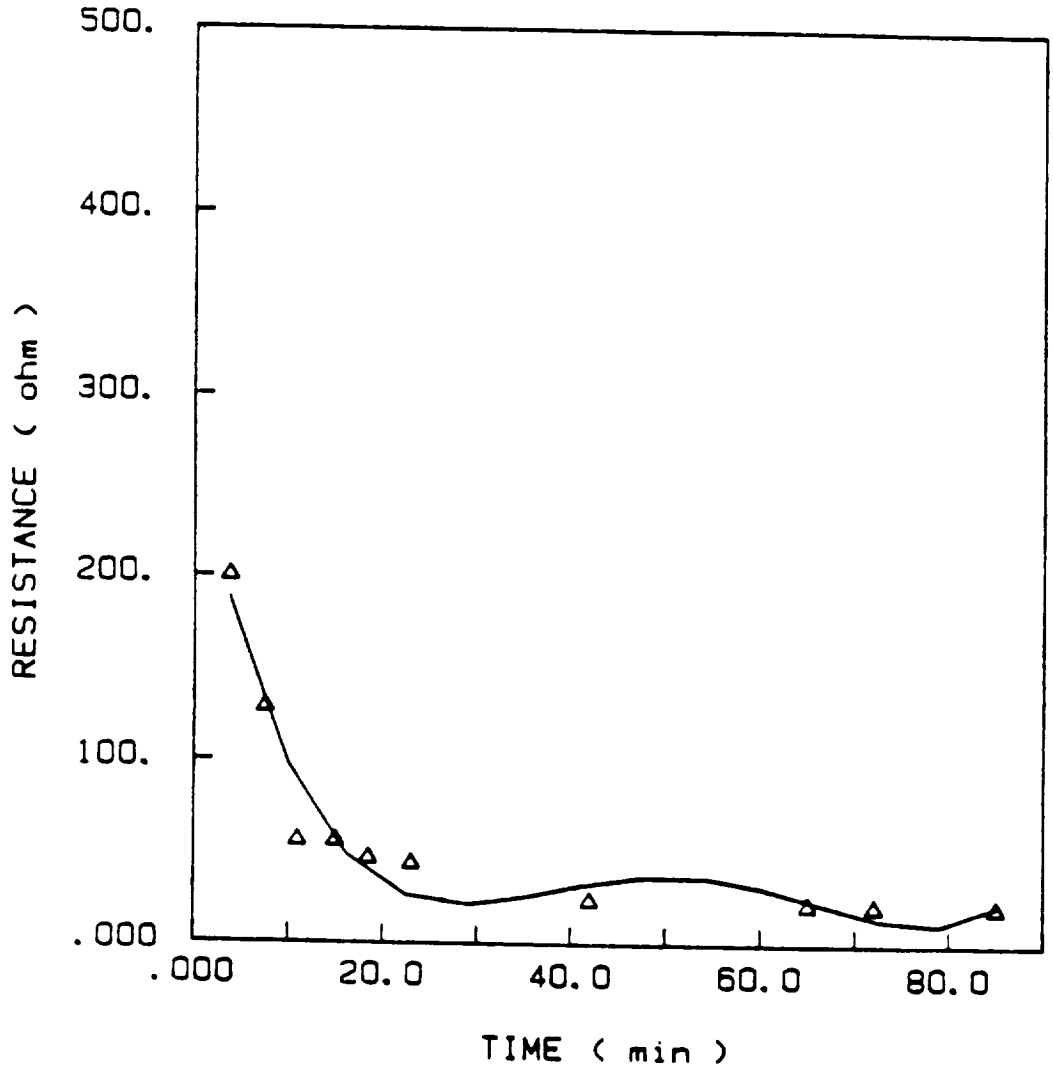

Figure 4.15 Variation of Resistance with Time for a Constant Voltage of 98 VAC.

from about 445 ohms to a final resistance of 21.2 ohms. This corresponds to a current of 4.62 amps after about 1 1/2 hours of operation. The new zirconia element operated for over 25 hours without failure. The commercial elements carried a measured maximum current of 4.6 amps, while the new element was found to carry currents of over 7 amperes. Higher current loads measured in the new element may resulted from techniques used to attach the lead wires.

The centerline temperatures that were measured for the the improved zirconia heating elements are shown in Figure 4.16. Also shown in Figure 4.16 is a comparison of the temperature readings between the thermocouple measurements of the centerline temperatures within the alumina crucibles and the pyrometer readings through the viewing hole. The reason for this wide difference in the readings was due to differences between the aperture of the pyrometer and the diameter of the viewing hole provided by the manufacturer. This difference would be very significant if the furnace in its current configuration were to be used in materials processing experiments.

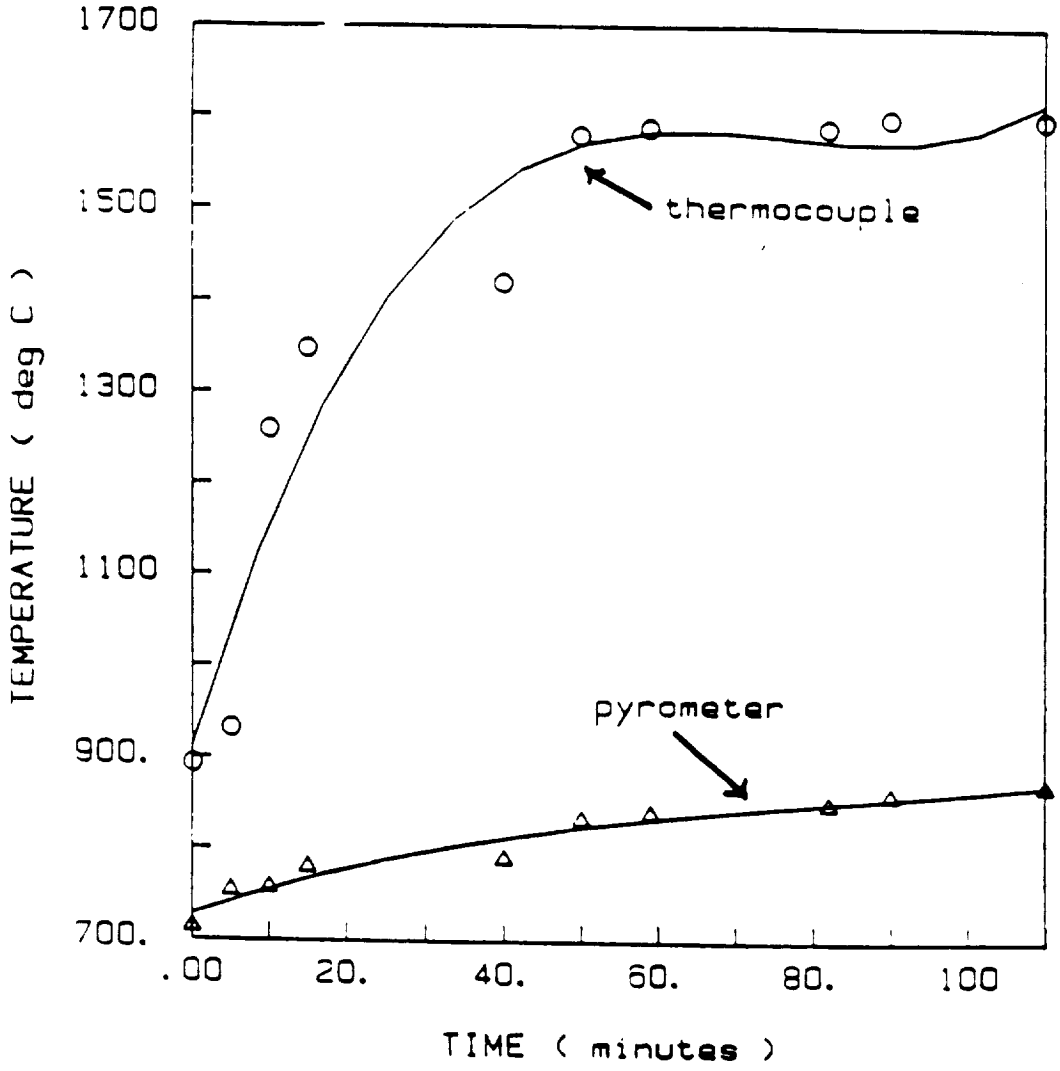

Figure 4.16 Centerline Temperatures as Measured by a Thermocouple compared to Temperatures Measured by Optical Pyrometer for Experiment Set #2.

CHAPTER 5

CONCLUSIONS AND RECOMMENDATIONS

5.1 CONCLUSIONS

In the one dimensional radiation/conduction analyses it was shown that the transmissivity of a material has a significant effect on the temperature profile when radiation is considered at such high temperatures. Considering the physical model, it was shown that the crucible wall appears thermally thinner than its physical thickness. Since the hot zone is within the crucible wall, temperature measurements made using optical pyrometry need to be adjusted if adequate control is to be achieved. It has been demonstrated that the variable radiation properties are significant in the analysis of radiation/conduction problems at such extreme temperatures.

The two dimensional model proved to be very successful in modeling the furnace crucible. The results have provided a greater detailed understanding of the components of this advanced high temperature furnace. The parametric study of the ratio of the crucible wall to the liquid iron sample, has shown that there is a significant increase in the temperature at the interface (between the liquid iron sample and the crucible wall) with decreasing crucible thickness. Also, the radiation effects on the sample are greatly reduced for thin crucible walls. This allows a greater portion of the iron sample to attain a more uniform radial temperature profile relative to the centerline. For a thick wall,

an optical pyrometer would have measured the average temperature of the crucible wall. Optical pyrometer measurements for a thin crucible wall would approximate the interfacial temperature at the liquid iron sample. The general conclusion from this portion of the study is to select as thin a crucible as will tolerate the loads applied during processing.

Initial performance data for a new zirconia element design was presented, and results show consistent performance and greater power handling capabilities. As discussed in the results, the higher current loads are a result of the improved junction used for this zirconia element. Procedural modification followed for the new element, indicate that the preheater power should not be shut off until the zirconia element has ignited. Therefore one has to either have two independent power supply sources for the preheater and main heater, or have a feedback control scheme that will monitor the current in the main zirconia element prior to disconnection of the preheater power.

Centerline temperature measurements using thermocouples recorded temperatures twice as high as the pyrometer measurements for equal power inputs. After modification of either the pyrometer focal length or increasing the diameter of the viewing hole, better correlations between these two temperature measurements will be possible. With the integration of the numerical modeling and the temperature measurements from the optical pyrometer, it may be possible to develop a feedback control scheme for use with these furnaces. Electronics with variable emissivities accessible from a digital computer would greatly aid in the accurate measurement of

the wall temperature when using commercially available optical pyrometers.

5.2 RECOMMENDATIONS

Several improvements could be made in the area of control for this type furnace. Detailed studies are needed to verify the extent and sensitivity of the zirconia elements to water vapor. Experiments are needed that will measure the centerline temperature of the furnace while solidifying several pure metal systems. This approach will provide a consistent reference for numerical modeling and to both calibrate the experimental apparatus.

A suggested experimental setup is shown in Figure 5.1. For this open loop control scheme, the computer would contain a numerical model capable of predicting the temperature profile of the furnace sample based on accurate optical pyrometer measurements. The computer could also estimate the average emissivity based on the spectral bandpass of the emitting wall as a function of temperature. This value would serve as input to the optic pyrometer, thus minimizing another source of potential error that occurs when an average emissivity is used over the entire range of operating temperatures. In addition the computer should be equipped with current monitors to control both the preheater and main heater power supplies.

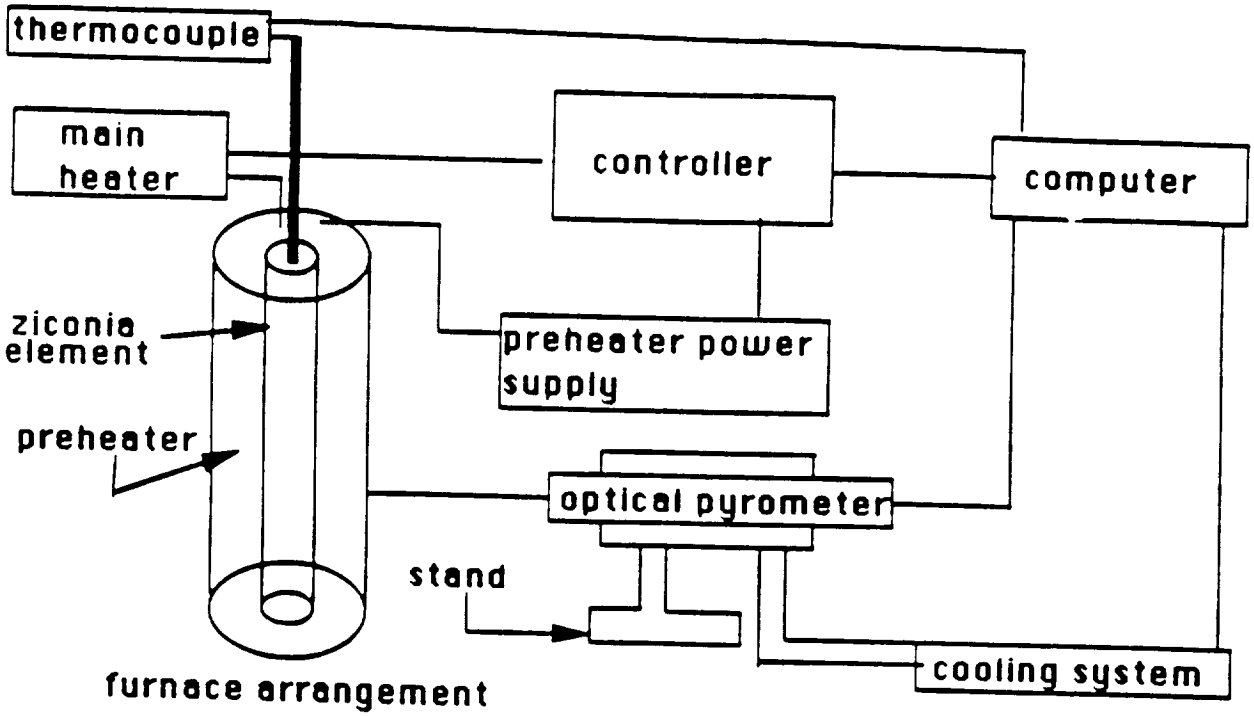

Figure 5.1 Recommended Layout of the Experiment including Auxiliary Systems.

APPENDICES

APPENDIX A

TEMPERATURE MEASUREMENT DEVICES

I. THERMOCOUPLES

TYPE S

Platinum-10% Rhodium - Platinum

Temperature Range 335 - 1750°C

Error ± 2.3°C

Resolution 1°C

TYPE K

Chromel - Alumel

Temperature Range 200 - 1250°C

Error ± 2.0°C

Resolution 1°C

II. OPTICAL PYROMETER

TYPE OS-1000-HT

Optics

Spectral Response	2.0 - 2.5 microns
Resolution	50:1(1°),90% energy
Minimum Spot Size	1.5 cm at 76 cm

Accuracy

±1% of reading, ±1 digit at 25°C head temperature

APPENDIX B: FORTRAN PROGRAM FOR ONE DIMENSIONAL RADIATION/CONDUCTION MODEL

```
      PARAMETER (ND = 100, ND2 = 200)
      EXTERNAL AFUNC, THERM1, THERM2,ADSIMP
      DIMENSION A(ND,ND),B(ND),T(ND),W(ND),
     $ DIFF(ND),AFT(8),ER(2),TC(ND),QT(ND),
     $ WW(ND),EE(ND),FT(ND2),DIST(ND)
C
      SIGMA = 5.669E-12
      TOL = 1.0E-6
      IER = 0
      OPEN (6,FILE = 'CRUC1.DAT',STATUS = 'NEW')
C INITIALIZE THE MATRICES
      DO 1 I = 1, ND
         B(I) = 0.0
         T(I) = 0.0
         W(I) = 0.0
         WW(I) = 0.0
         DO 1 J = 1, ND
            A(I,J) = 0.0
   1  CONTINUE
C RANGE OF WAVE LENGTHS AND INITIAL GUESS TEMPERATURES
      WRITE(*,*) 'ENTER T(1)   T(ND)'
      READ(*,*) T(1), T(ND)
      WRITE(*,*) 'ENTER SL AND BL '
      READ(*,*) SL, BL
      H = 1/ND
      DIST(1) = 0.0
      DO 6 I = 2, ND
         DIST(I) = DIST(I-1) + H
 6    CONTINUE
      COUNT = 0.0
 200  IF (COUNT.GT.0.0) THEN
         IF (FLX2.GT.FLX1) THEN
            T(ND) = T(ND) + 3.0
            P = T(ND)
         ELSE
            T(ND) = T(ND) - 2.5
            P = T(ND)
         ENDIF
      ELSE
         WRITE(6,*)'COUNTER  =  ',COUNT
      ENDIF
      DO 5 I = 1, 8
         AFT(I) = ADSIMP(AFUNC,SL,BL,TOL,IER,I)
 5    CONTINUE
      CALL RAD(ND,T,B,H,SL,BL,ND,FLX1)
      WRITE(*,*) 'FROM RADIATION FLUX AT JOINT = ',FLX1
      DO 2 I = 1, ND
         FT(I) = T(I)
 2    CONTINUE
      CALL CONDUCT(ND,T,H,HH,ND,FLX1,FLX2)
C
```

```
      WRITE(*,*) 'FROM CONDUCTION FLUX AT JOINT = ',FLX2
      DO 3 I = 1, ND2
         FT(I+10) = T(I)
 3    CONTINUE
      COUNT = COUNT + 1
      IF(COUNT.GT.100.0)GOTO 300
C CONDITION FOR STOP
      IF(COUNT.GT.0.0) THEN
        ER(2) = ER(1)
        ER(1) = ABS(FLX2 - FLX1)
        ERA = ABS(ER(1) - ER(2))
        IF (ERA.GT.1.0E-2) THEN
           WRITE(*,*)'ERROR IN  FLUXES  ',ERA
           GOTO 200
        ELSE
           WRITE(*,*)'ERROR AND FLUX1 FINAL ',ERA,FLX1
        ENDIF
      ELSE
      ENDIF
 300  WRITE(*,*) '# OF ITERATIONS = ',COUNT
      WRITE(*,*)'ERROR IN FLUX AT JOINT = ',ERA
      WRITE(*,*)'FLUX AT RAD/COND JOINT = ',FLX1,FLX2
      DO 4 I = 1, ND2
         WRITE(*,*)I,' = ',FT(I)
 4    CONTINUE
      STOP
      END
C
      SUBROUTINE RAD(ND,T,B,H,SL,BL,ND,FLX1)
      DIMENSION A(ND,ND),B(ND),T(ND),W(ND),DIFF(ND),AFT(8)
     $          TC(ND),QT(ND),WW(ND),EE(ND),FLXR(ND),
     $          PT(ND)
      T(1) = Q
      T(ND) = P
      PT(1) = T(1)
      COUNT2 = 0.0
      SIGMA = 5.669E-12
      TOL = 1.0E-6
      IER = 0
      WW(1) = 0.0
      WWW = 0.0
      DO 423 I = 2 , ND
       WW(I) = H + WWW
       WWW = WWW +H
 423  CONTINUE
C
      Z = (T(1) - T(ND))/ND
      DO 4 I = 2, ND-1
         T(I) = T(1) - I*Z
         PT(I) = T(I)
 4    CONTINUE
      DO 41 I = 1,ND
        QT(I) = T(I)/T(1)
 41   CONTINUE
```

```
      MM = 1
C ADJUSTING GUESS VALUES
      IF(MM.GT.0)GOTO 212
 37   DO 42 I = 2, ND-1
         IF(PT(I).GT.T(I)) THEN
           PT(I) = T(I)
           T(I) = T(I) + 0.5*DIFF(I)
           QT(I) = T(I)/T(1)
         ELSEIF(PT(I).LT.T(I))THEN
           PT(I) = T(I)
           T(I) = T(I) - 0.5*DIFF(I)
           QT(I) = T(I)/T(1)
         ELSE
         ENDIF
 42   CONTINUE
 212  Y=1.0
      DO 22 I = 1,ND
           TC(I) = 0.01*THERM1(T(I))
 22   CONTINUE
C GENERATE MATRIX [A] and [B]
      A(1,1) = 1.0
      A(ND,ND-1) = TC(ND) + TC(ND-1)
      A(ND,ND) = -A(ND,ND-1)
      DO 2 I = 2, ND-1
        A(I,I-1) = (0.5*(TC(I-1) + TC(I)))/(H**2)
        A(I,I) =-(0.5*TC(I-1) + TC(I) +
     $       0.5*TC(I+1))/(H**2)
        A(I,I+1) = (0.5*(TC(I) + TC(I+1)))/(H**2)
 2    CONTINUE
C
      CALL FORCE(ND,QT,W,B,AFT,SL,BL,TOL,IER)
      B(1) = 1.0
      B(ND) = AFT(2)*SIGMA*(T(ND)**4)
      CNTERM =(SIGMA*(T(1)**3))/AFT(3)
      DO 5 I = 2, ND-1
         B(I) = -1.0*(CNTERM*B(I))
 5    CONTINUE
C
      CALL GAUSS(ND,A,B)
C
      DO 666 I = 1, ND
         QT(I) = B(I)
         T(I) = T(1)*B(I)
 666   CONTINUE
      DO 8 I = 1, ND
         W(I) = T(1)*B(I)
         WRITE(*,*)WW(I),' , ',W(I)
 8    CONTINUE
      FLXR(ND)= (3.*T(ND) - 4.*T(ND-1) + T(ND-2))/(2.*H)
      FLX1 = 0.4*SIGMA*(T(2)**4 - T(1)**4) + FLXR(ND)*
     $          THERM1(T(ND))
      DO 13 I= 2 , ND
          DIFF(I) = ABS(PT(I) - T(I))
 13   CONTINUE
```

```
C      CONDITION FOR STOP
       MM = MM+1
       COUNT2 = COUNT2 + 1.0
       IF (COUNT2.GT.20.0) GOTO 300
       DO 14 I = 1, ND
         IF(DIFF(I).GT.0.5) GOTO 37
 14    CONTINUE
 300   WRITE(*,*)' TOTAL ITRS FOR RADIATION ---- ',COUNT2
       RETURN
       END
C
       SUBROUTINE CONDUCT(ND,T,H,HH,ND,FLX1,FLX2)
       DIMENSION A(ND,ND),B(ND),T(ND),U(ND),DIFF(ND),
      $          BFLX(2),TC(ND),QT(ND),UU(ND),EE(ND),
      $          FLXC(ND)
C
       T(1) = T(ND)
       COUNT3 = 0.0
       SIGMA = 5.669E-12
       TOL = 1.0E-6
       IER = 0
       UU(1) = 0.0
       UUU = 0.0
       DO 423 I = 2 , ND
        UU(I) = HH + UUU
        UUU = UUU +HH
 423   CONTINUE
       Z = 1.0
       DO 4 I = 2, ND
          T(I) = T(I-1) - Z
 4     CONTINUE
C GENERATE MATRIX [A] and [B]
       DO 41 I = 1,ND
         QT(I) = T(I)/T(1)
 41    CONTINUE
       MM = 1
C ADJUSTING GUESS VALUES
       NDD = ND - 1
       IF(MM.GT.0)GOTO 212
 37    DO 42 I = 2, ND-1
          IF(BFLX(1).GT.BFLX(2))THEN
            IF(I.EQ.NDD)T(ND) = T(ND) - 0.5
            T(I) = T(I) - 0.1*DIFF(I)*T(1)
            EE(I) = QT(I)
            QT(I) = T(I)/T(1)
          ELSE
            IF(I.EQ.NDD)T(ND) = T(ND) + 0.5
            T(I) = T(I) + 0.1*DIFF(I)*T(1)
            EE(I) = QT(I)
            QT(I) = T(I)/T(1)
          ENDIF
 42    CONTINUE
 212   Y=1.0
```

```
      DO 22 I = 1,ND
           TC(I) = 0.01*THERM2(T(I))
 22   CONTINUE
      A(1,1) = 1.0
      A(ND,ND-1) =-(TC(ND)+TC(ND-1))
      A(ND,ND) = -A(ND,ND-1)
      A(ND,ND-1) = 1.0
      DO 2 I = 2, ND-1
        A(I,I-1) = (0.5*(TC(I-1) + TC(I))
        A(I,I) = -(0.5*TC(I-1) + TC(I) + 0.5*TC(I+1))
        A(I,I+1) = (0.5*(TC(I) + TC(I+1))
 2    CONTINUE
      B(1) = 1.0
      DO 5 I = 2, ND
         B(I) = 0.0
 5    CONTINUE
C
      CALL GAUSS(ND,A,B)
C
        DO 666 I = 1, ND
         QT(I) = B(I)
         T(I) = B(I)*T(1)
 666    CONTINUE
      DO 8 I = 1, ND
         U(I) = T(1)*QT(I)
         WRITE(*,*)UU(I),' , ',U(I)
 8    CONTINUE
        BFLX(2)=BFLX(1)
        FLXC(1)= (-3.*T(1) + 4.*T(2) -T(3))/(2.*HH)
        WRITE(*,*)'CONDUCTION flux at 1 = ',FLXC(1)
        FLXC(ND)= (3.*T(ND) - 4.*T(ND-1) +
     $       T(ND-2))/(2.*HH)
        WRITE(*,*)'CONDUCTION flux at ND = ',FLXC(ND)
        FLX2 = FLXC(1)
        BFLX(1) = FLXC(ND)
        FLX2 = THERM2(T(1))*FLXC(1)
        DO 13 I= 2 , ND
          DIFF(I) = ABS(QT(I) - EE(I))
  13  CONTINUE
C     CONDITION FOR STOP
      WRITE(*,*)'CONDUCTION iterations = ',MM
      MM = MM+1
      COUNT3 = COUNT3 + 1.0
      IF (COUNT3.GT.20.0) GOTO 300
      DO 14 I = 1, ND
        IF(DIFF(ND).GT.1.0E-6) GOTO 37
 14   CONTINUE
 300  WRITE(*,*)'TOTAL ITRS FOR CONDUCTION ---- ',COUNT3
      RETURN
      END
C
      SUBROUTINE FORCE(ND,ST,W,SS,AFT,SL,BL,TOL,IER)
      DIMENSION ST(ND),W(ND),SS(ND),AFT(8)
      REAL Y,XY,AFUNC
```

```
      SIGMA = 5.669E-12
      DO 1 I = 1, ND
C
      SSE = 0.0
C
C     GAUSSIAN QUADRATURE
C
      DO 2 J = 1 , 2
        IF (J.EQ.1) THEN
          Y = -0.57735027
          LAMDA = SL
        ELSE
          Y = 0.57735027
          LAMDA = BL
        ENDIF
C
        XY = 5.0E-5*Y + 5.0E-4
C
        A = AFT(1)*(ST(I)**4)
        B = ((1.0 - AFT(2))*0.1281)/
     $      (2.0*0.1281*(1.0 - AFT(2))
     $      + ((AFT(1))*SIGMA*(ST(I)**4)
     $      *((ST(1)*1600)**4)))
        C = AFT(3)*(ST(I)**4)
        D = (AFUNC(1.0,8))*(ST(I)**4)*
     $      ((AFUNC(XY,1))-AFT(4))
        F = 2.0*(1.0 - (AFUNC(XY,6)))
        G = (AFUNC(XY,6))*(ST(I)**4)
        H = 1.0/0.1281
C
        AILOG = 1.0 - XY
        SSE = SSE + 5.0E-5 * (4.0 * G
     $        - 2.0 * (AFUNC(XY,2)) *
     $        (G + 2.0*F*B* ( (-G - F*A) - H*(C-A) ) + A)
     $        + 4.0*B* (-G - F*A - H*(C-A))
     $        * ( 1.0 + (0.5772 - 1.0 + alog(AILOG)) *
     $          (1.-XY) - ((1.-XY)**2)/2.0) - 2*D )
 2    CONTINUE
        SS(I) = SSE
 1    CONTINUE
      RETURN
      END
C
      REAL FUNCTION AFUNC(X,ID)
      REAL X
      INTEGER ID
   5  GOTO (10,20,30,40,50,60,70,80,90) ID
  10  AFUNC = -0.5772 - alog(X) + X - (X**2)/4.0
      goto 90
  20  AFUNC = 1.0 + (0.5772 - 1.0 + alog(X))*X -
     $       (X**2)/2.0
      goto 90
  30  AFUNC = 0.5 - X + 0.5*(-0.5772 + 1.5 - alog(X))*X**2
     $        + (X**3)/6.0
```

```
      goto 90
   40 AFUNC = ((-0.0001 * (X**5) + 0.0031*(X**4) -
     $     0.0523*(X**3) + 0.3834 * (X**2) - .9968 * X +
     $     .8177) * (1.003**4) * (-0.5772 - alog(1.003E-5)
     $     + 1.003E-5 - (1.003E-5**2)/4.0)
     $     - (-0.0001*(X**5) + 0.0031 * (X**4) - 0.0523 *
     $     (X**3) + 0.3834 * (X**2) - .9968 * x + .8177) *
     $ (1.003**4) *(-0.5772 - alog(X) + X - (X**2)/4.0))
      goto 90
   50 AFUNC = (1.0 + (0.5772 - 1.0 + alog(X))*X -
     $   (X**2)/2.0) * (-0.0001*(X**5) + 0.0031*(X**4) -
     $   0.0523*(X**3)+  0.3834*(X**2) - .9968*X + .8177)
      goto 90
   60 AFUNC = -0.0001*(X**5) + 0.0031*(X**4) -
     $    0.0523*(X**3) +
     $         0.3834*(X**2) - .9968*X + .8177
      goto 90
   70 AFUNC = .0004*X + .4432
      goto 90
   80 AFUNC = 1.0/(0.5 - 1.0 + 0.5*(-0.5772 + 1.5 -
     $  alog(1.0))*1.0**2 + (1.0**3)/6.0)
C
   90 RETURN
      END
C
C THERMAL CONDUCTIVITY OF ALUMINA
C
      REAL FUNCTION THERM1(X)
      REAL X
      THERM1 = .0019*X + 6.0
      RETURN
      END
C
C THERMAL CONDUCTIVITY OF IRON SAMPLE
C
      REAL FUNCTION THERM2(X)
      REAL X
      THERM2 = .0219*X + 2.6
      RETURN
      END
C-------------------------------------------------------------
C THIS FUNCTION CALCULATES THE INTEGRAL OF THE FUNCTION IN THE
C REAL FUNCTION 'AFUNC', USING ADAPTIVE QUADRATURE WITH SIMPSON'S
C RULE.
C       A = LOWER BOUND  OF THE INTEGRAL
C       B = UPPPER BOUND OF THE INTEGRAL
C       TOL = MAXIMUM ERROR OF THE QUADRATURE
C       IER = ERROR.  IER = 129 IF THE ALGORITHM COULD NOT CONVERGE.
C-------------------------------------------------------------
C
      REAL FUNCTION ADSIMP(AFUNC, AA, BB, TOLL, IER,Q)
C
      REAL AA, BB, TOLL, AFUNC
      INTEGER Q
```

```
      DOUBLE PRECISION EST,R(20),V(20),FR(20),
     *     FS(20),FT(20),FU(20),FV(20),ERR,S2F,SF, HMIN, TOL
      LOGICAL FIN
      INTEGER LEV,IER
C INITIALIZE
      IER = 0
      A = DBLE(AA)
      B = DBLE(BB)
      TOL = DBLE(TOLL)
      HMIN = (BB-AA)/2.D0**19
      EST = 0.D0
      R(1) = A
      V(1) = B
      IF (A.EQ.B) RETURN
    1 LEV = 1
      FR(1) = DBLE(AFUNC( SNGL( R(1) ) ,Q) )
      FS(1) = DBLE(AFUNC( SNGL( (V(1)-R(1))/4.D0 + R(1) ) ,Q) )
      FT(1) = DBLE(AFUNC( SNGL( (V(1)-R(1))/2.D0 + R(1) ) ,Q) )
      FU(1) = DBLE(AFUNC( SNGL( (V(1)-R(1))*.75D0 + R(1) ) ,Q) )
      FV(1) = DBLE(AFUNC(SNGL(V(1)),Q))
      FIN = .FALSE.
C
C ENTER THE MAIN LOOP
C
100   IF (FIN) RETURN
C
C CALCULATE S2(F) AND SF(F)
C
        S2F = (V(LEV)-R(LEV))/12.D0*(FR(LEV)+FV(LEV)+2.D0*FT(LEV) +
     *       4.D0*(FS(LEV) + FU(LEV)))
        SF = (V(LEV)-R(LEV))/6.D0*(FR(LEV)+FV(LEV) + 4.D0*FT(LEV))
C
C GET THE TOLERANCE FOR THIS STAGE
        ERR = 2.D0*TOL*(V(LEV)-R(LEV))/(B-A)
C
C IF THE ERROR IS TOO HIGH, GO TO THE NEXT SMALLER STAGE.
C OTHERWISE, DO THIS STAGE.
C
        IF(DABS(S2F-SF).GT.ERR) GO TO 200
          EST = EST + S2F
          ADSIMP = SNGL(EST)
C
C CHECK FOR ENDING CRITERIA. IF LEVEL = 1 AND V(LEV) = B, STOP
C
        IF ((LEV.GT.1).OR.(V(LEV).LT.B)) GO TO 150
          FIN = .TRUE.
          GO TO 100
  150   CONTINUE
C
C OTHERWISE, SET UP FOR THE NEXT STAGE
C
        R(LEV - 1) = V(LEV)
        FR(LEV - 1) = FV(LEV)
        FT(LEV - 1) = FU(LEV - 1)
```

```
      FS(LEV - 1) = DBLE(AFUNC(SNGL((V(LEV-1)-R(LEV-1))
     *                              /4.D0+R(LEV-1)),Q)
      FU(LEV-1) = DBLE(AFUNC(SNGL((V(LEV-1)-R(LEV-1))*.75D0 +
     *                                              R(LEV-1)),Q)
      LEV = LEV - 1
      GO TO 100
C
C IF IT DIDN'T WORK OUT, GO TO THE NEXT HIGHER LEVEL
  200 CONTINUE
C
C SET UP THE BOUNDARIES AND FUNCTIONS FOR THE NEXT LEVEL CALCULATIONS
C
      IF (LEV.EQ.20) GOTO 225
      R(LEV+1) = R(LEV)
      V(LEV+1) = (R(LEV)+V(LEV))/2.D0
      FR(LEV+1) = FR(LEV)
      FT(LEV+1) = FS(LEV)
      FV(LEV+1) = FT(LEV)
      FS(LEV+1) = DBLE(AFUNC(SNGL( (V(LEV+1)-R(LEV+1))/4.D0 +
     *                                              R(LEV+1)),Q)
      FU(LEV+1) = DBLE(AFUNC(SNGL((V(LEV+1)-R(LEV+1))*.75D0 +
     *                                              R(LEV+1)),Q)
      LEV = LEV+1
C
C CHECK FOR ERROR. IF NOT ERROR, GO BACK AND DO THE NEXT LOOP
C
      IF((V(LEV)-R(LEV)).GE. HMIN) GO TO 100
  225   IER = 129
      BB = SNGL(R(LEV))
      RETURN
      END
C
      SUBROUTINE GAUSS(M,C,RR)
      DIMENSION C(M,M),RR(M)
      DD=0.0
      DO 23 L=1,M
         DO 21 K=1,M
            DD=DD+C(L,K)*C(L,K)
   21    CONTINUE
   23 CONTINUE
      PD=SQRT(DD)
      DET=1.0
C     ----------MAXIMIZATION OF PIVOT ELEMENTS ------------
      DO 101 L = 1,M
      BIG=C(L,L)
      ABIG=ABS(C(L,L))
      IBIG=L
      DO 15 I = L,M
         SIZE=C(I,L)
         ASIZE=ABS(C(I,L))
         IF (ASIZE.LE.ABIG)GO TO 15
         BIG=SIZE
         IBIG=I
   15 CONTINUE
```

```
      DET=DET*BIG
C SWAP ROWS FOR MAXIMUM OF C(L,L)
      IF (L.EQ.IBIG)GOTO 26
      DO 25 J=L,M
      CBIG=C(IBIG,J)
      C(IBIG,J)=C(L,J)
      C(L,J)=CBIG
   25 CONTINUE
      RBIG=RR(IBIG)
      RR(IBIG)=RR(L)
      RR(L)=RBIG
   26 RR(L)=RR(L)/BIG
      DO 151 J=L,M
  151 C(L,J)=C(L,J)/BIG
      DO 201 K = 1,M
      A=C(K,L)
      IF(K.EQ.L) GOTO 201
      DO 11 J=L,M
   11 C(K,J)=C(K,J)-C(L,J)*A
      RR(K)=RR(K)-RR(L)*A
  201 CONTINUE
  101 CONTINUE
      CTX=ABS(DET)/PD
      RETURN
      END
```

APPENDIX C: FORTRAN PROGRAM FOR TWO DIMENSIONAL RADIATION/CONDUCTION MODEL

```
      PARAMETER (ND = 100, ND2 = 200)
      EXTERNAL AFUNC, THERM1, THERM2,ADSIMP
      DIMENSION A(ND,ND),B(ND),T(ND),TT(5,5),W(ND),
     $ DIFF(ND),AFT(8),ER(2),TC(ND),QT(ND),
     $ WW(ND),EE(ND),FT(ND2),DIST(ND)
C
      SIGMA = 5.669E-12
      TOL = 1.0E-6
      IER = 0
      OPEN (6,FILE = 'CRUC1.DAT',STATUS = 'NEW')
C INITIALIZE THE MATRICES
      DO 1 I = 1, ND
         B(I) = 0.0
         T(I) = 0.0
         W(I) = 0.0
         WW(I) = 0.0
         DO 1 J = 1, ND
            A(I,J) = 0.0
    1 CONTINUE
C RANGE OF WAVE LENGTHS AND INITIAL GUESS TEMPERATURES
      WRITE(*,*) 'ENTER T(1)   T(ND)'
      READ(*,*) T(1), T(ND)
      WRITE(*,*) 'ENTER SL AND BL '
      READ(*,*) SL, BL
      H = 1/ND
      DIST(1) = 0.0
      DO 6 I = 2, ND
         DIST(I) = DIST(I-1) + H
    6 CONTINUE
      COUNT = 0.0
  200 IF (COUNT.GT.0.0) THEN
         IF (FLX2.GT.FLX1) THEN
            T(ND) = T(ND) + 3.0
            P = T(ND)
         ELSE
            T(ND) = T(ND) - 2.5
            P = T(ND)
         ENDIF
      ELSE
         WRITE(6,*)'COUNTER  =  ',COUNT
      ENDIF
      DO 5 I = 1, 8
         AFT(I) = ADSIMP(AFUNC,SL,BL,TOL,IER,I)
    5 CONTINUE
      CALL RAD(ND,T,B,H,SL,BL,ND,FLX1)
      WRITE(*,*) 'FROM RADIATION FLUX AT JOINT = ',FLX1
      DO 2 I = 1, ND
         FT(I) = T(I)
    2 CONTINUE
      CALL CONDUCT(TT,T,H,HH,ND,FLX1,FLX2)
C
```

```
      WRITE(*,*) 'FROM CONDUCTION FLUX AT JOINT = ',FLX2
      COUNT = COUNT + 1
      IF(COUNT.GT.100.0)GOTO 300
C CONDITION FOR STOP
      IF(COUNT.GT.0.0) THEN
        ER(2) = ER(1)
        ER(1) = ABS(FLX2 - FLX1)
        ERA = ABS(ER(1) - ER(2))
        IF (ERA.GT.1.0E-2) THEN
           WRITE(*,*)'ERROR IN  FLUXES  ',ERA
           GOTO 200
        ELSE
           WRITE(*,*)'ERROR AND FLUX1 FINAL ',ERA,FLX1
        ENDIF
      ELSE
      ENDIF
 300  WRITE(*,*) '# OF ITERATIONS = ',COUNT
      WRITE(*,*)'ERROR IN FLUX AT JOINT = ',ERA
      WRITE(*,*)'FLUX AT RAD/COND JOINT = ',FLX1,FLX2
      DO 4 I = 1, ND2
         WRITE(*,*)I,' = ',FT(I)
 4    CONTINUE
      DO 3 I = 1, 5
        DO 3 J = 1,5
          WRITE(*,*)I,',',J,' = ',TT(I,J)
 3    CONTINUE
      STOP
      END
C
      SUBROUTINE RAD(ND,T,B,H,SL,BL,ND,FLX1)
      DIMENSION A(ND,ND),B(ND),T(ND),W(ND),DIFF(ND),AFT(8)
     $          TC(ND),QT(ND),WW(ND),EE(ND),FLXR(ND),
     $          PT(ND)
      T(1) = Q
      T(ND) = P
      PT(1) = T(1)
      COUNT2 = 0.0
      SIGMA = 5.669E-12
      TOL = 1.0E-6
      IER = 0
      WW(1) = 0.0
      WWW = 0.0
      DO 423 I = 2 , ND
       WW(I) = H + WWW
       WWW = WWW +H
 423  CONTINUE
      Z = (T(1) - T(ND))/ND
      DO 4 I = 2, ND-1
         T(I) = T(1) - I*Z
         PT(I) = T(I)
 4    CONTINUE
      DO 41 I = 1,ND
        QT(I) = T(I)/T(1)
 41   CONTINUE
```

```
      MM = 1
C ADJUSTING GUESS VALUES
      IF(MM.GT.0)GOTO 212
 37   DO 42 I = 2, ND-1
        IF(PT(I).GT.T(I)) THEN
          PT(I) = T(I)
          T(I) = T(I) + 0.5*DIFF(I)
          QT(I) = T(I)/T(1)
        ELSEIF(PT(I).LT.T(I))THEN
          PT(I) = T(I)
          T(I) = T(I) - 0.5*DIFF(I)
          QT(I) = T(I)/T(1)
        ELSE
        ENDIF
 42   CONTINUE
 212  Y=1.0
      DO 22 I = 1,ND
           TC(I) = 0.01*THERM1(T(I))
 22   CONTINUE
C GENERATE MATRIX [A] and [B]
      A(1,1) = 1.0
      A(ND,ND-1) = TC(ND) + TC(ND-1)
      A(ND,ND) = -A(ND,ND-1)
      DO 2 I = 2, ND-1
        A(I,I-1) = (0.5*(TC(I-1) + TC(I)))/(H**2)
        A(I,I) =-(0.5*TC(I-1) + TC(I) +
     $       0.5*TC(I+1))/(H**2)
        A(I,I+1) = (0.5*(TC(I) + TC(I+1)))/(H**2)
 2    CONTINUE
C
      CALL FORCE(ND,QT,W,B,AFT,SL,BL,TOL,IER)
      B(1) = 1.0
      B(ND) = AFT(2)*SIGMA*(T(ND)**4)
      CNTERM =(SIGMA*(T(1)**3))/AFT(3)
      DO 5 I = 2, ND-1
         B(I) = -1.0*(CNTERM*B(I))
 5    CONTINUE
C
      CALL GAUSS(ND,A,B)
C
      DO 666 I = 1, ND
         QT(I) = B(I)
         T(I) = T(1)*B(I)
 666    CONTINUE
      DO 8 I = 1, ND
         W(I) = T(1)*B(I)
         WRITE(*,*)WW(I),' , ',W(I)
 8    CONTINUE
      FLXR(ND)= (3.*T(ND) - 4.*T(ND-1) + T(ND-2))/(2.*H)
      FLX1 = 0.4*SIGMA*(T(2)**4 - T(1)**4) + FLXR(ND)*
     $          THERM1(T(ND))
      DO 13 I= 2 , ND
          DIFF(I) = ABS(PT(I) - T(I))
 13   CONTINUE
```

```
C     CONDITION FOR STOP
      MM = MM+1
      COUNT2 = COUNT2 + 1.0
      IF (COUNT2.GT.20.0) GOTO 300
      DO 14 I = 1, ND
        IF(DIFF(I).GT.0.5) GOTO 37
 14   CONTINUE
 300  WRITE(*,*)' TOTAL ITRS FOR RADIATION ---- ',COUNT2
      RETURN
      END
C
      SUBROUTINE CONDUCT(TT,T,H,HH,ND,FLX1,FLX2)
      DIMENSION T(ND),U(ND),DIFFC(5,5),BT(25)
     $          BFLX(2),TCC(5,5),QT(25),UU(25),EE(25),
     $          FLXC(25),TT(5,5),BB(25),AA(25,25)

      GG = 1/5
      HH = 1/5
      DO 1 I = 1, 5
         TT(1,I) = T(ND)
 1    CONTINUE
      COUNT3 = 0.0
      SIGMA = 5.669E-12
      TOL = 1.0E-6
      IER = 0
      MM = 1
C ADJUSTING GUESS VALUES
      IF(MM.GT.0)GOTO 212
 37   DO 42 N = 2, 5
        DO 42 M = 1, 5
           TT(N,M) = TT(N,M) - 0.1*DIFFC(N,M)*T(1,1)
         ELSE
           TT(N,M) = TT(N,M) + 0.1*DIFFC(I)*TT(1,1)
         ENDIF
 42   CONTINUE
 212  Y=1.0       DO 22 N = 1,25
         DO 22 M = 1, 25
           TCC(N,M) = 0.01*THERM2(T(N,M))
 22   CONTINUE
C GENERATE MATRIX [A] and [B]
C
C     R = GG**2/HH**2
      AB = ADSIMP(AFUNC,SL,BL,TOL,IER,I)
      DO 1 N = 2, 24
        DO 1 M = 2, 24
          A(N,M-1) = (1/AB**3)*0.5*(TCC(N-1,M)+TCC(N,M))
          A(N,M)   =  -((AB**3 + HH*N)*(R/HH*N*(AB**3)))*
     $                 0.5(TCC(N-1,M) - TCC(N+1,M))
          A(N,M+1) = (1/AB**3)*0.5*(TCC(N+1,M)+TCC(N,M))
          A(N-1,M) = (R/HH*N)*0.5*(TCC(N-1,M)+TCC(N,M))
          A(N+1,M) = (R/HH*N)*0.5*(TCC(N+1,M)+TCC(N,M))
 1    CONTINUE
C  BOUNDARY CONDITIONS
C
```

```
C
      DO 2 NN = 1, 5
         TT(NN,1) = T(NN,2)
 2    CONTINUE
      DO 3 NN = 1, 5
         TT(NN,5) = T(NN,4)
 3    CONTINUE
      DO 4 MM = 1, 5
         TT(1,MM) = TT(1,1)
 4    CONTINUE
      DO 5 MM = 1, 5
         TT(5,MM) = TT(4,MM)
 5    CONTINUE
C
      I = 1
      DO 6 M = 1, 5
          DO 6 N = 1, 5
            BB(I) = T(N,M)
            EE(I) = BB(I)
            I = I + 1
 6    CONTINUE
C
      DO 55 I = 1, 25
         BT(I) = 0.0
 55   CONTINUE
C
      DN = 25
      CALL GAUSS(DN,A,BT)
C
C
      I = 1
      DO 66 M = 1, 5
          DO 66 N = 1, 5
            T(N,M) = BT(I)
            BB(I) = BT(I)
            I = I + 1
 66   CONTINUE
C
        BFLX(2)=BFLX(1)
        FLXC(1)= (-3.*BB(1) + 4.*BB(2) -BB(3))/(2.*HH)
        WRITE(*,*)'CONDUCTION flux at 1 = ',FLXC(1)
        FLXC(25)= (3.*BB(25) - 4.*BB(24)+
     $       BB(23))/(2.*HH)
        WRITE(*,*)'CONDUCTION flux at 25 = ',FLXC(25)
        FLX2 = FLXC(1)
        BFLX(1) = FLXC(25)
        FLX2 = THERM2(BB(1))*FLXC(1)
        DO 13 I= 2 , 25
          DIFFC(I) = ABS(BB(I) - EE(I))
  13  CONTINUE
C     CONDITION FOR STOP
      WRITE(*,*)'CONDUCTION iterations = ',MM
      MM = MM+1
      COUNT3 = COUNT3 + 1.0
```

```
      IF (COUNT3.GT.20.0) GOTO 300
      DO 14 I = 1, ND
        IF(DIFF(ND).GT.1.0E-6) GOTO 37
 14   CONTINUE
 300  WRITE(*,*)'TOTAL ITRS FOR CONDUCTION ---- ',COUNT3
      RETURN
      END
C
      SUBROUTINE FORCE(ND,ST,W,SS,AFT,SL,BL,TOL,IER)
      DIMENSION ST(ND),W(ND),SS(ND),AFT(8)
      REAL Y,XY,AFUNC
C
      SIGMA = 5.669E-12
      DO 1 I = 1, ND
C
      SSE = 0.0
C
C     GAUSSIAN QUADRATURE
C
      DO 2 J = 1 , 2
        IF (J.EQ.1) THEN
          Y = -0.57735027
          LAMDA = SL
        ELSE
          Y = 0.57735027
          LAMDA = BL
        ENDIF
C
        XY = 5.0E-5*Y + 5.0E-4
C
        A = AFT(1)*(ST(I)**4)
        B = ((1.0 - AFT(2))*0.1281)/
     $      (2.0*0.1281*(1.0 - AFT(2))
     $      + ((AFT(1))*SIGMA*(ST(I)**4)
     $      *((ST(1)*1600)**4)))
        C = AFT(3)*(ST(I)**4)
        D = (AFUNC(1.0,8))*(ST(I)**4)*
     $      ((AFUNC(XY,1))-AFT(4))
        F = 2.0*(1.0 - (AFUNC(XY,6)))
        G = (AFUNC(XY,6))*(ST(I)**4)
        H = 1.0/0.1281
C
        AILOG = 1.0 - XY
        SSE = SSE + 5.0E-5 * (4.0 * G
     $        - 2.0 * (AFUNC(XY,2)) *
     $        (G + 2.0*F*B* ( (-G - F*A) - H*(C-A) ) + A)
     $        + 4.0*B* (-G - F*A - H*(C-A))
     $        * ( 1.0 + (0.5772 - 1.0 + alog(AILOG)) *
     $          (1.-XY) - ((1.-XY)**2)/2.0) - 2*D )
 2    CONTINUE
        SS(I) = SSE
 1    CONTINUE
      RETURN
      END
```

```
        DO 666 I = 1, DN
         QT(I) = B(I)
         T(I) = B(I)*T(1)
666     CONTINUE
      DO 8 I = 1, ND
         U(I) = T(1)*QT(I)
         WRITE(*,*)UU(I),' , ',U(I)
8     CONTINUE
C
      REAL FUNCTION AFUNC(X,ID)
      REAL X
      INTEGER ID
5     GOTO (10,20,30,40,50,60,70,80,90) ID
10    AFUNC = -0.5772 - alog(X) + X - (X**2)/4.0
      goto 90
20    AFUNC = 1.0 + (0.5772 - 1.0 + alog(X))*X -
     $       (X**2)/2.0
      goto 90
30    AFUNC = 0.5 - X + 0.5*(-0.5772 + 1.5 - alog(X))*X**2
     $        + (X**3)/6.0
      goto 90
40    AFUNC = ((-0.0001 * (X**5) + 0.0031*(X**4) -
     $     0.0523*(X**3) + 0.3834 * (X**2) - .9968 * X +
     $    .8177) * (1.003**4) * (-0.5772 - alog(1.003E-5)
     $     + 1.003E-5 - (1.003E-5**2)/4.0)
     $     - (-0.0001*(X**5) + 0.0031 * (X**4) - 0.0523 *
     $     (X**3) + 0.3834 * (X**2) - .9968 * x + .8177) *
     $ (1.003**4) *(-0.5772 - alog(X) + X - (X**2)/4.0))
      goto 90
50    AFUNC = (1.0 + (0.5772 - 1.0 + alog(X))*X -
     $   (X**2)/2.0) * (-0.0001*(X**5) + 0.0031*(X**4) -
     $   0.0523*(X**3)+  0.3834*(X**2) - .9968*X + .8177)
      goto 90
60    AFUNC = -0.0001*(X**5) + 0.0031*(X**4) -
     $    0.0523*(X**3) +
     $         0.3834*(X**2) - .9968*X + .8177
      goto 90
70    AFUNC = .0004*X + .4432
      goto 90
80    AFUNC = 1.0/(0.5 - 1.0 + 0.5*(-0.5772 + 1.5 -
     $  alog(1.0))*1.0**2 + (1.0**3)/6.0)
C
90    RETURN
      END
C
C THERMAL CONDUCTIVITY OF ALUMINA
C
      REAL FUNCTION THERM1(X)
      REAL X
      THERM1 = .0019*X + 6.0
      RETURN
      END
C
C
```

```
C
C THERMAL CONDUCTIVITY OF IRON SAMPLE
C
      REAL FUNCTION THERM2(X)
      REAL X
      THERM2 = .0219*X + 2.6
      RETURN
      END
C-------------------------------------------------------------
C THIS FUNCTION CALCULATES THE INTEGRAL OF THE FUNCTION IN THE
C REAL FUNCTION 'AFUNC', USING ADAPTIVE QUADRATURE WITH SIMPSON'S
C RULE.
C       A - LOWER BOUND  OF THE INTEGRAL
C       B - UPPPER BOUND OF THE INTEGRAL
C       TOL - MAXIMUM ERROR OF THE QUADRATURE
C       IER - ERROR.  IER - 129 IF THE ALGORITHM COULD NOT CONVERGE.
C-------------------------------------------------------------
C
      REAL FUNCTION ADSIMP(AFUNC, AA, BB, TOLL, IER,Q)
C
      REAL AA, BB, TOLL, AFUNC
      INTEGER Q
      DOUBLE PRECISION EST,R(20),V(20),FR(20),
     *     FS(20),FT(20),FU(20),FV(20),ERR,S2F,SF, HMIN, TOL
      LOGICAL FIN
      INTEGER LEV,IER
C INITIALIZE
      IER = 0
      A = DBLE(AA)
      B = DBLE(BB)
      TOL = DBLE(TOLL)
      HMIN = (BB-AA)/2.D0**19
      EST = 0.D0
      R(1) = A
      V(1) = B
      IF (A.EQ.B) RETURN
    1 LEV = 1
      FR(1) = DBLE(AFUNC( SNGL( R(1) ) ,Q) )
      FS(1) = DBLE(AFUNC( SNGL( (V(1)-R(1))/4.D0 + R(1) ) ,Q) )
      FT(1) = DBLE(AFUNC( SNGL( (V(1)-R(1))/2.D0 + R(1) ) ,Q) )
      FU(1) = DBLE(AFUNC( SNGL( (V(1)-R(1))*.75D0 + R(1) ) ,Q) )
      FV(1) = DBLE(AFUNC(SNGL(V(1)),Q))
      FIN = .FALSE.
C
C ENTER THE MAIN LOOP
C
100   IF (FIN) RETURN
C
C CALCULATE S2(F) AND SF(F)
C
        S2F = (V(LEV)-R(LEV))/12.D0*(FR(LEV)+FV(LEV)+2.D0*FT(LEV) +
     *       4.D0*(FS(LEV) + FU(LEV)))
        SF = (V(LEV)-R(LEV))/6.D0*(FR(LEV)+FV(LEV) + 4.D0*FT(LEV))
C
```

```
C GET THE TOLERANCE FOR THIS STAGE
        ERR = 2.D0*TOL*(V(LEV)-R(LEV))/(B-A)
C
C IF THE ERROR IS TOO HIGH, GO TO THE NEXT SMALLER STAGE
C OTHERWISE, DO THIS STAGE.
C
        IF(DABS(S2F-SF).GT.ERR) GO TO 200
          EST = EST + S2F
          ADSIMP = SNGL(EST)
C
C CHECK FOR ENDING CRITERIA. IF LEVEL = 1 AND V(LEV) = B, STOP
C
        IF ((LEV.GT.1).OR.(V(LEV).LT.B)) GO TO 150
          FIN = .TRUE.
          GO TO 100
  150   CONTINUE
C
C OTHERWISE, SET UP FOR THE NEXT STAGE
C
        R(LEV + 1) = V(LEV)
        FR(LEV + 1) = FV(LEV)
        FT(LEV + 1) = FU(LEV + 1)
        FS(LEV + 1) = DBLE(AFUNC(SNGL((V(LEV-1)-R(LEV-1))
     *                              /4.D0+R(LEV-1)),Q))
        FU(LEV-1) = DBLE(AFUNC(SNGL((V(LEV-1)-R(LEV-1))*.75D0 +
     *                                                R(LEV-1)),Q))
        LEV = LEV + 1
        GO TO 100
C
C IF IT DIDN'T WORK OUT, GO TO THE NEXT HIGHER LEVEL
  200 CONTINUE
C
C SET UP THE BOUNDARIES AND FUNCTIONS FOR THE NEXT LEVEL CALCULATIONS
C
        IF (LEV.EQ.20) GOTO 225
        R(LEV+1) = R(LEV)
        V(LEV+1) = (R(LEV)+V(LEV))/2.D0
        FR(LEV+1) = FR(LEV)
        FT(LEV+1) = FS(LEV)
        FV(LEV+1) = FT(LEV)
        FS(LEV+1) = DBLE(AFUNC(SNGL( (V(LEV+1)-R(LEV+1))/4.D0 +
     *                                                R(LEV+1) ),Q) )
        FU(LEV+1) = DBLE(AFUNC(SNGL((V(LEV+1)-R(LEV+1))*.75D0 +
     *                                                R(LEV+1) ),Q) )
        LEV = LEV+1
C
C CHECK FOR ERROR. IF NOT ERROR, GO BACK AND DO THE NEXT LOOP
C
      IF((V(LEV)-R(LEV)).GE. HMIN) GO TO 100
  225   IER = 129
      BB = SNGL(R(LEV))
      RETURN
      END
C
```

```
      SUBROUTINE GAUSS(M,C,RR)
      DIMENSION C(M,M),RR(M)
      DD=0.0
      DO 23 L=1,M
         DO 21 K=1,M
            DD=DD+C(L,K)*C(L,K)
 21    CONTINUE
 23   CONTINUE
      PD=SQRT(DD)
      DET=1.0
C     ----------MAXIMIZATION OF PIVOT ELEMENTS ------------
      DO 101 L = 1,M
      BIG=C(L,L)
      ABIG=ABS(C(L,L))
      IBIG=L
      DO 15 I = L,M
         SIZE=C(I,L)
         ASIZE=ABS(C(I,L))
         IF (ASIZE.LE.ABIG)GO TO 15
         BIG=SIZE
         IBIG=I
  15  CONTINUE
      DET=DET*BIG
C SWAP ROWS FOR MAXIMUM OF C(L,L)
      IF (L.EQ.IBIG)GOTO 26
      DO 25 J=L,M
      CBIG=C(IBIG,J)
      C(IBIG,J)=C(L,J)
      C(L,J)=CBIG
  25  CONTINUE
      RBIG=RR(IBIG)
      RR(IBIG)=RR(L)
      RR(L)=RBIG
  26  RR(L)=RR(L)/BIG
      DO 151 J=L,M
 151  C(L,J)=C(L,J)/BIG
      DO 201 K = 1,M
      A=C(K,L)
      IF(K.EQ.L) GOTO 201
      DO 11 J=L,M
  11  C(K,J)=C(K,J)-C(L,J)*A
      RR(K)=RR(K)-RR(L)*A
 201  CONTINUE
 101  CONTINUE
      CTX=ABS(DET)/PD
      RETURN
      END
```

BIBLIOGRAPHY

Adams, J.A. and Rodgers, D.F., *Computer-Aided Heat Transfer Analysis*, McGraw-Hill Book Co. NY (1973).

Ames, W.F., *Numerical Methods for Partial Differential Equations*, Barnes and Noble, NY (1969).

Anderson, E.E. and Viskanta, R., "Effective Conductivity for Conduction - Radiation by Taylor Series Expansion", *Int. J. Heat Mass Transfer*, vol 14, pp 1216 - 1220 (1971).

Anderson, E.E., Viskanta, R., Stevenson, W.H., "Heat Transfer through Semitransparent Solids", *Journal of Heat Transfer, Transaction ASME*, vol 95, n 2, pp 179 - 186 (1973).

Armaly, B.F. and El-Baz, H.S., "Influence of the Refractive Index on the Radiative Source Functions of an Isotropically Scattering Medium", *J. Quant. Spectrosc. Radiat. Transfer*, vol 18, pp 419 - 424 (1977).

Bates, J.L., McNeilly C.E., Rasmussen J.J., "Ceramics in Severe Environments", *Materials Science Research* vol 5, ed by W.W. Kriegel, H. Palmour III, Plemun Press, NY pp 11 - 26 (1971).

Beattie, J.R. and Coen, E., "Spectral Emission of Radiation by Glass", *J. of Applied Physics*, vol 11, pp 151 - 157 (1960).

Carslaw, H.S. and Jaeger, J.C., *Conduction of Heat in Solids* 2nd ed, Oxford Univ. Press, London (1959).

Chang, Yan-Po and Smith, S. Jr., "Steady and Transient Heat Transfer by Radiation and Conduction in a Medium Bounded by two Coaxial Cylindrical Surfaces", *Int. J. Heat Mass Transfer*, vol 13, pp 69 - 80 (1970).

Chung, T.J., Kim, J.Y., "Two-Dimensional, Combined-Mode Heat Transfer by Conduction, Convection, and Radiation in Emitting, Absorbing, and Scattering Media - Solution by Finite Elements", *Journal of Heat Transfer, Transaction ASME*, vol 106 n 2 pp 448 - 452 (1984).

Chupp, R.E. and Viskanta, R., "Development and Evaluation of a Remote Sensing Technique for Determining the Temperature Distribution in Semitransparent Solids", *Journal of Heat Transfer, Transaction ASME*, vol 96 n 3 pp 391 - 397 (1974).

Crosbie, A.L. and Dougherty, R.L., "Two-Dimensional Radiative Transfer in a Cylindrical Geometry with Anisotropic Scattering", *J. Quant. Spectrosc. Radiat. Transfer*, vol 19, pp 551 - 569 (1980).

Crosbie, A.L. and Linsenbardt, T.L., "Two-Dimensional Isotropic Scattering in a Semi-Infinite Medium", *J. Quant. Spectrosc. Radiat. Transfer*, vol 19, pp 257 - 284 (1978).

Dua, S.S. and Cheng P., "Multi-Dimensional Radiative Transfer in Non-Isothermal Cylindrical Media with Non-Isothermal Bounding Walls", *Int. J. Heat Mass Transfer*, vol 18, pp 245 - 259 (1975).

Edwards, D.K. and Matovosian, R., "Scaling Rules for Total Absorptivity and Emissivity of Gases", *Journal of Heat Transfer, Transaction ASME*, vol 106, pp 685 - 689 (1984).

Eryou, N.D. and Glicksman, L.R., "An Experimental and Analytical Study of Radiative and Conductive Heat Transfer in Molten Glass", *Journal of Heat Transfer, Transaction ASME*, vol 94 n 2, pp 224 - 230 (1972).

Fernandes, R. and Francis, J., "Radiative Heat Transfer in an Absorbing, Emitting, and Scattering Cylindrical Medium", *Journal of Heat Transfer, Transaction ASME*, vol 106, n 4, pp 888 - 891 (1984).

Fowle, A.A., Strong, P.f., Comstock,D.F., and Sox, C., "Computer Program to Predict Heat Transfer Through Glass", *AIAA Journal*, vol 7, pp 478 - 483 (1969).

Gerald, C.F. and Wheatly, P.O., *Applied Numerical Analysis*, Addison-Wesley Publishing Co. CA (1984).

Gille, J. and Goody, R.,"Covection in a Radiating Gas", *Journal of Fluid Mechanics*, vol 20, pp 47 - 49 (1964).

Gordaninejad, F. and Francis, J., "A Finite Difference Solution to Transient Combined Conductive and Radiative Heat Transfer in an Annular Medium", *Journal of Heat Transfer, Transaction ASME*, vol 106, n 4, pp 888 - 891 (1984).

Grief, R., "Energy Transfer by Radiation and Conduction with Variable Gas Properties", *Int. J. Heat Mass Transfer*, vol 7, pp 891 - 900 (1964).

Heinisch, R.P. and Viskanta, R., "Transient Combined Conduction Radiation in an Optically Thick Semi-Infinite Medium", *AIAA Journal*, vol 6, n 7, pp 1409 - 1411 (1968).

Ho, C.H. and Ozisik, M.N., "Combined Conduction and Radiation in a Two-Dimensional Rectangualar Enclosure", *Numerical Heat Transfer* vol 13 n 2 pp 229 - 239 (1988).

Holman, J.P., *Heat Transfer*, 5th ed McGraw-Hill Book Company, NY (1981).

Keller, H.H., Holdredge, E.S., "Radiation Heat Transfer for Annular Fins of Trapezoidal Profile", *Journal of Heat Transfer, Transaction ASME*, vol 94, n 1, pp 113 - 116 (1970).

Kellett, B.S., "The Steady Flow of Heat Through Hot Glass", *Journal of the Optical Society of America*, vol 42, n 5, pp 339 - 343 (1952).

Kesten, A.S., "Radiant Heat Flux Distribution in a Cylindrically-Symmetric Nonisothermal Gas with Temperature-Dependent Absorption Coefficient", *J. Quant. Spectrosc. Radiat. Transfer*, vol 8, pp 419 - 434 (1968).

Kingery, W.D. and Bowen, H.K., *Introduction to Ceramics*, 2nd ed., John Wiley and Sons, NY (1976).

Kreith, F. and Bohn, M.S., *Principles of Heat Transfer*, 4th ed., Harper & Row Publishers, NY (1986).

Lardner T.J., "Approximate Solutions of Combined Conduction-Radiation Problems", *AIAA Journal*, vol 7, n 1, pp 167 - 169 (1969).

Lick, W., "Transient Energy Transfer by Radiation and Conduction", *International Journal of Heat and Mass Transfer*, vol 8, pp 119 - 127 (1965).

Lii, C.C. and Ozisik, M.N., "Transient Radiation and Conduction in an Absorbing, Emitting, and Scattering Slab with Reflective Boundaries", *International Journal of Heat and Mass Transfer*, vol 15, pp 1175 - 1179 (1972).

Modest, M.f. and Azad, F.H., "Evaluation of the Radiative Heat Flux in Absorbing, Emitting and Linear-Anisotropically Scattering Cylindrical Media", *Journal of Heat Transfer, Transaction ASME*, vol 103 pp 350 - 356 (1981).

Modest, M.F. and Stevens, D.S., "Two-Dimensional Radiative Equilibrium of a Gray Medium between Concentric Cylinders ", *J. Quant. Spectrosc. Radiat. Transfer*, vol 19, pp 353 - 365 (1978).

Nishimura, M., Hasatami, M., and Sugiyama, S., "Simultaneous Heat Transfer by Radiation and Conduction. High Temperature One Dimensional Heat Transfer in Molten Glass", *Int. Journal of Chemical Engineering*, vol 8, pp 739 - 745 (1968).

Olfe, D.B., "Application of a Modified Differential Approximation to Radiative Transfer in a Gray Medium Between Concentric Spheres and Cylinders", *J. Quant. Spectrosc. Radiat. Transfer*, vol 8, pp 899 - 907 (1968).

Omega Complete Temperature Measurement Handbook and Encyclopedia, vol 26, Omega Engineering, Samford, CT (1988).

Padney, D.K., "Combined Conduction and Radiation Heat Transfer in Concentric Cylindrical Media", *Journal of Thermophysics and Heat Transfer* vol 3, pp 75 - 82 (1989).

Patankar, S.V., *Numerical Heat Transfer and Fluid Flow*, Hemisphere Publ. Corp., Washington, DC (1980).

Rohsenow, W.M., Hartnett, J.P., and Ganic, E., *Handbook of Heat Transfer*, 2nd ed McGraw-Hill Book Co., NY (1985).

Siegel, R., "Net Radiation Method for Transmission Through Partially Transparent Plates", *Solar Energy*, vol 15, pp 273 - 276.

Siegel, R. and Howell, J.R., *Thermal Radiation Heat Transfer*, 2 nd Ed., McGraw-Hill Book Company, NY (1980).

Smith, J.P., *SINDA User's Manual*, TRW System Report No. 14690-H001-R0-00, NASA Contract NAS 9-10435 (1971).

Sohal, M.S., Howell, J.R., "Determination of Plate Temperature in Case of Combined Conduction, Convection and Radiation Heat Exchange", *Int. J. Heat Mass Transfer*, vol 16, pp 2055 - 2066 (1973).

Sparrow, E.M. and Cess, R.D., *Radiation Heat Transfer*, McGraw-Hill Co., NY (1970)

Steward, F.R. and Cannon, P., "The Calculation of Radiative Heat Flux in a Cylindrical Furnace Using the Monte Carlo Method", *Int. J. Heat Mass Transfer*, vol 14, pp 245 - 262 (1971).

Toulokian, Y.S., *Thermophysical Properties of High Temperature Solid Materials*, vol 4, Part I, Thermophysical Properties Research Center, Purdue University (1967).

Viskanta, R. and Anderson, E.E. "Heat Transfer in Semitransparent Solids", *Advances in heat Transfer* vol 11, Academic Press, Inc., NY, pp 317 - 441 (1975).

Viskanta, R. and Grosh, R.J., "Effect of Surface Emissivity on Heat Transfer by Simultaneous Conduction and Radiation", *Int. J. Heat Mass Transfer*, vol 5, pp 729 - 734 (1962).

Viskanta, R. and Grosh, R.J., "Heat Transfer by Simultaneous Conduction and Radiation in an Absorbing Medium", *Journal of Heat Transfer, Transaction ASME*, C 84, pp 63 - 72 (1962).

Viskanta, R. and Hirleman, E.D., "Combined Conduction Radiation Heat Transfer Through an Irradiated Semitransparent Plate", *Journal of Heat Transfer, Transaction ASME*, vol 100, pp 169-174 (1978).

Viskanta, R. and Kim, D.M., Heat Transfer through Irradiated, Semi-transparent Layers at High Temperature", *Journal of Heat Transfer, Transaction ASME*, vol 102, pp 182-184 (1980).

Wang, L.S., Tien, C.L., "A Study of Various Limits in Radiation Heat-Transfer Problems", *Int. J. Heat Mass Transfer*, vol 10, pp 1327 - 1338 (1967).